



UPPSALA
UNIVERSITET

UPTEC K 16015

Examensarbete 30 hp
September 2016

Wear on Alumina Coated Tools and the Influence of Inclusions when Turning Low-Alloy Steels

Master Thesis - Chemical Engineering

Sebastian Öhman



UPPSALA
UNIVERSITET

Teknisk- naturvetenskaplig fakultet
UTH-enheten

Besöksadress:
Ångströmlaboratoriet
Lägerhyddsvägen 1
Hus 4, Plan 0

Postadress:
Box 536
751 21 Uppsala

Telefon:
018 – 471 30 03

Telefax:
018 – 471 30 00

Hemsida:
<http://www.teknat.uu.se/student>

Abstract

Wear on Alumina Coated Tools and the Influence of Inclusions When Turning Low-Alloy Steels

Sebastian Öhman

In this master thesis, performed at Sandvik Coromant Västberga (Stockholm), a comprehensive study has been made to investigate the wear on textured alumina (Inveio™) coated cutting tools when turning low-alloy steels. Specifically, wear studies have been made on tools' rake faces when turning two separate batches of SS2541, after an initial turning time of 4 min. A particular focus has been given to elucidate what particular role the inclusions might have for the wear of the alumina coating on the tools. Evaluation of tool wear has been made by employing several different analytical techniques, such as LOM, SEM, Wyko, Auger-spectrometry (AES), EPMA and XRD.

The results shows that the arisen wear marks on both tested tool types may be divided into three separate and highly distinguishable wear zones, denoted here in this work as “wear bands”. Largest amount of wear tended to occur initially at the topmost part of the 3rd wear band. This was true for both tested tool types. This area demonstrated a characteristic 'lamellar' wear pattern, composed of narrow and structured ridges. All the tools tested demonstrated the adhesion of workpiece materials of various composition that formed into smeared layers in these formed ridges. Depth-profiling Auger-spectrometry revealed that a significant amount of calcium was present in the machined alumina coating layers. This suggests that a reaction between the calcium-containing inclusions found in the steel and the alumina coating layer had occurred during the performed turning tests. These results are contradictory to the general belief that alumina is chemical inert during machining and has previously, to the authors knowledge, not yet been published.

Based on the results from this thesis and from a literature review concerning the behavior of α -alumina during deformation, a new theoretical wear model has been developed. In this model, it is emphasised that the sliding of hard inclusions from the steel may activate pyramidal slip systems in the textured alumina coating. This causes a nano-crystallisation and/or amorphisation in the topmost part of the coating, which facilitates the further wear of these coated tools.

Handledare: Marianne Collin
Ämnesgranskare: Urban Wiklund
Examinator: Erik Lewin
ISSN: 1650-8297, UPTec K16 015
UPPSALA

Populärvetenskaplig sammanfattning på svenska

Förslitningen av aluminiumoxidbelagda verktyg och inflytandet av inneslutningar vid svarvning av låglegerade stålsorter

I detta arbete har förslitningen av aluminiumoxidbelagda skärverktyg undersökts vid svarvningen av låglegerade stålsorter. Undersökningarna har framförallt syftat till att undersöka den initiala förslitningen av verktygens så kallade spånsida (eng: rake face).

Arbetet har inkluderat användningen av flera olika analystekniker för att kunna identifiera, kartlägga och karaktärisera förslitningen av verktygen. Detta har bland annat inkluderat flera olika typer av mikroskopiska tekniker, såsom ljusoptisk mikroskopi (LOM), elektronmikroskopi (SEM) och vitljusprofilometri (Wyko), men även andra undersökningar från Augerspektroskopi (AES), röntgendiffraction (XRD) samt elektronprobmikroanalys (EPMA).

I svarvningsundersökningarna har två olika typer av verktygssorter används, vilka går under beteckningen CNMA eller CNMG. Dessa verktyg är tillverkade av hårdmetall, som utgörs av mycket små, finfördelade oorganiska volframkarbidpartiklar som har ingjutits i en metallisk matris med hög seghet. Vanligtvis består denna matris utav kobolt. Kombinationen av dessa hårda volframkarbidpartiklar och den sega matrisen skapar ett material som både är mycket hårt och relativt segt. Detta ger hårdmetall mycket goda egenskaper för skärande bearbetningsprocesser av metall.

Genom att belägga hårdmetallen med olika typer av ytskikt kan förslitningsmotståndet hos verktygen ytterligare förbättras. I bearbetningen av stål utgörs dessa ytskikt vanligtvis av ett tunt multiskikt. Detta multiskikt består vanligtvis av ett tunt lager aluminiumoxid deponerat ovanpå ett titankarbonitridskikt, som förbinder aluminiumoxiden till det underliggande hårdmetallsubstratet. Aluminiumoxid har visat sig ha mycket goda egenskaper som gjort materialet särskilt lämpligt till att användas inom skärande bearbetningsprocesser av stål. Detta beror mestadels av materialets höga hårdhet, dess goda värmehållfasthet samt kemiska inerthet, vilket betyder att aluminiumoxid är relativt obenäget att reagera med andra element.

På senare tid har utvecklingen av teknikerna för att deponera dessa ytskikt på skärverktygen kraftigt förbättrats. Detta har möjliggjort till att man numera kan tillverka ytskikt bestående av föreningar (exempelvis aluminiumoxid) som är helt riktade i bestämda kristallografiska planriktningar och orienteringar. Genom detta kan man kraftigt förbättra egenskaperna för dessa typer av ytskikt. Inom Sandvik Coromant kallas dessa ytskikt, som utgörs av aluminiumoxidkristaller riktade i en och samma orientering, för Inveio™.

I examensarbetet har fyra olika typer av svarvningstester utformats för att se hur verktygen förslits. I dessa har två former av låglegerat stål använts, tillhörande samma stålsort men där det ena stålet hade genomgått en kalciumbehandling (medan det andra inte hade det).

Kalciumbehandlingar används frekvent av stålindustrin för att på olika sätt modifiera de så kallade inneslutningarna som finns inuti stålet. Dessa inneslutningar utgörs av mikroskopiskt små oorganiska partiklar av varierande storlek, struktur och kemisk sammansättning. Ofta härrör dessa inneslutningar som föroreningar från själva tillverkningen av stålet. Även om dessa partiklar i många fall kan anses vara en naturlig del av stålet, är de även kända för att kunna påverka stålets egenskaper negativt. Detta gäller framförallt stålets mekaniska egenskaper samt korrosionsmotstånd.

Inneslutningarna tros även kunna spela en viktig roll för hur skärverktygen förslits vid bearbetningen av stål. Inom litteraturen har därför en omfattande forskning bedrivits för att fastställa deras exakta roll och inverkan på hur verktygen förslits.

Emellertid har man dock, trots flera försök genom historien, ej helt uteslutande kunnat fastställa deras exakta roll till förslitningsförloppet. Många av de slutsatser och resultat som har presenterats är tvetydliga, och det finns fortfarande många frågeställningar och oklarheter kring inneslutningarnas roll som är obesvarade. Exempelvis har inneslutningarna både tillskrivits till att kunna förvärta förslitningen av verktygen men också för att faktiskt kunna skydda dem. I båda dessa fall har inneslutningarnas roll för förslitningen ofta kunnat kopplas till deras förmåga att bilda tunna, utsmetade oxidskikt ovanpå skärverktygen. Dessa skikt har av många ansetts kunna verka skyddande för verktygen under bearbetningsprocessen, men har likväl också rapporterats kunna accelerera förslitningen av dem. Därför har ett av målen med detta examensarbete varit att undersöka och försöka klargöra vilken roll inneslutningarna kan tänkas ha till förslitningen av de skärverktyg som har använts i detta examensarbete.

Från de erhållna resultaten i denna rapport kan man konstatera att förslitningen av verktygen kan uppdelas i tre olika separata områden, som uppvisar olika utseenden och karaktäristiska mönster. Dessa har här benämnts som tre olika nötningsband på verktygen, från 1 till 3, där det första nötningsbandet ligger närmast skärejden av verktygen. I dessa band visar resultaten på att förslitningen koncentreras mestadels i övergångsregionen mellan det andra och tredje nötningsbandet, vilket uppstår en bit in på verktygens spånsidor. Detta område uppvisar ett karaktäristiskt "lamell-liknade" utseende, bestående av ordnade gropar och skårer som alternerar i ett mycket ordnat mönster.

Vid undersökningen av detta område med den mycket yt-känsliga mättekniken Auger, har man för detta examensarbete erhållit mycket intressanta resultat. Man har här kunnat påvisa att en signifikant mängd kalcium – från tre oberoende försök – har lyckats tränga sig in i det allra översta (0.5 μm) toppskiktet av aluminiumoxiden. Eftersom tvärsnittsbilder gjorda i SEM inte kan påvisa någon mekanisk påverkan av själva kristallkornen, är det sannolikt att kalciumet här har trängt sig in i aluminiumoxiden via en diffusionskontrollerad mekanism. Det vill säga, att man fått en reaktion mellan kalcium och aluminiumoxiden under själva svarvningsprocessen.

Dessa resultat går stick i stäv med den allmänna uppfattningen om att aluminiumoxiden är kemiskt inert vid skärande bearbetning och har, till författarens kännedom och till dags dato, ej tidigare publicerats.

Baserat på de erhållna resultaten och en litterär sammanställning av flera forskningsrapporter från andra, angränsande forskningsområden har en ny modell kunnat presenteras som beskriver förslitningen av aluminiumoxidskiktet. Modellen är uppbyggd i fem individuella steg och utgår ifrån den atomära uppbyggnaden av aluminiumoxidkristallen och de atomära mekanismer som sker inuti den vid plastisk deformation. Modellen har i detta arbete benämnts som *ATBM* – "Amorphous transitional breakdown model". Denna teoretiska modell betonar vikten av att hårda abrasiva partiklar – i synnerhet från stålets inneslutningar – kan aktivera så kallade pyramidala glidsystem inuti aluminiumoxidkristallerna. Dessa glidsystem tros kunna spela en viktig roll för hur dessa kristaller i verktygens beläggningar förslits och till sist hur verktygen slutligen går sönder.

Table of Contents

1	Introduction.....	6
1.1	Background.....	6
1.2	Aim and objectives.....	7
2	Theoretical background.....	9
2.1	Coated cemented carbides.....	9
2.2	The machining processes and turning.....	9
2.2.1	Important cutting parameters.....	10
2.2.2	Tool geometry.....	11
2.3	Tribological aspects of turning.....	12
2.3.1	Shearing zones.....	13
2.3.2	Chip- and wear band formation.....	14
2.4	Assessment of wear mechanisms and wear types.....	15
2.5	Wear Types.....	19
3	Steel as a workpiece material.....	21
3.1	Challenges and demands.....	21
3.2	Wear protecting coatings.....	22
3.3	Properties of alumina.....	22
3.3.1	Crystal structure.....	24
3.3.2	Anisotropic behaviour and the effect of crystal orientation.....	26
4	The role of the inclusions on the tool wear.....	27
4.1	General description of inclusions.....	27
4.1.1	Layer formation.....	29
5	Literature survey.....	30
5.1	Review of published articles.....	30
6	Experimental procedure.....	32
6.1	Tools.....	32
6.2	Workpiece materials.....	33
6.3	Performed turning tests.....	36
6.3.1	DP1 – Test of tool life.....	36
6.3.2	DP2 – Turning of Ca-treated SS2541 using liquid coolant.....	37
6.3.3	DP3 – Dry turning of Ca-treated SS2541.....	37
6.3.4	DP4 – Turning of non Ca-treated SS2541 using liquid coolant.....	37
6.4	Material Analyses.....	37
6.4.1	SEM-imaging.....	37
6.4.2	Etching.....	39
6.4.3	Surface conductivity enhancement.....	39
6.4.4	Surface profilometry.....	40
6.4.5	Auger-microscopy (depth profiling).....	40
6.4.6	Microprobe analysis (EPMA).....	41
6.4.7	X-ray crystallography (XRD).....	41

7	Results.....	42
7.1	DP1	42
7.2	DP2	44
7.3	DP3	46
7.4	DP4	47
7.5	Cross-sectional imaging	48
7.6	Layer formation.....	51
7.7	Surface analyses.....	52
7.7.1	Profilometry.....	52
7.7.2	Auger	53
7.7.3	XRD.....	54
7.7.4	EPMA.....	55
8	Discussion	58
8.1	Summary of main results	58
8.2	Analyses of the results	60
8.2.1	I. – Possible chemical wear	62
8.2.2	II. – Indication for a phase transformation of alumina.....	64
8.3	Amorphous transitional breakdown model.....	66
8.3.1	General description of slip and dislocation movement	68
8.3.2	I – Shear deformation and basal twinning formation.....	70
8.3.3	II: Activation of pyramidal slip systems due to the sliding of hard inclusions..	72
8.3.4	III: Nano-crystallisation and/or amorphisation	74
8.3.5	IV: Microcrack formation	75
8.3.6	V: Coupling of micro cracks and end of tool-life.....	75
9	Suggestions for further work.....	77
10	Summary and conclusions.....	78
11	Acknowledgements.....	81
12	References.....	82

Abbreviations

AES	<i>Auger spectroscopy</i>
ATBM	<i>Amorphous transitional breakdown model</i>
Al ₂ O ₃	<i>Alumina</i>
BSE	<i>Back-scatter electron (detector)</i>
BUE	<i>Built-up edge</i>
BUL	<i>Built-up layer</i>
CAD	<i>Computer-aided design</i>
CAM	<i>Computer-aided machining</i>
CFD	<i>Chip flow direction</i>
CRSS	<i>Critical Resolved Shear Stress</i>
EDS	<i>Energy-dispersive X-ray spectroscopy</i>
EHT	<i>Extra high tension (voltage)</i>
EPMA	<i>Electron probe micro-analysis</i>
f.c.c	<i>Face-centred cubic</i>
h.c.p	<i>Hexagonal close-packed</i>
i.a	<i>Inter alia – “Among others”</i>
i.e	<i>Id est – “That is”</i>
In situ	<i>“in place, in position”</i>
LOM	<i>Light optical microscopy</i>
PD	<i>Plastic deformation</i>
RSS	<i>Resolved Shear Stress</i>
SE	<i>Secondary electron (detector)</i>
SEM	<i>Scanning electron microscopy</i>
TEM	<i>Transmission electron microscopy</i>
VPSE	<i>Variable pressure secondary electron (detector)</i>
Wyko	<i>White-light optical profilometry</i>
WC/Co	<i>Tungsten carbide/cobalt (tool substrate)</i>
XRD	<i>X-ray diffraction</i>

1 Introduction

1.1 Background

Throughout the history of mankind, the usage of different materials have played a central role for the development of our societies. The continuous improvement of these materials has not only shaped the way we live our lives as of today, but have also enabled for the technological advancements made in many other scientific areas, including the fields of medicine, transportation, communication, energy and space technology.

Arguably, there has been no more important material for the expansion of humanity than the usage of steel. This incredibly multi-functional and versatile material has laid the foundation for the economic growth of our civilization, not least by promoting the industrial revolution when Henry Bessemer invented the world's first method to inexpensively mass-produce steel in 1855. [1] Hence, steel has not only formed the backbone for many of the social and technological conveniences we have seen in modern years, but also contributed to our vastly improved living conditions in general.

Today, steel constitutes to one of the most common materials used by the manufacturing industries, and the shaping of this material corresponds to one of the most important machining applications worldwide. Steel machining is mainly performed by the use of hard cemented carbide tools, which are typically coated with a thin and protective ceramic coating. In essence, the wear of these tools correspond to one of the most important factors governing the outcome from the entire machining process. For instance, tool wear governs aspects such as the product qualities of the shaped component, the machining productivity and, ultimately, also the profitability from the entire machining process. For these reasons, it is desirable to prolong the longevity of the used cutting tools and to impede the development of wear, as this could cause premature tool failures. Accordingly, these two improvement areas are commonly requested by the manufacturing industries that the producers of these tools have to address.

In order to achieve these improvements, a comprehensive and detailed understanding for the mechanisms controlling the wear of the tools is needed. In this respect, a vast number of scientific journals have been published on the topic of "tool wear" when machining of different steel materials.

However, in spite of more than 50 years of extensive studies have been made, there are still many questions remaining to be resolved. For example, many of the results presented in the literature on the subject have proven being quite ambiguous, and a comparison of the results between dissimilar authors are more often than not contradictory.

Although it is believed that much of the tool wear when machining steels may be ascribed to the small inorganic precipitates found inside the steel matrix, their exact role for the wear progression has not yet been fully elucidated. These precipitates, which are commonly known as *inclusions*, have been shown to form stable oxide layers on top of the tool's surfaces during

a machining process. It has been debated whether these type of layers may be detrimental or possibly even beneficial for the cutting tools' longevity.

Accordingly, this thesis work has intended to shed some new lights into the topic about tool wear when machining of steels, in particular for turning low-alloy steels, when using alumina-coated (Inveio™) cutting tools. It is believed that the findings from this thesis, along with the provided literature reviews and discussions, may contribute to unravel some of the erratic and ambiguous historical findings in this field. Moreover, the proposed model in the discussion-part (page 66) of this thesis may also aid the further development of these cutting tools, especially for new machining applications using recently developed steel grades. Such steel grades include so called "clean steels", which contain very low levels of inclusions.

1.2 Aim and objectives

The purpose with this thesis has been to investigate the wear on two different types of alumina-coated cutting tools when turning two separate batches of low-alloy steel. A particular focus has been given to evaluate the initial wear on the tools' rake faces and how this wear progresses itself in the textured alumina coating (Inveio™). Moreover, a special attention has been given to link the wear on the tools to the inclusions found inside the workpiece material.

In this work, the term 'initial' implies that the machining time was deliberately chosen so that no wear through of the outer alumina coating should have occurred. For this reason, wear studies was made exclusively in this outer alumina coating layer.

The two different types of tool inserts used in this thesis were denoted as CNMA and CNMG. These inserts belong to a similar grade (GC4325) but have different geometries on their rake faces. In essence, CNMG-tools utilizes a 'chip-breaking geometry aimed at decreasing the cutting forces and facilitate the overall machining process, whilst CNMA-tools were completely planar. A chip-breaking geometry tends to increase the overall wear resistance of the tool. Therefore, by using both of these tools in the performed turning tests, it was possible to achieve a comparison of the effect from this chip-breaker on the tool wear.

In order to evaluate the performance of the machined cutting tools, four different type of turning tests have been made on two separate batches of a low-alloy SS2541 steel. In one of these batches the steel had undergone a calcium-treatment, whereas the other batch had not. The purpose with this was to evaluate what effect the calcium-treatment had for the wear development of the tools. The calcium-treatment is frequently used by the steelmakers in order to modify the inclusions in the steel. This makes them softer and thus less abrasive on the tools' surfaces.

The four turning tests, denoted as DP1, DP2, DP3, DP4, respectively, may be summarized according to following list:

1. DP1, longevity test using Ca-treated steel and liquid coolant.
2. DP2, initial turning test using Ca-treated steel and liquid coolant.
3. DP3, initial turning test using Ca-treated steel but no liquid coolant.
4. DP4, initial turning test using a non Ca-treated steel and liquid coolant.

The used analytical techniques for this work includes many microscopical techniques such as light optical microscopy (LOM), scanning electron microscopy (SEM) and white light surface profilometry (Wyko). Additionally, several qualitative analytical techniques have been made from depth profiling Auger-spectroscopy (AES), X-ray diffraction (XRD) and electron probe micro-analysis (EPMA).

Based on these turning tests and the employed analytical methods, the objective with this work has been to:

- Investigate wear on two different geometries of alumina-coated cutting tools, CNMA & CNMG (grade GC4325 Inveio™), when turning low-alloy steel.
- Characterise, clarify and attempting to explain the arisen wear on the tools' rake faces.
- Elucidate what role the steel's inclusions might have for the wear of these tools.

2 Theoretical background

2.1 Coated cemented carbides

Cemented carbide is a composite material composed of a fine-distribution of small, hard tungsten carbide particles (WC) embedded into a ductile metallic matrix. This matrix consists usually of cobalt and/or other elements. The combination of the hard tungsten carbide particles and the ductile cobalt-matrix forms a material that has relatively high hardness whilst still having good toughness. This makes the material particularly suitable for metal cutting applications.[2]

Tool inserts are fabricated from a powder metallurgical process, in which tungsten carbide and cobalt powder is mixed together and spray-dried into a granular brick that is subsequently die-pressed. This brick is then sintered for several hours at temperatures above the melting point of cobalt. In this sintering process, a diffusion process occurs between neighbouring WC particles and the melted cobalt, which upon cooling forms into a solid, dense material.[3,4]

Usually, cemented carbide tools are also coated by a thin, ceramic coating. This drastically increases the durability of the tool. These coatings have several functions, including to limit unwanted reactions between the workpiece material and the tool substrate.[5]

2.2 The machining processes and turning

The basic principle of any machining process is to shape a workpiece-material to a useful component by the removal of excess material. This can be achieved in numerous of different ways, and includes procedures such as grinding, milling, drilling and not least turning.

Among these many ways to machine a material, it is generally considered that turning is the most commonly used method employed by the manufacturing industries worldwide. Turning is well-known for being able to produce components having very narrow surface tolerances. For this reason, the technique has been widely adopted by the aerospace and automotive industries, where the tolerances in surface finish for the shaped component can be extremely narrow. By using turning, components can be made having a surface roughness value not deviating more than 0.0025 mm, or possibly even less.[6–9]

Turning is commenced by the fastening of a suitable workpiece material into an engine lathe holder, which thereafter is brought into rotation during the entire machining process. The removal of material then occurs from the pressing of a hard tool bit (cutting tool) into the rotating workpiece. This initiates the creation of two new surfaces, namely, the newly machined surface from the workpiece and its removed surface, which are commonly denoted as the *chip*.[6,8–10]

Today, there are many different turning applications available, and their purpose and inherent complexity depends largely on what demands that are put on the desired component that are about to be machined. In general, the main differences among these turning applications is the movability of the tool insert holder.

In the most simple form of turning, known as longitudinal, the tool is moved perpendicular towards the rotating workpiece along a single, fixed axis direction.[6] However, for more complex turning procedures, such as facing and grooving, it is even possible to utilise multiple coordinate axes in order to shape the workpiece into the desired shape. These advanced turning applications are often computer-assisted by so called CAD/CAM systems, which enable the programming of the tool's movement along a predetermined course consisting of a number of three-dimensional coordinates.[9]

2.2.1 Important cutting parameters

The turning process has several important parameters known to govern the qualities of the machined component to a very large degree.[7,9,11] The most commonly mentioned are usually the:

- *Cutting speed* (v), which describes the relative motion between the rotating workpiece and the moving cutting tool. This parameter is usually given in the units of m/min.
- *Feed rate* (f_n), describing at what velocity the workpiece material is brought into contact with the cutting tool and expressed by the unit mm/workpiece revolution.
- *Cutting depth* (A_p), which simply relates to how deep the tool inserts penetrates the workpiece material.

Jointly for all these parameters is that they control the material-removal rate Q of the turning process. The relationship between these parameters for the rate of material removal is frequently expressed by the simplified formula

$$Q = v \times f_n \times A_p \quad (\text{eq 2.2.1})$$

Thus, by altering one or several of these parameters, an inevitable effect on the material-removal rate will be achieved.

A high value of Q is often desired in turning, as this will then reduce the time needed to shape the workpiece into its final component. From the equation above it would therefore seem that a maximisation of the three factors would give the highest achievable material-removal rate. However, this is generally not true because the parameters in the equation affects turning in detrimental ways as well. This include an increase of the wear of the tools.

In essence, the parameters v , f_n and A_p governs the amount of heat developed in the tool-workpiece interfaces during machining. Therefore, an improper balance between these parameters will usually give rise to excessive heat development in these interfaces. This may, in turn, accelerate the wear of the tools and thereby also influence the geometrical accuracy for the finished component. Consequently, it is often necessary to optimise these individual cutting parameters so that an ideal material removal rate can be attained whilst still keeping the wear rate and surface tolerances of the component at a respectable level.

This optimal combination of cutting data is typically unique for a particular machining application. For example, it depends on the properties of the used cutting tools, the workpiece material, the used machining instrument, the usage of coolants and so on. Thus, different machining applications will require a different set of cutting parameters in order to obtain the best possible material-removal rate. For a particular machining process, this optimal combination is usually determined by empirical means.[6,7,12–14]

2.2.2 Tool geometry

Figure 2.1 displays a general image displaying a modern cutting tool insert. The different sides of the tool are marked in the image.

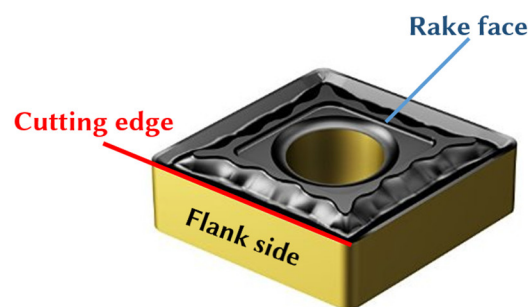


Figure 2.1. Schematic overview of a cutting tool insert

The tool's top side is denoted as its *rake face*, whilst its sides are referred as its 'flank sides' or 'flank face'. During turning, the conditions at the flank side and rake face will be quite dissimilar from each other since they will be in contact with the workpiece material in different ways.

Essentially, the rake face of the tool will be sliding against the chip from the workpiece, whilst the flank side will slide against the newly machined surface. This creates two very different contact situations between the tool and the workpiece which thereby also generates different amounts of heat. Typically, the temperatures reached on the rake face are much higher than the ones reached on the flank side. This is one of the primary reasons to why the cutting tool usually may display different wear behaviours on its rake face compared to its flank side.

A patterned geometry can also be seen on the tool's rake face in Figure 2.1. This is an important part of many cutting tools' overall function and consists usually of two features, namely, a positive rake angle and a chip breaker. These serve the common purpose to facilitate the chip formation process on the rake face, in particularly by easing its removal and decreasing the chip's contact length with the tool. These actions tends to result in an overall increase of the tool's wear resistance on its rake face when comparing with tools without a chip-breaking geometry.[10]

2.3 Tribological aspects of turning

Tribology is defined as the study of interacting surfaces in relative motion, and the subject addresses aspects such as friction, wear and heat generation. Thus, tribology is an important topic that describes many of the unique phenomena generated in the contact situations between the tool and the workpiece during a machining process.[15] In general, there are two different types of contact situations that may arise in the tool-workpiece interfaces. These are, respectively, a *continuous contact* or an *intermittent contact*.

A continuous contact is characterised by the fact that the tool rarely releases from the workpiece during the machining process, meaning that the tool is in continuous contact with the workpiece as long as the machining process proceeds. This type of contact situation is common in turning and is often correlated to the development of very high cutting temperatures in the arisen tool-workpiece interfaces.

The second type of contact situation that may develop is called intermittent. Even though intermittent turning procedures also exist[16], this type of contact situation is regularly more attributed to machining processes such as milling. Contrary to a continuous contact, this contact situation involves the periodical release of the tool from the workpiece. The tribological conditions for intermittent machining processes are therefore usually very different to the ones seen from a continuous contact. Due to these different contact situations, the wear behaviour from the tools used in turning and milling will often be quite dissimilar; hence, these are not readily comparable to each other.

Nevertheless, irrespectively from what type of contact situation that is used, it is well-known that a machining process generate many unique and important tribological features on the tool's surfaces. For example, the removal of material in turning usually requires very high cutting forces. These are needed in order to shear the workpiece material from its bulk matrix. Moreover, these forces increase significantly if the hardness of the workpiece material is substantial.

These generated forces are also distributed over a very small surface on the tool insert's rake face. The size range of this area is approximately about 1-2 mm². This implies that the pressures induced in the tool-workpiece interfaces during a machining process can be substantial, i.e. typically reaching values in the magnitude of several GPa.[10,17–20]

Moreover, a machining process is often associated with very high frictional forces. These are considered to be one of the main causes of the extensive heat developed during machining. The origin of this friction is partly due to a shearing of asperity junctions that are formed between the tool and the workpiece in their respective contact zones.[15,18,21] In short, these asperity junctions represent contact points at which the tool and the workpiece is in true microscopic contact to each other on an atomic scale.

Normally, the quantity of available asperity junctions will be limited to a discrete number of load-bearing points. These will increase in their size with increasing load. For this reason, due to the large contact pressures and temperatures that arise in the tool-workpiece interfaces, the available asperity junctions will grow into a state where almost the entire junction of the two surfaces are in true microscopic contact. This is a phenomenon not commonly seen among other tribological applications and is a feature commonly attributed to machining processes only.[15,22]

It is important to note that although the surfaces in contact between the tool and workpiece is indeed small from a microscopic point of view, the relative ratio of points in true microscopic contact is large. This has several important implications for the machining process in general.

First, it is estimated that nearly 70 percent of all the heat that is generated during a machining process derives from the shearing of these junctions. The remaining 30 percent originates from the heat developed due to the internal shear occurring within the workpiece material itself.[21] Thus, the large amount of asperity junctions in true contact will not only be the principal reason for the arisen frictional forces, but also to the extensive development of heat in the machining process. [15,22,23]

To summarize this section, the unique tribological conditions arising from a machining process, which includes turning, implies that:[18,20]

- ✓ Nearly the entire areas of interface between the tool and the workpiece is brought into microscopic contact
- ✓ The forces, both in terms of frictional- and cutting forces, that are acting in the tool-workpiece interfaces are generally severe and acting on relatively small surface areas ($\sim 2 \text{ mm}^2$)
- ✓ An extensive amount of heat is generated in the tool-workpiece interfaces during the machining process

2.3.1 Shearing zones

From a machining process, there are mainly three different regions that exist which governs the arisen tribological conditions on the surfaces of the tool. These regions are referred to as 'zones' and are denoted as the primary, secondary and tertiary shearing zone, respectively. In essence, these zones represent the areas where most heat develops during a machining process, and their respective positions can be seen from *Figure 2.2*. The primary shearing zone distinguishes itself for being the only zone that occurs in the workpiece material itself. The other two mentioned zones (i.e. secondary and tertiary) are instead expressing the shearing contact between the tool and the workpiece. Since wear is a contact-governed phenomenon, it is predominantly these two zones where the wear on the tools occurs.

In terms of the secondary shear zone, it expresses the contact that arises from the tool's rake face and the workpiece's chip. The tertiary shear zone expresses a similar situation, yet for the interface between the flank side and the newly machined surface.[18] Since the main interest for this thesis has been to investigate the wear behaviour of the tool's rake face, a detailed description of the secondary shear zone will follow, and the description of flank wear will be left-out for this work.

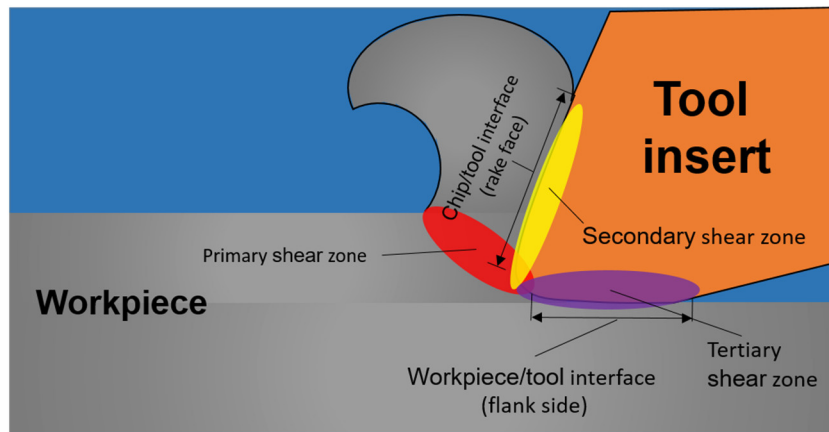


Figure 2.2. Illustrative description of the three different shearing zones developed during a turning process. These zones are all related to the heat generated during the machining process and relate to the wear seen on the tools.

2.3.2 Chip- and wear band formation

The ploughing from the tool through the workpiece material is the main cause to the wear developed in the secondary shear zone. This ploughing causes the plastic deformation of the workpiece, leading to the formation of a chip that slides against the tool's rake face. The formation of this chip may be described briefly in a step-wise manner, where the chip:[11,18]

- i. Is formed.
- ii. Slides and sticks to the tools surface.
- iii. Grow in its size.
- iv. Curls and reaches a critical length.
- v. Releases from the workpiece.
- vi. (Preferably) leaves the tool-workpiece interface entirely.

Notably, these individual steps occur at different locations on the tool's rake face in a subsequent order, from the cutting edge and down towards the inner part of the tool insert. As a further fact, the severity and nature of the interaction between the chip and the tool differs between these noted steps. This give rise to areas on the tool's rake face having dissimilar wear behaviours and wear characteristics.

In particular, the simultaneous adhesion and slipping of the chip, in which some parts of the chip sticks to the tool's surface whilst other parts undergo sliding, creates localised stress fields and regions on the tool where the frictional forces are intense yet different from each other[18,23]. This is usually visualized by the formation of distinctive and separated "wear bands" on the rake face, running parallel with the cutting edge and perpendicular to the *chip-flow direction* (CFD). These bands can be seen in *Figure 2.3*.

The generated heat within each of these formed "wear bands" tends to not be entirely equal. This is because the frictional forces, along with the amount of heat that may diffuse into the passing chip, varies between these bands. As a result, the temperatures developed on the tool's rake face are not uniformly distributed but instead divided among these bands. This is usually expressed by the formation of a temperature gradient on the tool's rake face which runs from the areas where the cutting forces (and also temperatures) are highest to the areas where the cutting forces are lowest.[14,24,25] Commonly, this gradient follows the same direction as the CFD.

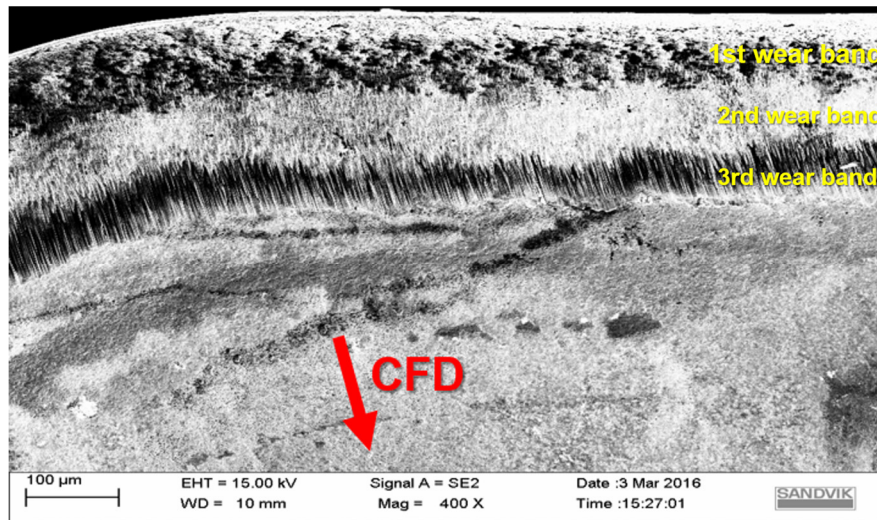


Figure 2.3. SEM-image taken on a cutting tools rake face displaying three characteristic wear-band regions running parallel to the cutting edge and perpendicular to the CFD.

2.4 Assessment of wear mechanisms and wear types

Formally, wear is defined as the undesirable material-loss caused from a tribological arisen contact situation where two reciprocally acting surfaces are involved[15,26]. As a general applicable rule, nearly all tribological contact situations generate some kind of wear. Moreover, wear is nearly always an irreversible process that, ultimately, leads to the failure and loss of function for a particular material in an application.

Even though wear is indeed inevitable, it still constitutes to one of the most highly unwanted parts for any machining operation. Consequently, an increased wear resistance of the tools and a prolonged functional machining time are two features commonly requested by the manufacturing industries for these tools.[27]. By achieving this, more reliability in the production line will be attained. This translates in turn to an increased machining efficiency, less downtimes in production, less need for operator maintenances and, ultimately, decreased costs for the each shaped component.[6]

In the discussion of machining processes and turning, there are numerous of different ways the tools can wear. It is therefore important to make a clear and comprehensible description of all the possible wear behaviours that may arise on the tools in a machining process.

In this respect, it is especially important to separate the underlying *mechanisms* causing a wear from the *types* that are actually visualised and able to be distinguished on the tools (Figure 2.4). Accordingly, 'wear' constitutes to two different components, namely, the chemical, physical, tribological and mechanical interactions that may give rise to a specific wear development, and the way this particular wear may be viewed in the form of a wear type.[11,14]

Usually, a wear type is composed of several coordinated wear mechanisms that may occur at the same time, in a subsequent order, or both. These wear mechanisms can also both be counteracting for the wear progression but are more often synergetic, i.e. their combined presence enhances the wear and rate of wear on the tool's surfaces. This results in a wear progression that usually constitutes of several complex and linked events. It is therefore sometimes very

difficult to distinguish a single wear mechanism out from several co-existing mechanisms[13,28,29].

In addition, since wear is a phenomenon that mostly occurs at the junction between surfaces in real contact, it is the properties of these two surfaces that primary dictates the severity and behaviour of the wear. In other words, wear is a surface-sensitive process that shows little dependency, if even any, to the bulk properties from the two materials in contact[15]. For this reason, surface-sensitive material parameters, such as heat transfer coefficients, chemical affinities and shearing strength, are the main parameters that influence the development of wear on the tools. Moreover, the overall morphology and topography of the two surfaces in contact are also important to the wear.

In literature there is a vast number of different terminologies used to describe the many different mechanisms and types of wear that may be present during a machining process [14,15]. The ones used in this work constitutes to the most regularly used in the literature concerning machining applications.

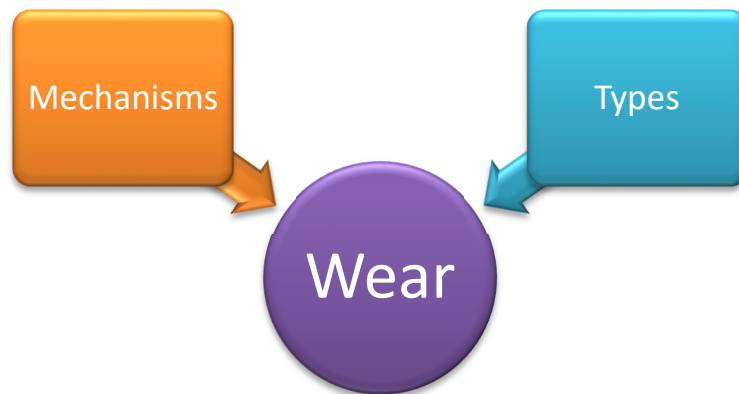


Figure 2.4. Wear in machining applications is composed of two separable components. Namely, the mechanisms giving rise to material loss from the tool and how these are expressed and identified on its surfaces (i.e a wear type).

2.4.1.1 Abrasive wear

Abrasive wear arises when hard, local asperities from one surface slides and scratch a softer counter-surface[23,26]. The wear mechanism may also appear due to the scratching from hard particles or agglomerates that are trapped in the interface between the tool and the workpiece.[11,15,26] These particles usually consist of different inorganic compounds, such as oxides, borides and silicates, that commonly originates from the workpiece material. This is especially true when machining different steel materials.[6] In addition, work-hardened wear debris from the workpiece may also contribute to the abrasive wear seen on the tools.[11,15]

There are two main parameters that are known to govern the severity from abrasive wear, namely, the hardness value of the machined workpiece material and the topographical appearance of the two surfaces in contact.[15] Typically, a workpiece material having a high hardness value and a large surface roughness with many sharp asperities will increase the abrasive wear of the tools. Furthermore, if the machined material contains any of the hard particles mentioned above, the abrasive wear usually becomes more pronounced on the tools.

Unlike many other wear mechanisms, it should also be mentioned that the abrasive wear shows remarkably little influence, if any, on the arisen temperature at the tool-chip interface[11].

The resistance from the tool against abrasive wear can be improved primarily by accomplishing two different things; namely by increasing the tool's hardness value and decreasing the contact length of the tool-chip interface[11].

2.4.1.2 Adhesive wear

Adhesive wear arises as a result of the many asperity junctions that are formed between the tool and the machined workpiece material during a machining process.[15,26] These junctions create small 'sticking zones' and micro-welds[6,11] that cause the ripping of material from the weaker counter surface.[30] This is induced by the severe shearing forces that is present in the tool-workpiece interface.[6,26]

Adhesive wear usually increases with increasing temperature until reaching a maximum value[11]. Accordingly, wear originating from an adhesive wear mechanism can be lowered by tailoring the used cutting parameters. In this way, the detrimental temperature range may be avoided.[18]

2.4.1.3 Chemical wear

Chemical wear is a generic term used to denote various types of wear caused by the chemical reactions that may occur between tool and the workpiece during a machining process. Alternatively, chemical wear may also be induced on the tools from a reaction with the machining environment, which is known as corrosion.[11] Nonetheless, a reaction between the tool and the workpiece is commonly the main cause for the observed chemical wear. This type of reaction is based on diffusion, which denotes the random movement of matter – such as molecules or atoms – from one surface to another.

In a machining application, the reaction between the tool and the workpiece is most commonly expressed in the form of a diffusion-dissolution wear model. In short, this model describes how matter from the tool is diffused into the workpiece material and then subsequently gets removed with the passing chip, thus resulting in the development of wear.[23]

There are three main factors that influence the chemical wear progression, namely, the temperature, the contact lengths and the chemical affinities between the various elements that exist in the tool and the workpiece[11]. It is generally considered that the temperature has one of the largest influence on the chemical wear rate since the rate of diffusion increases with temperature[31]. Thus, chemical wear is mainly reduced by decreasing the temperatures in the tool-workpiece interface.

2.4.1.4 Thermo-mechanical wear

Thermo-mechanical wear, also known as 'thermo-plastic' wear, describes the combined wear on the tool caused from the thermal and mechanical induced stresses that are developed in the tool-workpiece interface[11]. These coordinating stresses may either cause wear on its own, for example in the form of development of cracks or, alternatively, promote the effects from other wear mechanisms. To exemplify, these include the chemical- and adhesive wear mechanisms.

The wear seen on the tools due to an applied thermo-mechanical load is possible because many materials intrinsic properties are greatly affected when the temperature gets elevated.[18] This fact is especially true for materials' mechanical properties which usually deteriorate heavily when the temperature is raised above a certain threshold.[14]

For cemented carbides, the material properties that are most affected due to increasing temperature include, among other things, its hardness value[32]. At elevated temperatures, these tools become more susceptible for plastic deformation. This might induce unwanted alterations of the surface qualities for the shaped component and also increase the risk for sudden material-loss of the tool due to chipping and edge fracturing. For this reason, the thermo-mechanical wear on the tools is commonly noted in literature as one of the largest sources of errors in the machining process. [18,33]

The development of thermal-mechanical wear may usually be lowered by applying measures aiming to decrease the heat developed in the tool-workpiece interfaces. The most common way to achieve this is to use liquid coolants and lubricants during the machining operation. In addition, heat-resistant coatings of the tool may also be used to decrease the thermo-mechanical loads.

2.5 Wear Types

All of the described wear mechanisms above are able to give rise to certain wear features and wear characteristics that may be observed on the tool surfaces throughout the machining process. These are known as different 'wear types'. Similar to the wear mechanisms, there exists a vast number of different denotations to describe the many available types of wear that may arise on the tools from a machining process. Nevertheless, these wear types share a common feature in that they are able to be categorised based on their ability to influence the geometrical accuracy of the shaped workpiece component.[14]

Below, the reader will find the description of five different wear types that may arise on the tool's rake face from a machining process. Note that all possible wear types have not been listed here, but rather, the ones judged to be the most likely to occur on the tool's rake face during an initial turning process.

2.5.1.1 Crater wear

Crater wear is a generic term used to describe all the distinguishable wear-features that are able to be seen on the cutting tools rake face after a machining process. As the name suggest, this wear is characterised by the formation of a crater that hollows out the rake face. This is a gradual process which successively influence the geometry of the rake face. Eventually, crater wear leads to tool fracture, usually by segmental loss of fragments of the rake face (so called chipping) or edge breakage which renders the tool completely unusable.

In essence, there are two underlying wear mechanisms commonly associated being the most influential for the formation of crater wear on the tool's rake face. These are, respectively, abrasive wear and/or chemical wear. However, both adhesive- and thermo-mechanical wear may contribute to the crater formation on the tools as well.

2.5.1.2 Plastic deformation

Plastic deformation (PD) denotes the permanent geometrical change of the tool due to exposure of high temperatures and/or mechanical loads. Thus, this wear type is mostly governed by thermo-mechanical wear mechanisms. Frequently, plastic deformation is demonstrated from a depression or impression (i.e. a buckling) of the tool's rake face, which ultimately results in edge fracture.[11]

Formally speaking, it should be noted that plastic deformation by itself is not a cause of wear since no material-loss is involved in the PD-process. However, since plastic deformation is known to lead to edge fracture and chipping of fragments from the tool insert (which influence the geometrical accuracy for the shaped component), it is still commonly classified as a wear type.[11]

2.5.1.3 Flaking

Flaking denotes the loss of the wear-protecting coating on the cutting tool insert which exposes the underlying cemented carbide substrate. Usually, flaking implies that small pieces of the coating layers fall off the tool. This usually occurs as a single, isolated incident. Thus, unlike many of the other described wear types which are a continuous process, flaking happens usually in a non-continuous manner.

Flaking may occur primarily due to the influence of two different wear mechanisms, namely, adhesive wear and excessive thermo-mechanical loads. In the first case, a strong chemical affinity between the workpiece and the coating layer promotes the ripping of this layer from the underlying tool substrate. This is particularly significant if the adhesion between the coating and the tool substrate is weak.

Secondly, the induced thermo-mechanical wear may induce flaking due to the differences in thermal expansion between the substrate and the coating. When a thermal load is applied on the tools, this difference may result in different expansions of the coating and the substrate which induces tensions in the coating layer and possible subsequent flaking of the coating layer.

2.5.1.4 Cracks

Cracks is a broad and rather inelaborate term for the visible discontinuities and separations on the rake face surface. These may appear in various forms and sizes and also propagate in various directions.

The causing of cracks may mainly be ascribed to the thermo-mechanical wear that is induced on the tools during machining. Usually, cracks occur because of thermal fluctuations which causes a microscopic fatigue of the tool's surface. This is caused by the differences in thermal expansion coefficient between the tool's substrate and its coating layer when the tool is cooled off.

Ultimately, the formation of cracks can lead to the simultaneous loss of large pieces of fragments from the tool's rake face. They may also promote the effects of other wear types such as chemically-induced crater wear, since the formation of cracks tend to increase the surface reactivity from the tool. Hence, the wear due to crack formation may entail that the tool becomes more susceptible for unwanted diffusion and chemical reactions.

2.5.1.5 Smearing/Built-up Edge

Smearing is a type of wear that arises due to the adhering of workpiece layer on top of the tool surface. This type of wear has many names in the literature, and is commonly referred to as either smearing, transfer-layer, built-up edge (BUE), built-up layer (BUL), 'belag', adhered layer, etc.

Similar to plastic deformation, this wear type is not formally speaking a 'wear' since it involves a material-gain rather than a material-loss. In addition, the detrimental effects from these smeared workpiece layers are also a highly debatable topic in the literature. Some authors have even suggested that these layers may act as protecting rather than promoting the wear. Nonetheless, it is well-known that the formation of these layers may induce unwanted geometrical deviations for the shaped component, particularly if this adhered layers grows into a macroscopic, visible size.

Smearing is particularly common when machining highly ductile materials having relatively low thermal conductivity and a facility to work-harden. These type of workpiece materials include many stainless-steels, especially austenitic ones.

In the cases where smearing has been reported for being detrimental and causing wear on the tools, it has commonly been attributed for being caused by a chemical wear (from diffusion-dissolution) and/or an adhesive wear mechanism. This topic will be addressed later on in this report.

3 Steel as a workpiece material

3.1 Challenges and demands

Steel has shown to have several inherent properties that has arguably made it to be one of the most commonly selected material in today's modern society. The many favourable properties of the material, such as its high mechanical strength, easy formability, long-lasting durability, good availability and comparably low-cost, have all contributed to this widespread use.

Moreover, steel is regularly considered to be an incredible versatile material with excellent capabilities to control the properties of. The vast number of different alloying elements that can be used, along with the various types of different after-treatments that may be employed, means that the chemical composition and microscopic appearances of steel can be greatly controlled. These parameters are highly linked to the material's overall mechanical properties. Thus, this implies that the properties of steel can be tailor-made to suit a wide range of different applications and usages to a very large degree.

Nevertheless, this versatility has also likely contributed to several of the challenges when machining this type of material. Many of these challenges relates to the very high temperatures that are developed in the tool-workpiece interfaces when machining steel[27,34]. These can easily reach levels up to 1000°C. This fact, along with the numerous amount of different alloying elements that are present in the steel, means that the material often becomes highly reactive towards the tools used in the machining process.[35,36] Consequently, the tool inserts used in the machining of steels are not only highly susceptible for a few but several different contemporary wear mechanisms. These commonly include thermo-mechanical wear, chemical wear, adhesive wear and also abrasive wear.

In addition, the presence of inorganic precipitates and inclusions in the steel matrix are well-known to play an important part in the development of wear on the tools. Their exact role is however still quite ambiguous, and they have in literature both been attributed to increase the wear of the tools whilst other sources suggest that they may instead impede the development of wear. This is a topic that will be discussed in further detail in section 4 of this thesis.

3.2 Wear protecting coatings

Over the years, a large focus has been made on implementing measures to suppress the wear on the cutting tools to the furthest extent possible. There are many ways this can be achieved. One of them includes the use of various types of wear-protecting coatings, which are usually made of one or several ceramic compounds.[24,37] These type of coatings were first introduced in the 1970[27,37] and are most commonly deposited from a chemical vapour technique (CVD).

In order to efficiently impede the development of wear on the tools during machining of steel, the used coating must be targeted at counteracting the relevant wear mechanisms that may occur.[6,14,28,29]. Since many different wear mechanisms are possible when machining steels, the demands put on the chosen coating for this particular application may be many.

Essentially, the choice for the most suitable coating material should be done based on the following three listed criteria:

- I. High hardness, to resist the plastic deformation and abrasive wear of the tool's rake face.
- II. Adequate temperature resistance, to resist the thermal-effects from the high temperatures developed when machining steel.
- III. Chemical inertness, to avoid reactions and to decrease the possibility for a chemical wear mechanism.

A strong candidate that fulfil these criteria have shown to be alumina-based coatings (Al_2O_3).[5,28] These type of coatings constitute to one of the most promising candidates to be used on tools during steel machining. [13,27,38]. The use of alumina-based coatings has enabled manufacturing industries to have much higher cutting speeds[5] when machining steel, which has vastly improved the productivity for this particular machining application[28,29,39,40].

3.3 Properties of alumina

Alumina (Al_2O_3) is a highly abundant ceramic material known for its many favourable properties, such as its excellent chemical inertness[27,34,37,39,40], high melting temperature[5,41], good heat resistance (i.e. "hot hardness")[37–39] and high hardness value[28,29,40]. The strong chemical bonds present in the material, which in their character are mostly ionic (~66%) but also partially covalent (~33%)[42], have mainly been attributed for giving rise to these features. In addition, whereas many materials' hardness value deteriorates heavily as the temperature rises, the hardness value of alumina stays remarkably intact, even at relatively high temperatures (i.e temperatures less than 1000°C)[34,42,43].

A further interesting characteristic with alumina is its ability to exist in numerous of different crystallographic shapes, known as *polymorphs*, which all demonstrates different material properties and dissimilar material behaviours[44]. These may be categorised based on the crystal's packaging of oxygen anions, which can either adopt a face-centred cubic structure

(fcc) or a hexagonal (hcp) ditto. Usually, these different polymorphs are denoted by Greek letters. A list of the most common polymorphs of alumina are listed in *Table 3.1* below. The lattice parameters, that is, the relative positions of each atom that constitute to the alumina crystal's unit cell, diverges between these polymorphs. This constitute to the main reason for their differently displayed material characteristics.[40,44].

Table 3.1. List of known polymorphic phases of alumina, which are categorised based on their displayed packaging of oxygen anions (fcc or hcp). These different phases are denoted by a Greek letter.[44]

Face-centred cubic (fcc)	Hexagonal close-packed (hcp)
γ - , η - (Cubic)	α - (trigonal)
θ -, θ' -, θ'' -. λ - (monoclinic)	κ - (orthorombic)
δ - (tetragonal or orthorombic)	χ - (hexagonal)

Among these listed polymorphs, it is known that the α -phase¹ of alumina is the only one that is thermodynamically stable[45]; the other existing polymorphs are *metastable* and will hence decompose gradually into this stable α -phase[34,44]. This degradation occurs through a step-wise mechanism involving one or several phase transformations. These are greatly accelerated if the metastable alumina phases are exposed to high temperatures and/or pressures.

For this reason, the thermodynamically stable α -phase is commonly considered to be the most favourable phase to utilize in a machining application. [5,39] Additionally, this phase also demonstrates the most superior mechanical properties of all listed polymorphs above.[27,34,39,40]

¹ The α -phase of alumina is commonly referred to in literature as either corundum or sapphire. This is somewhat misleading since both corundum and sapphire are naturally occurring minerals of alumina that also contain small traces of various metallic impurities. In addition, the term 'sapphire' is also widely used in literature to denote single-crystalline alumina.

3.3.1 Crystal structure

The crystal structure of α -alumina (*Figure 3.1*) adapts a hexagonal-like shape (rhombohedral) with a trigonal crystal symmetry. It consists of two different sub-lattices, where the larger O^{2-} -anions occupy the outer lattice-shell points whilst the substantially smaller Al^{3+} cation occupies a portion of the available octahedral interstitial sites in the crystal. The strong ionic charge of these two atoms give rise to considerable columbic interactions in the crystal[46], which highly influence its lattice parameters and therefore also its geometrical appearance.

For instance, the large divergence in electronegativity between Al^{3+} and O^{2-} (in accordance to the Pauling scale[47]) implicates that these two ions will strongly attract each other. Accordingly, this would energetically favour relatively small ionic bonding distances between them. In the case of alumina crystal, this translates into a compression of the α -alumina crystal's sidewalls, resulting in a typically small a-value (0.475 nm) for the crystal, as seen in *Figure 3.2*. [34,39,40,48]

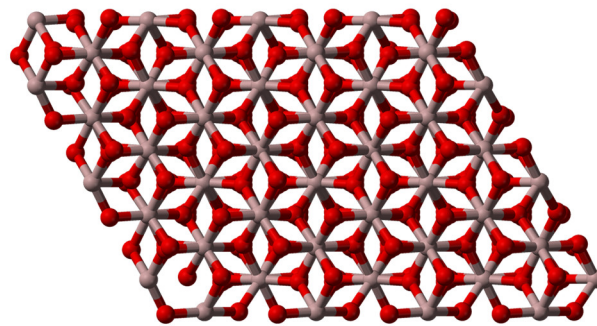


Figure 3.1. Three-dimensional “ball-and-stick” model depicting the atomic arrangement between oxygen (red) and aluminum (grey) in its trigonal crystal lattice. Each aluminum atom is surrounded by 6 oxygen atom which forms a three-dimensional tetrahedron[49]. (Image originating from Wikimedia Commons, used under Public Domain).

Similarly, the strong columbic interactions induced in the alumina crystal between equally charged ions also give rise to large electrostatic repulsions in the crystal lattice[46]. This is particularly true for the Al^{3+} cation, which carries a large positive charge (+3). Therefore, the Al^{3+} cations inside the crystal will require the maximum available spacing between them in order to sufficiently avoid any energetically unfavourable repulsions between them.[46,48,50]

To account for this, the Al^{3+} cations are capable to outstretch the crystal lattice in its vertical direction, which give rise to a relatively large c-value for α -alumina (1.297 nm)[44,51] in comparison to other hcp-crystals. This elongation is possible since not all of the octahedral sites found in the alumina crystal are actually occupied; only two-thirds of these sites contain an Al^{3+} -cation. This enables the Al^{3+} -cations to displace themselves towards an empty octahedral vacancy, which places them into an energetically lower and more ‘relaxed’ configuration.[48,52]

These cationic displacements, in turn, are subsequently followed by a distortion of the oxygen-sub-lattice, in which the larger oxygen atoms are slightly displaced from their ideal hexagonal positions. In this way, the α -alumina crystal adapts a more rhombohedral-like shape instead of a purely hexagonal.[39,44,48]

The partial filling of the octahedral holes in α -alumina results in an irregular stacking sequence of the cations in crystal. In this stacking sequence, a single Al^{3+} is surrounded by three neighbouring O^{2-} anions in two dimensions, which forms a triangular sheet with a centred Al^{3+} cation[52]. In three dimensions, two O^{2-} anions are located above and below this centred Al^{3+} cation, thus resulting in a tetragonal 3D-configuration, as viewed in *Figure 3.1*. Due to the slight displacement of the Al^{3+} -cation, its ionic radius extend itself slightly above the normal plane of the O^{2-} anions, resulting in a “puckered” appearance[52]. This “puckering” causes anomalies to the atomic stacking sequence in the α alumina’s crystal, which consequently becomes more jagged. It is strongly believed that this jagged appearance from the cations plays an important role for the behaviour of the alumina crystal, in particular on how it is plastically deformed. This, in turn, relates to the wear behaviour of the alumina crystal.[48]

Interestingly, the distribution of cations in the crystal have, for the other metastable polymorphic phases of alumina, been shown to differ from this optimal 2/3 ratio. In contrast to the stable α -alumina, these metastable phases also have cations located in a portion of the available tetragonal interstices in the crystal. These tetragonal sites are substantially smaller in size in comparison with their octahedral counterparts. In addition, they are also more closely located to each other in the crystal lattice. This inevitably leads to more unfavourable and energetic demanding cationic configurations when these sites are being occupied.

This information is important, since it not only explains the metastability of alumina’s numerous polymorphs, but also links the crystal geometrical appearance of alumina as being strongly reliant on its cationic configuration. Since a material’s overall behaviour, properties and characteristics are linked to its crystallographic appearances, it implies that many of the characteristic features from alumina depends on its inherent arrangement of Al^{3+} -cations.[44]

In other words, the Al^{3+} -cations and the arrangement of these cations in the alumina crystal constitutes to the single most important factor governing the overall properties of the material. Due to this, they may also explain the actual wear behaviour of alumina and how this material deforms on an atomic scale. This is an interesting topic that will be discussed in further detail in the wear model presented in the discussion part of this thesis.

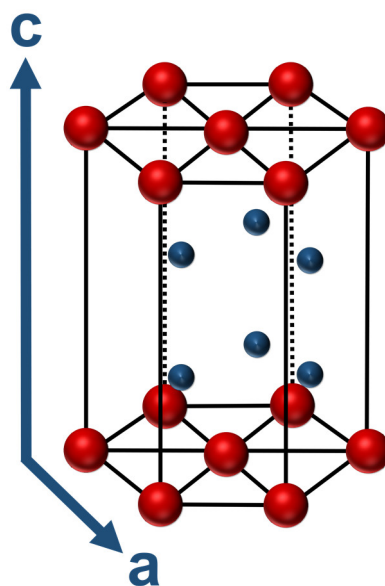


Figure 3.2. Schematic illustration of the structure from an α -alumina single-crystal. Figure displays the relative atomic position between the outer positioned O^{2-} -anions (red) and the inherent Al^{3+} -cations (blue), which are located in a portion of the available octahedral interstices in the crystal’s interior (Illustration made by the author).

3.3.2 Anisotropic behaviour and the effect of crystal orientation

The combined effects from the two different types of electrostatic interactions that occurs in α -alumina causes the crystal to have an appearance with a relative small base (because of favourable Al^{3+} - O^{2-} interactions) and a large height (because of unfavourable Al^{3+} - Al^{3+} interactions). For the crystal, this corresponds into an relatively high c/a-ratio[48,51], meaning that the lattice parameters are substantially different from each other in its horizontal and vertical directions. This is a common feature being observed among many materials having a hexagonal crystal appearance.

In the case of alumina, this particular crystal structure is known to induce some unexpected and erratic material behaviours, especially when it comes to the material's mechanical properties. To exemplify, it is noted that alumina does not generally display the same isotropic properties in compression as it does during tension.[53]. This is actually commonly observed among many cubic materials, such as many metals.

Moreover, it has been shown that the Young's modulus from single-crystalline α -alumina can differ with as much as 30 percent, depending on what loading direction that is used[54]. Consequently, the material properties of alumina are known to be highly *anisotropic*, i.e. strongly reliant on its crystallographic orientation. This is especially true for alumina's mechanical, thermal, electrical and optical properties.[55]. In polycrystalline alumina, these material differences are mostly nullified due to the large amount of crystal grains present in various different directions. However, if single-crystalline phases of alumina may be isolated, the differences in material properties between crystals in dissimilar directions can be substantial.[41,51,54,56]

The variation of material properties due to crystallographic orientation are commonly denoted as the 'texture effect', and the utilisation of this effect corresponds to one of the most modern ways to enhance the wear-resistant properties of alumina-based coatings. In particular, different wear rates have been observed depending on what crystal orientation is used in the coating[53]. In tribological applications it has been found that a compressional stress that is applied in the crystal's c-direction is the most favourable for the alumina crystal's wear resistance[57]. Along this direction, which is commonly denoted as the [0001] direction in crystallographic notations (Miller-Bravais indices), the alumina crystal displays its highest value in tensile strength. Similarly, the alumina crystal demonstrates its highest value in Young's elastic modulus, shear modulus and also thermal conductivity perpendicular to this [0001]-direction.[55] Thus, in machining applications where the stress being applied on the tools are mostly compressive but also shearing, it is possible to attain a significant increase of the ceramic toughness of alumina due to this texture effect.

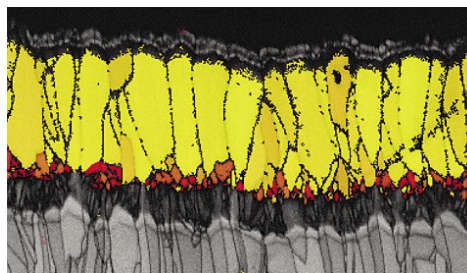


Figure 3.3. EBSD SEM-image displaying colored uni-directional (textured) alumina crystals deposited onto a cemented carbide tool substrate. The yellow-colored grains correspond to a growth direction of the crystals in its [0001] direction. (Image source: www.sandvik.coromant.com/en-gb/knowledge/technologies/inveio)

4 The role of the inclusions on the tool wear

Among the authors in the literature, it is a common belief that a large part of the arisen wear on the tools used to machine steel may be directly related to the steel's inclusions.[58] However, in spite that a lot of research has been made over the past years in order to elucidate their exact role for the wear, there has been little progress in this field.[38,59]

Early investigations showed that these inclusions could have beneficial properties for the wear resistance of the tools. This conclusion was made based on the formation of various types of inclusion layers on top of the tool's rake face. Several authors pointed out that the presence of these layers seemed to increase the longevity for the used cutting tool.

However, parallel to these promising findings there has also been several reports presented suggesting that the role of the inclusions is instead detrimental, and that these may promote the wear on the tools. Even if several attempts have been made to clarify and eliminate these contradictions, there are still many queries remaining as of today. Thus, the exact role for these inclusions on the tool wear are still a topic yet to be fully understood.

For this reason, it is deemed as being difficult to present a general consensus from the literature on what role these inclusions might have to the wear during the machining of steel. The behaviour from these inclusions may also differ and change largely depending on the machining conditions. This include what type of steel material that is going to be machined and what cutting parameters that are being used.

Therefore, this section will instead focus on presenting the general aspects of these inclusions and the main points suggesting both their beneficial and detrimental properties, respectively.

4.1 General description of inclusions

Inclusions denote the non-metallic impurities that are commonly present in the steel matrix. They are often in the form of small shaped particles, usually in the size range of a few micrometres. Even if they are commonly considered as being impurities, they are in fact a natural part of the steel material that derives from its many manufacturing processes.[60] In particular, this include the handling of steel's melted phase[8]. In these processes, additives may be added to the steel in order to more easily control the slag levels in the liquid melt. In addition, elements such as aluminium/calcium are commonly added to the melt in order to deoxidise/quench the steel melt from the presence of damaging free oxygen. Both these processes introduce foreign elements in the steel melt that can react and form to inorganic precipitates (i.e. inclusions).[8,61,62]

There are a certain number of elements that are commonly recognized for being able to form inclusions in the steel matrix[8]. These include the elements Ca, S, Mg, Si, Mn, Mo and Al, respectively, which are commonly present in the steel as various types of sulphides and oxide compounds[24,62,63]. The chemical composition and stoichiometric relationship for these compounds are usually highly variable and complex. This complexity is further enhanced by the fact that many of these elements, such as calcium and manganese, are highly soluble in each other[8,64]. This enables the formation of duplexed and composite inclusions[65] where the outer shell layer and the inner core of the inclusion may have very different chemical compositions.

In addition to the large spread in chemical composition, the inclusions found in the steel matrix may also display differences in its sizes and morphologies[8,64,65]. Hence, the many variations possible for the steel's inclusions implies that their inherent properties are very unevenly distributed. They may therefore influence the overall machinability of the steel in numerous of different ways, which are exemplified in *Table 4.1* below.[8,36]

Wear influence from inclusions when machining steels

Beneficial		Detrimental	
<i>Statement</i>	<i>Explanation</i>	<i>Statement</i>	<i>Explanation</i>
Lowers abrasive wear	<i>in situ</i> lubrication: Lower physical contact between tool and workpiece due to inclusion layer formation[8,65,66]	Increased abrasive wear	Inclusion particles scratches the surface and carries away tool material.[27]
Lower chemical wear	Layer acts as a diffusional barrier between the tool and the workpiece[8,66]	Increased chemical wear	Chemical dissolution of the tool's specimen into the formed inclusion layer[43]
Lower thermomechanical wear	Inclusion layer acts as a thermal barrier.[67–69]	Increased thermomechanical wear	BUE/BUL formation – Higher cutting temperatures
Lower cutting forces and increased machinability	Shear induced in inclusion layer instead of tool. Decreases friction[37]. Also, inclusions act as stress-raisers that facilitate chip formation. [8]	Decreased machinability. No observed effects on cutting forces.	BUE/BUL formation – Increased surface roughness. [65,70]

Table 4.1 Compilation of the main statements and corresponding explanations found in the literature for the most commonly mentioned attributes linked to the wear influence from the inclusions.

4.1.1 Layer formation

Many of the properties relating to the wear from the inclusions may be attributed to their ability to form stable layers on the tool's surfaces during a machining process. Specifically, the formation of these layers tend to occur on the tool's rake face. Commonly, they are regarded as a type of smearing of workpiece material, e.g. BUE/BUL, but this is not entirely correct. The layer formed by the inclusions tend to be much thinner in comparison with the formed BUE/BUL.[69,71]

In terms of the layer's chemical composition, it is generally noted to consist of a mixture from several different chemical compounds. These include CaO, MnO, MnS, (Mn,Ca)O, SiO₂ and Mg Al₂O₃ (spinel)[8,20,36,38,43,59,65]. The elemental distribution of these layers usually matches well to the same ratio found in the steel's inclusions. This suggest that these layers are indeed caused by these inclusions.[63,68,72]

The tendencies for formation of these layers are usually different depending on what area of the rake face they are formed onto.[24,36] This variation can be explained from to the unequal tribological conditions that occurs among these bands. Since these conditions are dependent on the cutting parameters, it is strongly believed that these may have an important meaning to the formation of these layers.

A detailed description for the mechanisms behind the formation of these layers have been made previously in the literature[20,66,69]. These are summarized into five linked and subsequent steps[66] and are briefly summarized below:

- I. Release of inclusions on the tool's rake face from the steel matrix
- II. Sufficient heating of the inclusions
- III. *Extrusion of inclusion across the rake face (layer formation)*
- IV. Cooling of layer
- V. Solidifying and continuous layer growth until steady-state is reached.

Thus, in order for these layers to be formed, it is necessary that the steel's inclusions are sufficiently heated prior to this step. In this respect, it has been shown that the inclusions found in the steel are able to transform into a highly viscous and "glassy" state once a certain temperature has been surpassed. This has been reported to occur approximately in the temperature range of 800°C - 1100°C. These temperatures are within the same range that may be reached when machining steels.[20,66,69]

However, it is important to note that temperature alone cannot entirely account for the formation of these layers. It also requires an application of a mechanical force in order to smear the inclusions across the tool's rake face. For this reason, the formation process of these layers are said to be *viscoplastic*, i.e. it requires both an appropriate temperature and an applied mechanical force in order to occur.[73] Therefore, the used cutting parameters are important for both the properties of these layers and also their ability to be formed on the tools.

This fact, along with the complex and varying chemical composition the inclusions might have in the steel workpiece material, may act as possible explanations for the many contradictory behaviours reported in the literature concerning these inclusion layers.

5 Literature survey

Due to the large popularity in the world to machine steel, it exists a vast number of different articles published about tool wear and the formation of inclusion layers when machining this material. The earliest reports made dates back to the late 1960ies. In terms of contemporary research, it has mainly been focused on investigating tool wear when machining newly developed steel grades.[6,8,61]. For example, these include duplexed steels and steel grades having very low levels of impurities and inclusions (referred to as “clean steels”).

This section will mainly focus on presenting the main achievements made in the field in regards to tool wear and layer formation when machining regular steel grades, such as low-alloyed and stainless steels. The ambition is to present the reader a mostly chronological overview of the literature available and also emphasise the contradictions and questionable topics related to these subject areas.

5.1 Review of published articles

Among the first persons that are commonly credited for having discovered the formation of inclusion layers on cutting tools are Opitz. In 1962, Opitz and his team of researchers published an article describing the formation of an oxide-rich layer on cemented carbide tools during the machining of calcium-deoxidised low-alloyed steels. They reported of an increased cutting tool life when these layers where formed, and linked this tool behaviour to the steel’s inclusions. In particular, they suggested that the employed calcium-treatment of the steels were of particular importance for this wear-reducing effect.[74]

In the following decade, Japanese scientists (K. Ohgo and K. Nakajima) presented results that were, in some instances, contradictory to Opitz findings. By using an electron probe micro-analyser (EPMA), K.Ohgo presented evidence that diffusion occurred between a non-coated cemented carbide tool and the deposited oxide layer. In particular, elements such as carbon and tungsten originating from the tool where found in the studied adhered oxide layer. Ohgo suggested that this indicated for an increased adhesive wear on the tools due to transfer of tool material to the passing chip.[75]

In addition, Ohgo presented one of the earliest theories suggesting the importance from the temperature for the layer formation and its properties. They also linked this to the used cutting parameters. During his conducted experiments, he noticed that the severity of his so-called ‘adhesive wear’ were different when an alteration of the cutting parameters was made. At low cutting speeds, a relatively thick built-up layer was formed on the tools that was clearly detrimental for the tool’s service life. However, when the cutting speed increased, an alteration of the chemical composition occurred. This type of layer demonstrated an increased tool life instead, in a similar manner discussed by Opitz.[74,75]

Ohgo also reported that the chemical composition of this layer mostly consisted of a mixture of compounds such as Al_2O_3 , SiO_2 , CaO , and that the layer's chemical composition was linked to that seen from the non-metallic inclusions found in the steel.[75] The authors X.D Fang and D.Zhang later presented results from EPMA that were similar to these findings, and further stated that the chemical composition in this adhered layers mostly consisted of ternary oxide phases belonging to the system $(\text{CaO}, \text{MgO}, \text{MnO})\text{-Al}_2\text{O}_3\text{-SiO}_2$. [36]. Several other authors have since then confirmed these observations.[38,59]

During the 1970s new techniques were introduced that enabled to deposit different types of wear-resistant coatings on the cemented carbide tools. This technological advancement greatly prolonged the tools overall service lives. Nonetheless, in some applications where these coated tools were used to machine Ca-deoxidised steels, a decrease in tool life was yet again observed. The authors Anders Nordgren and Arne Melander presented results were cemented carbide tools coated in a multilayer of $\text{TiC-Al}_2\text{O}_3\text{-TiN}$ worn out much more quickly when machining Ca-treated steels. Similar to Ohgo, they linked this rapid wear to a chemical dissolution wear mechanism of tool elements into the formed inclusion layer.[64] This dissolution model has since then been acknowledged by several more authors[43,76].

In 1998, Ruppi i.a published an article where he investigated the wear behaviour of different single-layered wear-protecting coatings on tools used to machine different steel grades. The purpose with this study was to elucidate the performance of each individual layer independent from one another. The coatings evaluated were TiC , Ti(C,N) and Al_2O_3 . Ruppi reported a significant increase in both machinability and tool life for all the coatings when they were deposited on the tools used in the machining of Ca-treated steels. That was, however, except for the one where the Al_2O_3 coating had been used. Of all the evaluated coatings, Al_2O_3 was the only one demonstrating a worsening in the wear resistance when machining Ca-treated steels. This was both seen as an increase in the wear on the flank side of the tools but also as an increased crater wear formation on the tools' rake faces.[77]

Interestingly, Ruppi did not attribute this increase in wear to a chemical dissolution mechanism, which several authors had previously been made, but attributed this behaviour to an increased abrasive wear mechanism instead. Similar to the dissolution wear model, this approach has also accepted by several other authors in the field.[6,8,27,61] Ruppi made this assumption based on the fact that no chemical reaction between the Al_2O_3 coating and the workpiece material could be observed.[77]

However, in 1986 Brandt and Mikus from Sandvik Coromant in Västberga actually demonstrated by experimental means that a reaction between alumina and an inclusion component, namely MgO , actually was possible. This is one of few articles on the subject that has proved that a reaction between Al_2O_3 and an inclusion constituent may be possible when turning steel.[78]

In later articles made by Ruppi, it was also declared that the wear on the Al_2O_3 coated tools during steel machining were due to plastic deformation.[72] This has, by some authors[43,76,79–81], been suggested for being a plausible explanation for the overall wear behaviour from Al_2O_3 . For example, it is noted that alumina may undergo a special type of plastic deformation, known as "superficial deformation" that only occurs in the topmost microscopic area of the material. This mechanism was initially presented by Dearnley[79]. In modern times, this type of deformation (and the wear it can lead to) has been ascribed to be a plausible feature on the newest type of textured alumina-based coatings[34], such as Inveio™.

6 Experimental procedure

6.1 Tools

Two different types of tool inserts have been used in the performed turning tests, denoted as CNMG and CNMA. These belong to a common grade (GC4325) yet have two different surface geometries on their respective rake faces. Whereas the CNMG tools utilize a chip-breaker, the geometry of the CNMA is instead completely plane. The two different geometries of the tools can be viewed in *Table 6.4* on page 34, which also specifies more data for these tools.

Both tested tools consisted of a WC/Co rhombohedral-shaped substrate coated with a wear-protecting, multi-layered CVD coating, as described in the tool datasheet in *Table 6.4* on page 35. The coating consisted of an outer, textured [0001] α -Al₂O₃ coating layer, which were deposited on top of a Ti(C,N) gradient that linked the outer, alumina coating to the tools' substrate. A cross-sectional image of this multi-layered coating can be viewed from *Figure 3.3* on page 26.

In addition, the CNMG-type of tools had also been coated by a thin outer TiN layer on top of the Al₂O₃ coating. This TiN coating was, however, blasted away from a post-treatment procedure. The intent with this procedure was to induce favourable residual stresses into the alumina coating, making it more resilient to flaking and crack formations.

Prior to all the performed turning test, a selection of suitable tool insert from each tool type were made based on two predetermined criterions that relates to the shape of the cutting edge. This was done to ensure that all the used tools had the same geometrical cutting edge appearance, which otherwise could, potentially, affect the performance from the tools used in the turning tests. Thus, the tools were selected so that the

- Length of the main cutting edge did not deviate more than +/- 5 μm from the mean value.
- W/H^2 (Ω) quotient for all the inserts were in the interval $1.1 < \Omega < 1.3$.

Cutting inserts from the different tool types were also subjected to material investigations in regards to their grain sizes, hardness and coating layer thickness. These values were compared with given tolerances from the large-scale production. All the tools used in the performed turning tests in this thesis were approved and within the given tolerances.

² The W/H-ratio relates to the point-roundness for the cutting edge of the tool.

6.2 Workpiece materials

The workpiece materials that has been used in the turning test consists of two separate batches from a low-alloyed, quenched and tempered[82], 34CrNiMoS6-steel. This particular steel is commonly labelled as either SS2541 (Swedish Standard) or, equivalently, AISI 4340 (American Iron and Steel Institute). Features of this steel includes type good hardenability, high tensile strength and relatively good toughness. For this reason, it is a common steel grade used by the manufacturing industries.[83,84]

One of the batches machined in the turning test had been Ca-treated whilst the other had not. This was done in order to compare the effects from the Ca-treatment, and how this might influence the wear progression of the machined tools. The Ca-treatment is used to alter the chemical composition and morphology of the inclusions found in the steel. The purpose with this is to make them softer and thus less abrasive against the tool's surfaces.

The chemical composition of the two used steel batches is given from *Table 6.1*, together with a list of mechanical properties (*Table 6.4*) and a specification of the type of inclusions found in this type of steel (*Table 6.5*).

WORKPIECE MATERIAL DATA SHEET

Table 6.1. Chemical composition of the two workpiece materials that has been used in the turning tests [83,85,86]

Weight percent- age wt.%	C	Si	Mn	P	S	Cr	Ni	Mo	Al	Ca	Other
Non calcium treated SS2541 (Batch nr 3091)	0.36	0.34	0.61	0.010	0.026	1.49	1.47	0.2	n/a	0.0003	
Calcium treated SS2541 (Batch nr 21419)	0.37	0.28	0.73	0.009	0.030	1.29	1.33	0.17	0.023	0.0005	0,23 (Cu)

Table 6.2. Listed properties for a general 34CrNiMoS6 steel grade (SS2541/AISI4340) [83,84]

Tensile strength [MPa]	850-1000
Hardness [HB]	248 – 302
Yield strength [MPa]	635
Young's modulus [10^3 N/mm ²]	210
Elongation to failure [%]	13
Izod impact strength [J]	40
Density (kg/dm ³)	7.85
Thermal conductivity[W/m K]	42

Table 6.3. Type of inclusions present in SS2541 (non Ca-treated) and their relative amount in percentage from the total [87]

Type of inclusion	Relative %-tot
Oxides	3.22
Oxisulphides	11.1
Sulphides	85.6

TOOL INSERTS DATASHEET


SIZE	120408	
TYPE OF COATING	CVD (Inveio™)	
GRADE	GC4325	GC4325**
SHAPE	CNMG	CNMA
APPEARANCE		
SURFACE GEOMETRY	-PM	-KR
TOOL GEOMETRY	Rhombic	Rhombic
ISO-CODE	CNMG120408	CNMA120408
NUMBER OF CUTTING EDGES	4	4
EFFECTIVE CUTTING EDGE LENGTH	12.1 mm	12.1 mm
CORNER RADIUS	0.8 mm	0.8 mm
DENSITY	14.6 g/dm ³	13.8 g/dm ³
HC	14.5	13,6
COM	6.9	6,3
HV3	1484	1493
GRADIENT	25 μm	n/a**
COATING THICKNESS	9 μm multi-layered CVD + 5 μm Al ₂ O ₃ + 1 μm outer TiN layer*	9.5 μm multi-layered CVD + 5 μm Al ₂ O ₃ + 1 μm outer TiN layer*
	<p><i>*The inserts used in this work are post-treated after coating. During the post-treatment the outer TiN-coating (about 1 μm thick) has been blasted away on the rake face.</i></p>	<p><i>**The CNMA type of tools that has been used in this work has been made to have a similar bulk composition to the one of CNMG.</i></p>

Table 6.4 List of specifications for the two types of tool inserts that has been used in the experimental procedures. [88,89]

6.3 Performed turning tests

Longitudinal turning tests were performed using an Okuma OSP P200LA turning machine. The geometry of the machined workpiece was in the form of a rolled bar (700×180 mm). The performance of the tested tool inserts, in terms of the development of wear, was then evaluated from four separately designed subtest in which both tool insert types (CNMA and CNMG) were used. These tests were denoted as DP1, DP2, DP3 and DP4, respectively. In all the performed turning tests the same cutting data were used in terms of the cutting speed v , feed rate f and cutting depth A_p . The values of each respective parameter is listed in *Table 6.5*.

During the cutting experiments, a water-soluble mineral-oil was used as a coolant. (Blasocut BC 935). The injection rate for the coolant was normal and did not deviate from ordinary conditions.[90,91]

Table 6.5. Used cutting parameters for the different performed turning tests.

Cutting speed (v)	Feed rate (f)	Cutting depth (A_p)	Use of coolants
220 mm/rev	0.2 mm	2 mm	Yes*, standard oil emulsion fluid
			*Except DP3

Table 6.6. Summary of the performed turning tests

	DP1	DP2	DP3	DP4
Test type	Longevity (tool life)	Initial wear	Initial wear	Initial wear
Workpiece material	Ca-treated SS2541	Ca-treated SS2541	Ca-treated SS2541	Non Ca-treated SS2541
Cutting fluid	Yes	Yes	No	Yes

6.3.1 DP1 – Test of tool life

DP1 was performed in order to evaluate the tools' longevity. In this first test, two cutting tool inserts from each type (CNMG and CNMA) were selected and turned until either one out of three tool life criterions were fulfilled. These were defined as:

- A V_B -value (referring to the length of the wear seen on the flank side) exceeding a value of 0.35 mm.
- Wear-through on the flank side, i.e. a substantial risk for fracture or chipping of the tool edge.
- Crater wear larger than 0.2 mm².

The turning procedures was done in 4 min interval sessions, after which time the corresponding wear marks on the flank- and rake face of the machined tool was measured and photographed using a stereo microscope at 6× magnification.

6.3.2 DP2 – Turning of Ca-treated SS2541 using liquid coolant

DP2 was designed with the specific purpose to evaluate the initial wear of the textured α - Al_2O_3 coatings after a turning time of 4 min. at this time, no wear-through of the outer alumina coating should yet have occurred, which meant that the wear patterns on the tools were located in the alumina coating layer.

Following this turning time, the machined tools were then photographed and measured in a similar manner as described for DP1. In total, eight cutting tool specimens from each tool type were produced from DP2.

6.3.3 DP3 – Dry turning of Ca-treated SS2541

DP3 was done in order to evaluate the performance of the tools when no liquid coolant was used during the machining. In all other cases, this test was designed exactly as to description in DP2.

6.3.4 DP4 – Turning of non Ca-treated SS2541 using liquid coolant

This test was also performed in the same manner and purpose as mentioned in DP2, except the fact that the workpiece material used in DP4 had been manufactured without any used Ca-treatment.

6.4 Material Analyses

6.4.1 SEM-imaging

High magnification imaging of worn tool inserts was obtained using a Zeiss Supra 40 and a Hitachi 4300 Scanning electron microscope (SEM), both equipped with a field emission gun (FEG) as electron source. Imaging was both carried out on worn, non-destructed tool specimens and polished cross-sections of worn rake face areas from destructed tool samples.

For the imaging of the non-destructed tools, an EHT-voltage of 10 kV was regularly used along with a working distance set at 10 mm. Prior to all the performed SEM-sessions, the samples were thoroughly cleaned by submerging the tools in an ultrasonic acetone solution for 10 minutes. After this, the tools were demagnetised and then placed in the SEM vacuum-chamber.

Tools were placed in a planar tool holder and imaged from a top view perspective, according to *Figure 6.1*, in order to obtain a full perspective of the various wear features on the tools rake face. Images were mostly taken by using the backscatter electron detector (BSE) and, when applicable, from the secondary electron detector (SE). The taken pictures were always aligned so that the cutting edge of the tools were displayed on the uppermost part of the images.

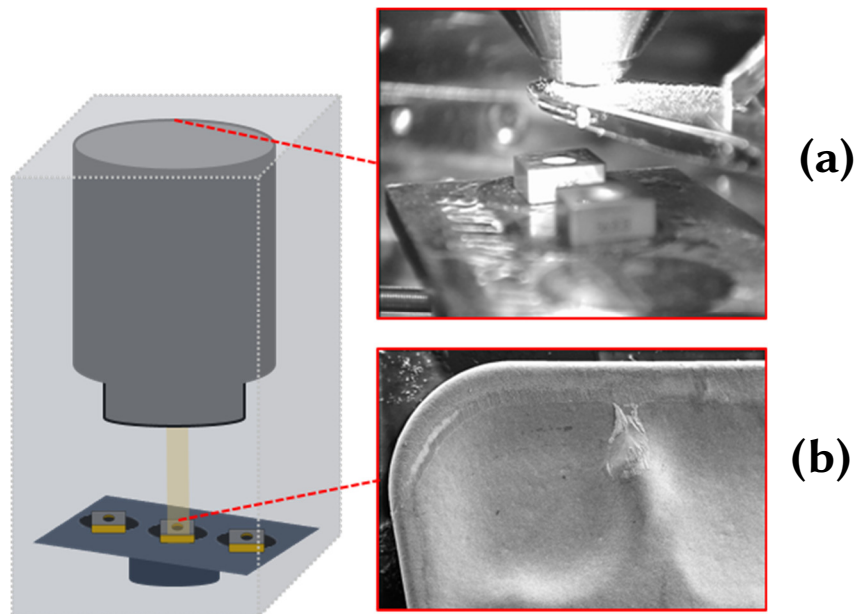


Figure 6.1. Schematic overview of the SEM-imaging of the turned cutting tool inserts. Imaging was performed from a top-down perspective where the tools had been placed on a planar tool-holder, as seen in (a). An example image of the imaged tool's rake face can be seen in (b) where the tool is aligned so that the cutting edge is shown in the uppermost part of the image.

Several different magnifications were used to image the wear seen on the rake face. The main area of interest for the imaging was chosen from a line perpendicular to the cutting edge, located at a distance of 1 mm in from the secondary edge of the tool (see *Figure 6.1 b*). Images were then taken along this line from the top cutting edge downwards on the tool's rake face.

6.4.1.1 Cross-sectional SEM imaging

In order to attain a detailed understanding for the wear seen on the rake face, polished cross-sections of CNMA-based tools belonging to DP2 were also imaged. Two differently oriented cross-sections were made. This was done by polishing the tool inserts in a 9 μm diamond suspension solution and then moulding them into a Bakelite pellet. Each performed cross-section was made on an a single CNMA cutting tool insert.

The first cross-section ran parallel with the main cutting edge, and was placed in level to the area of the tools where the wear on the rake face had appeared to occur in the fastest rate, see *Figure 6.2*. The second cross-section, in turn, were instead made to run perpendicular to the main cutting edge. This cross-section was located along the same tangent line described in the earlier section, i.e. 1 mm in from the left flank side.

SEM imaging was then taken from these samples, using relatively small working distances (5 – 7 mm) and low EHT-voltages (5-7 kV). This was done so that a channelling contrast could be achieved of the composing crystal grains in the Al_2O_3 coating, which could potentially reveal any underlying wear features of the coating that in other cases had not been possible to see from a top-down perspective only.

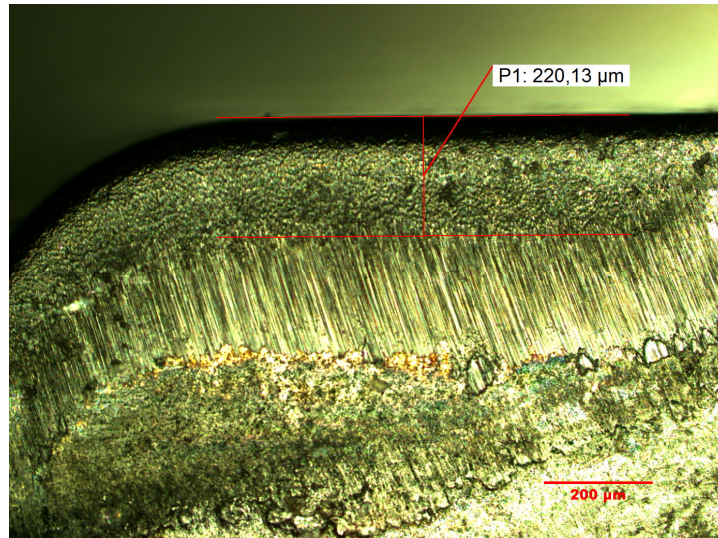


Figure 6.2. LOM-image of a CNMA cutting tool insert from DP2 displaying the location for the performed horizontal cross-section. The cut was placed approximately 220 μm below the main cutting edge of the tool. A second cross-section was made on another tool, which ran perpendicular to the cutting edge instead. This was located 1 mm in from left flank side of the tool.

6.4.2 Etching

In the case when workpiece material adheres on the tool's rake face during turning, for example in the form of a BUL, the real occurring wear mechanism of the Al_2O_3 layer might be concealed below this adhered layer. Therefore, in order to clarify that the observable wear marks on the tools really occurred in the Al_2O_3 coating, two samples were etched in boiling hydrochloric acid (37 %) for 5 minutes. This process was considered as being sufficient for eliminating any workpiece residues on the tool's surfaces.

6.4.3 Surface conductivity enhancement

Due to the non-conductivity from the Al_2O_3 surface, charging effects tended to occur when imaging the tools in the SE-detector. To circumvent this, some of the tested samples from DP2 were coated with a very thin (~ 2 nm) conductive nano-layer of gold, using a PVD sputter instrument (Cressington[®] 208 HR Sputter Coater). This efficiently removed all the surface charging effects from the samples without notably altering the surface topography of the evaluated tools.

6.4.4 Surface profilometry

3D Surface topography images of the tool samples were obtained using a white-light optical interferometry instrument (Veeco NT9100) running in VSI-mode. Images were taken from CNMA tools belonging to DP2 and DP4, respectively, and imaged at the transitional region between the 2nd and 3rd wear band (see *Figure 2.3*). This area corresponded to the region where the wear seen on the tools had appeared to be most pronounced. For DP2, this region was located approximately 280 μm below the main cutting edge, whilst for the DP4 this value was approximately 270 μm .

Three different magnifications were used to image the analysed tool samples, namely; 10 \times , 20 \times and 50 \times magnification. All the analysed tools used for Wyko were non-etched and coated with a nano-layer of gold in order to avoid image artefacts due to the displayed semitransparency from the Al_2O_3 -coating layer. Image analysis was then carried out using the commercially available software Vision[®].

6.4.5 Auger-microscopy (depth profiling)

Auger electron microscopy was performed by Mikael Olsson, Professor in Material Engineering, at Högskolan Dalarna. The Auger instrument provided a highly surface-sensitive analysis of the worn tool inserts, with the ability to detect small traces of various elements present in the topmost layer (~500 nm) of the alumina coating.

Three different cutting tool inserts from DP2 (Ca-treated), DP3 (Ca-treated, no liquid coolant) and DP4 (Non Ca-treated) were analysed, respectively, in four different 5 \times 5 μm areas located in the 3rd wear band of the tools, see *Figure 6.3*.

In the performed measurements, depth-profiling was used in order to achieve a detailed understanding of the elemental composition at different depths of the alumina layer. In this particular technique, the area of the tool being analysed was intermittently etched by a bombardment of energetic argon ions. It was then possible to plot the elemental composition as a function of sputtering depth at a nano-level.

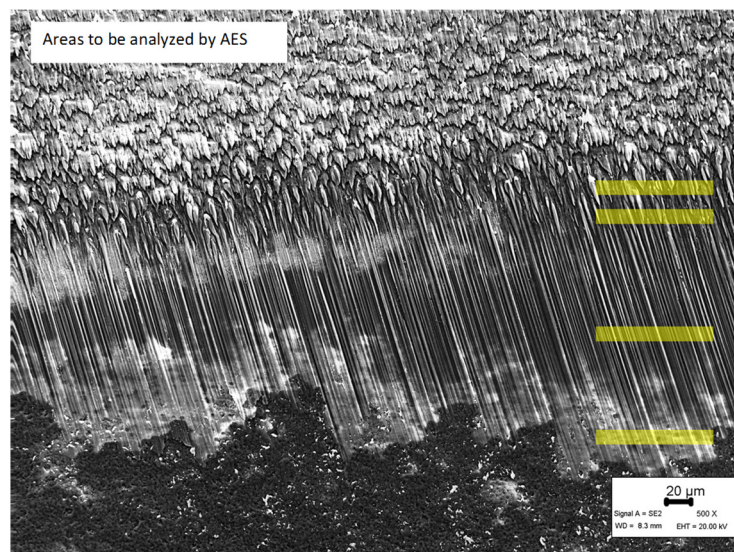


Figure 6.3. SEM image of worn cutting tool insert from DP2 displaying the location of the area of interest chosen for Auger analysis. The yellow fields are numerated as 1-4 from top to bottom in the image. Image taken with the cutting edge horizontally aligned.

6.4.6 Microprobe analysis (EPMA)

Analysis of the elemental composition for any adhered layers on the machined tools were made using a microprobe analyser (EPMA). Analyses were exclusively performed on a cross-sectional CNMA tool belonging to DP2. The cross section was made parallel to the cutting edge, as described in *section 6.4.1*.

The region of interest corresponded to an area in the topmost part of the 3rd wear band of the tool, i.e. the region where most wear seemed to have appeared initially. Prior to the making of the cross-section, the rake face of the tool was inspected in SEM which indeed revealed the presence of smeared workpiece layers. These were seen as inhomogeneous small areas of light phases contained in a secondary darker phase. To characterise these areas, they were elementally mapped in accordance to their chemical composition with the microprobe JEOL 8530F. Two different areas with different sizes were chosen for the analysis. The instrumental settings used in the mapping are listed below, together with a table listing all the twelve elements that were selected to analyse the presence of.

Table 6.7. Instrumental settings used for the elemental mapping from EPMA.

Acceleration voltage	15 keV
Probe current	150 nA
Dwell time	50 ms
Pixel size	Map 1: 0.1×0.1 µm; Map 2: 0.2×0.2 µm
Scan type	Stage scan

Table 6.8. Mapped elements along with the used instrumental channels and corresponding WDS-crystals for detection.

Element	Channel	Crystal
Mg	1	TAP
Mn	2	PETJ
Al	2	TAP
Cr	2	PETJ
Ca	3	PETH
S	3	PETH
Ni	3	LIFH
N	4	LDE5H
O	4	LDE1H
Ti	5	LIFH
Fe	5	LIFH
C	5	LDE6H

6.4.7 X-ray crystallography (XRD)

Powder XRD measurements were performed on a Bruker Discover D8 diffractometer with Davinci design and equipped with a IµS Microfocus Source (CuK_α radiation, $\lambda = 1.5418 \text{ \AA}$), a Eulerian cradle and a Vântec-500 2D area detector. A laser-video positioning system was used for the alignment of the sample. PXRD data were collected in the angular range $20^\circ < 2\theta < 95^\circ$. The XRD patterns were then analyzed with the software DIFFRAC EVA (Bruker) and High Score Plus (PANalytical).

7 Results

7.1 DP1

Table 7.1 demonstrates the wear progression on both types of tool inserts used in the performed turning tests of Ca-treated SS2541. The reader is recalled that the CNMG type of insert is equipped with a chip-breaking rake face geometry whilst CNMA is not.

From these images, it was discovered that signs of wear on the rake face were initially formed as bright contrast areas close to the lower left flank of the tool inserts. This wear tended to propagate rightwards on the rake face as the turning process proceeded. Eventually, they formed a bright band that ran parallel to the cutting edge of the tools. The width of this band increased at longer cutting times.






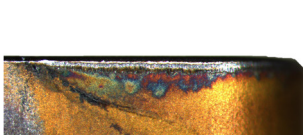
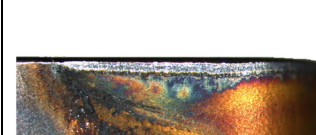

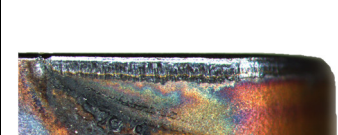
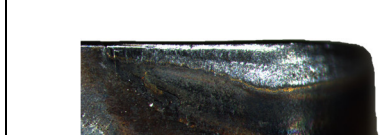
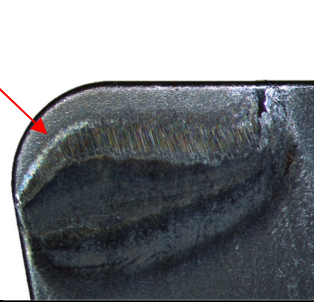


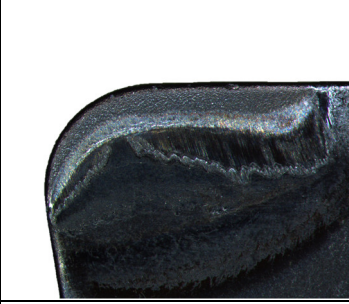
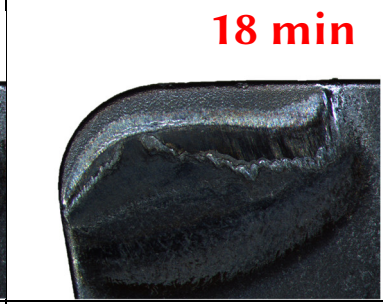
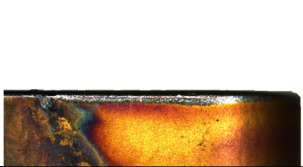
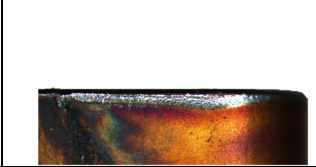
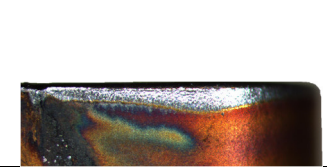
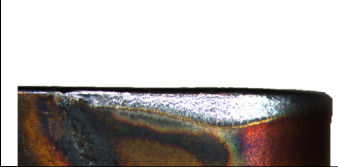
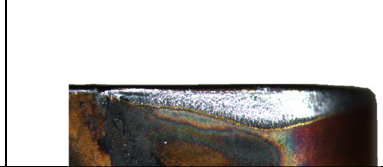
In addition to these white bands, signs of wear did also appear just below these bands on the worn tools. At later stages of the performed longevity tests, this area transformed into a crater on the rake face. Ultimately, one of the listed tool-life criteria were fulfilled for both tested inserts when the measured V_B -value exceeded 0.35 mm on the flank side. Thus, the tools used in the performed longevity tests failed because of plastic deformation, which is evident when viewing the images of the respective flank side from the tested tool inserts. By knowing that plastic deformation is mainly due to thermo-mechanical loads, it is suggested by these images that the experienced temperatures and pressures on the tools' surfaces were severe during the performed tests.

From a direct comparison of the tested tool insert types, it becomes evident that the CNMG tools demonstrated a much longer machining usability before they reached their tool-life criterion. The CNMG type of tools had a 10 min longer machining usability before they reached their tool-life ending criterion. In relative numbers, this corresponds to 55 % longer tool life for the CNMG type of tool insert in comparison with CNMA.

When studying the worn-out tool inserts in SEM, further details of the wear progression of the tools could be made. Here, it was shown that three separated wear bands, each displaying its own pattern and characteristic features, had appeared on the tools' rake faces. These different areas on the tools were denoted in a subsequent order from the cutting edge as the 1st, 2nd and 3rd wear band. These can be viewed from *Figure 7.1*.

The SEM-images show that both tested tool types demonstrated a similar microscopic appearance on their rake faces at the time when their respective tool-life criteria were reached. Considering that the same cutting conditions were used for both tested tool inserts, it may therefore be assumed that both tested tool types undergone a similar wear progression on their rake faces when turning SS2541. The large discrepancy in cutting tool-life from the tested tools may therefore be derived from the chip-breaking geometry equipped on the CNMG tools. This feature is well-known to enhance these type of tools overall machining usability.

Table 7.1. Visual comparison of the wear progression between two types of cutting tool inserts (CNMG and CNMA). Bright wear marks (marked by the red arrow) developed on the rake face from the lower left flank (close to the secondary cutting edge) and then gradually propagated rightwards as the turning process proceeded. At longer cutting times, this subsequently lead to the development of crater wear. Ultimately, the tool life criterion was fulfilled for both tested tool types due to plastic deformation.

		4 min	8 min	12 min	16 min	Tool-life criterion
CNMG	Rake					34 min 
	Flank					
CNMA	Rake					18 min 
	Flank					

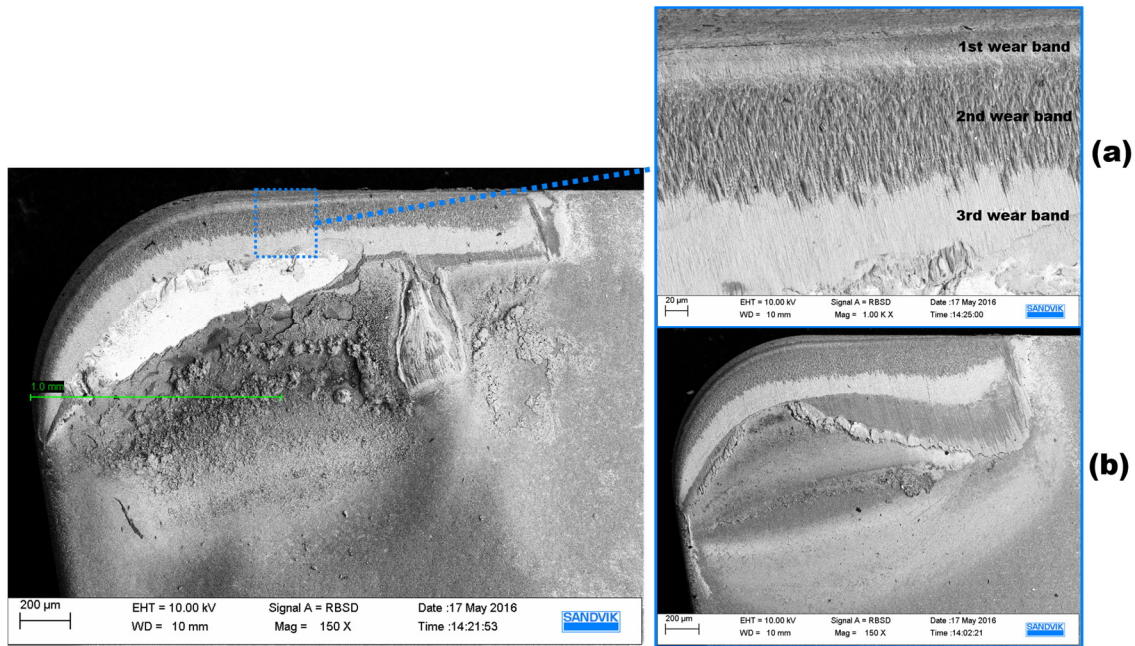


Figure 7.1. SEM image of a worn CNMG type of tool insert. An enlargement of the blue dotted area can be seen in image (a), revealing the formation of three separated wear band regions, each one having its own unique appearance. In (b) an image of a worn CNMA insert can be seen for comparison of the two tool type inserts.

7.2 DP2

SEM-imaging of the early-worn tool inserts from DP2 (Figure 7.2) confirmed the observation made in DP1 that wear on the tools' rake faces started in an area close to the secondary cutting edge. In this area, clearly visible and bright wear marks had appeared after 4 min of turning.

Similar to the tools from DP1, the tools from DP2 also demonstrated the formation of three highly distinctive wear band regions on its rake faces (Figure 7.3). Therefore, it was possible to deduce that the bright, initially-formed wear marks on these tools had mostly appeared in transitional zone between the 2nd and 3rd wear band. This observation was confirmed for both tested tool inserts types, i.e. both CNMG and CNMG. Accordingly, it appeared that this particular region of the tools demonstrated the highest wear rate.

The worn rake faces of the tools from DP2 were also evaluated in SEM using larger magnifications, as seen in Figure 7.3. This revealed that each formed band had its own distinguishing features and characteristic appearance.

In the first wear band, which was located closest to the tool's main cutting edge, a relatively smooth surface displaying only shallow indentation marks could be seen. However, below the 1st developed wear band, the topological features on the tools' rake faces surface had changed dramatically. In this area of the tools, which corresponded to the 2nd wear band, the alumina coating layer demonstrated a clearly deformed surface in which the alumina grains seemed to have been elongated in the chip-flow direction. The appearance in this zone could possibly be best described as being "tongue-like", with large overlapping droplet-shaped flakes. In some of the taken SEM-images, thin nano-sized cracks running parallel to the main cutting edge appeared in this region of the tools.

The second wear band region, in turn, transitioned smoothly to the final 3rd wear band that had appeared on the machined tools. This particular wear band was located a short distance in on the tools' rake faces, and had an appearance that clearly deviated from the other wear bands.

The surface topography of the 3rd wear band adapted a ridge-like and ordered appearance consisting of nearly equally spaced surface lines that ran mostly parallel with the chip-flow direction. These lines formed into a very thin and alternating 'lamellar structure' on the evaluated tools' rake faces. When measuring the approximate width of each lamella, it was found that they were somewhere in the nano-size region, typically around 100 nm or less. Additionally, cracks also appeared in this wear band, although these cracks propagated perpendicular to the main cutting edge. This was in contrast to the cracks that had appeared in the 2nd wear band that had grown mostly parallel with the main cutting edge.

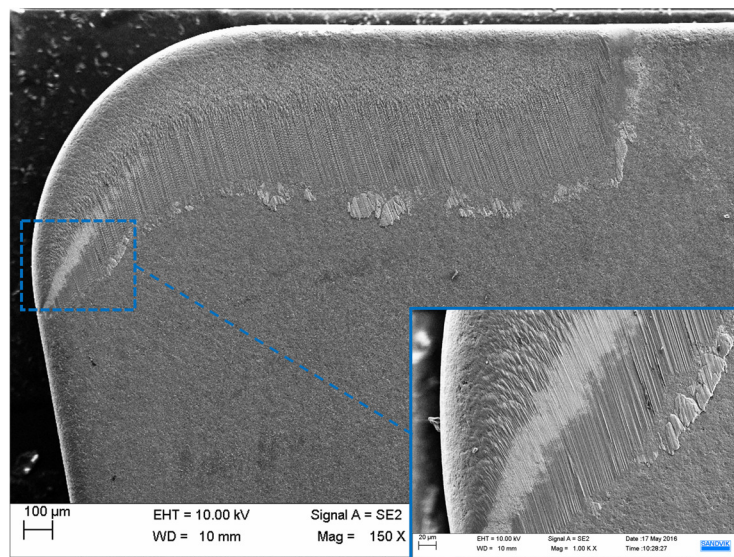


Figure 7.2. SEM image (SE-detector) of initially worn CNMA tool-insert displaying a bright wear area located close to secondary cutting edge of the tool's rake face. The viewed tool had been etched and gold-coated prior to imaging to avoid surface charging effects. The bright worn area was developed in the transitional region between the 2nd and 3rd wear band, thus suggesting that this area demonstrated the fastest initial wear rate on the tool insert.

In terms of the light-grey wear marks that had appeared on the examined tools, it was concluded that these most likely represented localised thinned areas of the alumina coating, which had revealed the underlying Ti(C,N) coating-layer. However, it was not considered that the alumina coating in these areas had worn-through entirely to the underlying Ti(C,N) layer. The reason for this was because the size of these bright wear marks grew somewhat when the used acceleration voltage (EHT-voltage) was increased in the SEM. In addition, these bright areas were still visible on the tools even though some were coated in gold prior to the imaging.

The fact that no wear-through had occurred in the alumina coating in its transitional region (i.e. 2nd to 3rd wear band region) was later confirmed when the cross-sectional samples of the tools were reviewed. These results can be found in section 7.5 and from Figure 7.6.

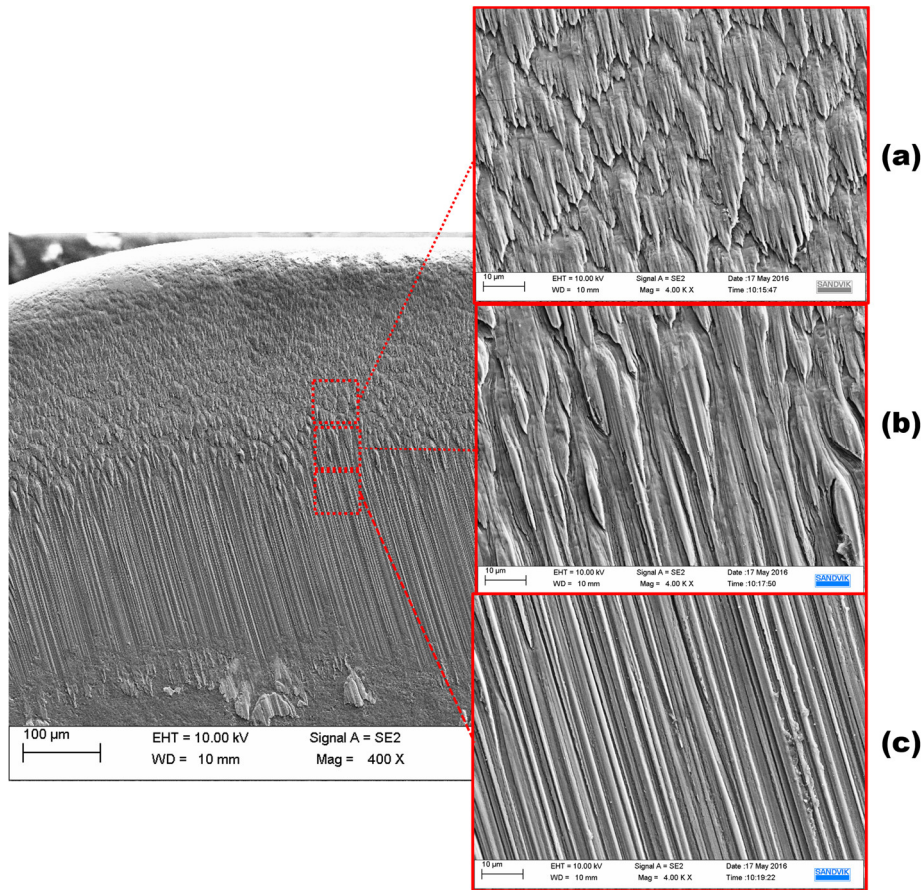


Figure 7.3. Inspection of the arisen wear band regions on the initially-worn CNMA tool inserts. At larger magnifications (4000 \times) the different wear band regions demonstrated clearly different and distinguishable surface appearances. (a) magnification of the 2nd wear band, (b) transitional zone between the 2nd and 3rd wear band, where the fastest wear rate had occurred (c) “lamellar structure” observed in the 3rd wear band. The tool had been etched and gold-coated prior to imaging.

7.3 DP3

SEM-imaging of the tools in DP3, which had been machined without any use of coolant, indicated that the wear on these tools had developed much faster in comparison with the tools from DP2 (where a coolant had been used). For instance, this was evident from the more pronounced and developed bright band area that had stretched itself much farther rightwards on the tools’ rake faces from DP3. This observation was true for both the CNMG and CNMA type of tools in DP3, although the white band seemed to have developed substantially more on the CNMG tools than for CNMA in DP3.

In addition, whereas the white band in DP2 had appeared in close proximity to the 2nd wear band on both tested tool types, the white band on the CNMG tools in DP3 were entirely located in the 3rd wear band. This is demonstrated in *Figure 7.4* on the following page. The position of this white band had been shifted slightly downwards, which had left a small gap between the 2nd and 3rd wear band where no white band formation had occurred. Otherwise, the tools machined in DP3 demonstrated a much similar appearance to the ones in DP2.

It was possible to distinguish adhered material on the tools from DP3, which most likely derived from the workpiece material. This adhered workpiece material appeared in all three

wear bands, however; it mostly appeared in the 2nd wear band of the tools. The appearance for this adhered material appeared predominantly in the form of homogeneously distributed “white spots”.

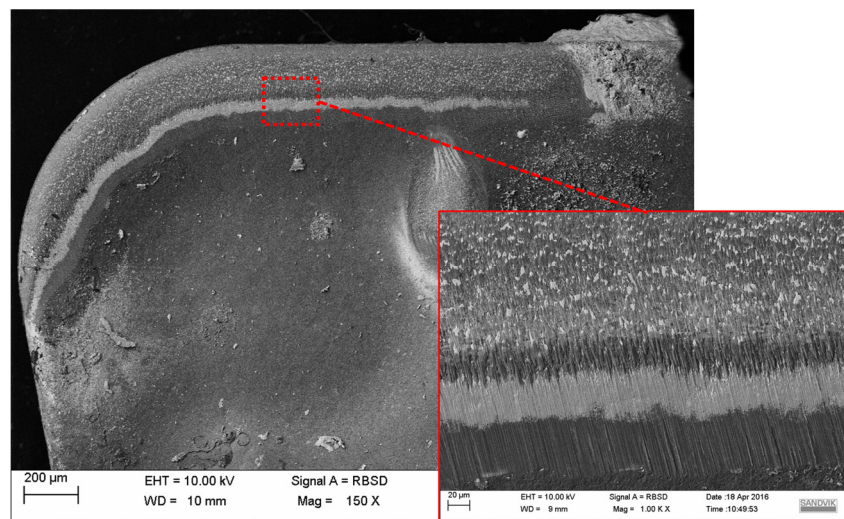


Figure 7.4. SEM image (BSE-detector) of machined CNMG tool from DP3 where no coolant media had been used. The image clearly demonstrated a much more developed worn “white band”, in comparison with the same tool type where a coolant media had been used in DP2 (see Figure 7.2 for comparison).

7.4 DP4

Before the results from DP4 are presented, the reader is recalled briefly that the steel work-piece material that had been machined in this turning test was not calcium-treated. This was a deviation from all other performed turning tests, where the machined steel material had been Ca-treated instead.

When studying the worn tools from DP4 in SEM, it became obvious that they demonstrated a clearly different wear progression in comparison with the tools used in the rest of the performed turning tests. In essence, there were no obvious signs of any worn white-band close to the secondary edge on these tools. This was a clear deviation from the tools used in the other performed turning tests. The different appearance of the machined tool in DP4 can be reviewed in Figure 7.5 below.

Another noticeable difference from DP4, especially when comparing with the similar DP2 test, is that the contact length of each individual wear band appeared to be much smaller in its length. This observation was especially true when comparing the width of the 3rd wear band. The width of the 3rd wear band on the worn tools from DP4 was significantly smaller in comparison with the worn tools from DP2.

Moreover, the position of the 3rd wear band had appeared much closer to the cutting edge on the tools from DP4 in comparison with DP2. A direct comparison between DP4 and DP2 revealed that the 3rd wear band on the CNMA type of tools in DP4 was located approximately 100 µm closer to the main cutting edge.

Furthermore, the tools used in DP4 demonstrated a topographical appearance of its 3rd wear band that clearly deviated from the one seen on the tools in DP2 (Figure 7.3 and Figure 7.5). In

particular, this was demonstrated by the fact that the tools in DP4 did not demonstrate the similar, ordered ‘lamellar structure’ in their 3rd wear band that had appeared on the tools from DP2. Rather, the worn surfaces in the 3rd wear bands on the tools from DP4 seemed to be much smoother and broadened.

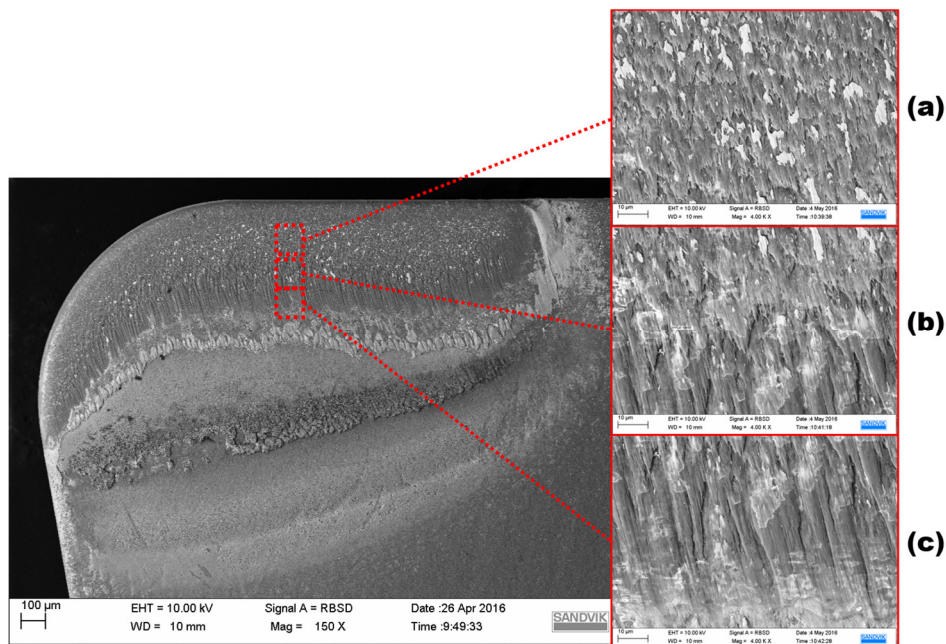


Figure 7.5. BSE-image of a CNMA tool from DP4, displaying a different wear behavior in comparison with the tools used in DP2. No presence of any formed white band in the topmost part of the 3rd wear band can be seen. In comparison with DP2, the arisen wear marks on the tools used in DP4 appeared as being much smoother. The white, hazy area seen in the magnified images are likely adhered material from the workpiece. (a) 2nd wear zone (b) transitional zone between 2nd and 3rd wear band (c) 3rd wear band.

7.5 Cross-sectional imaging

From the cross-sections that were made perpendicular to the main cutting edge on both tool types in DP2 (Figure 7.6), it was revealed that no wear-through had occurred on the outer alumina-coating layer after 4 min of turning. However, an area on both imaged tools where the alumina coating had been thinned was observed. This indicated that wear had been concentrated in this particular area of the tools.

The position of this area was slightly different when comparing CNMG with CNMA. On CNMG, this concentrated wear area appeared closer to the main cutting edge (~204 µm for DP2) than for CNMA (285 µm for DP2). In addition, the concentrated wear area on the CNMA type of tools were more elongated and covered a larger area of the inspected tool inserts.

It is interesting to note that this concentrated wear area corresponded to the transitional region between the 2nd and 3rd wear band for both the investigated tool types, i.e. the location where the white-band had tended to appear initially.

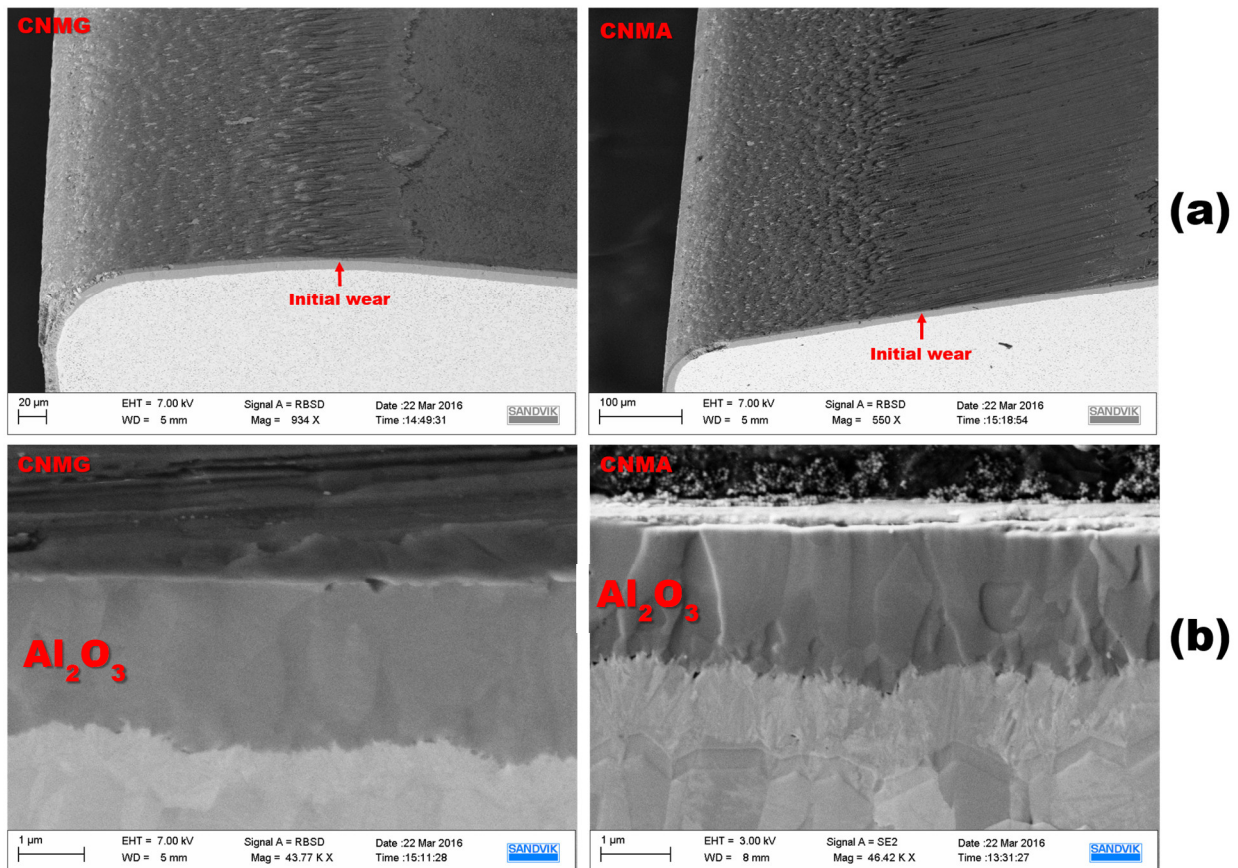


Figure 7.6. (a) BSE cross-sectional images of CNMG and CNMA tools displaying the location where most wear had appeared initially in the alumina-layer. (b) Magnification of the worn coating area imaged using channeling contrast. No prominent damage to the crystal grains in both imaged alumina coatings can be distinguished. All images taken on tools belonging to DP2.

When reviewing the cross-section made parallel to the main cutting edge in the BSE-detector (Figure 7.7 and Figure 7.8), it was noted that white, smeared fields had accumulated in the formed ridges of the 3rd wear band. Since the arisen contrast from a BSE-detector is mostly due to differences in atomic masses, it is strongly believed that these white fields represent foreign material that has adhered on the rake face. This material is most likely originating from the machined workpiece.

Besides these smeared materials, many of the SEM-images taken on the parallel cross-section also indicated for the presence of light-grey particles. These were unevenly distributed in the topmost part of the alumina coating, although they seemed to mostly appear just below the formed ridges of the worn tool.

At higher magnifications, the identified foreign particles became even more clearly visible. This was particularly true when viewing the cross section using the BSE-detector. The BSE-detector also revealed that some of these identified particles had agglomerated, and grown into larger regions. Interestingly, some of these agglomerates did seem to appear inside of the alumina matrix. This is especially apparent when viewing the close-up BSE image in Figure 7.8, which were taken using channeling contrast.

The channeling contrast on the parallel cross-section also revealed that the topmost part of the alumina coating appeared in a different contrast, and was more diffuse in comparison

with the taken vertical cross-section images (Figure 7.6). This diffuse region stretched approximately 1 μm down into the alumina coating, and corresponded to the area where most foreign light-grey particles seemed to have appeared.

A large interest was to characterize the chemical composition for these identified particles. However, due to the small sizes of these particles, typically in the nano-size region, it was not possible to identify them accurately by the equipped EDS-detector in the SEM-instrument. This necessitated the use from other analytical techniques, which was done at a later stage from EPMA. The results from this investigation can be viewed by the reader in section 7.7.4 .

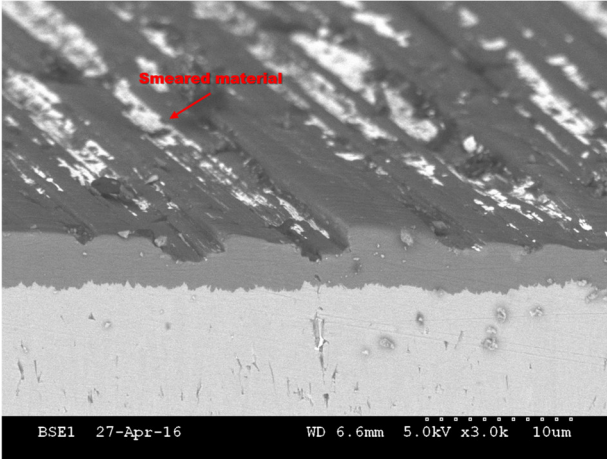


Figure 7.7. Cross-sectional imaging (parallel to the cutting edge) of a CNMA tool displaying the presence of white smeared material accumulated in the formed ridges, located in the transitional region between the 2nd and 3rd wear band. Image from a tool belonging to DP2.

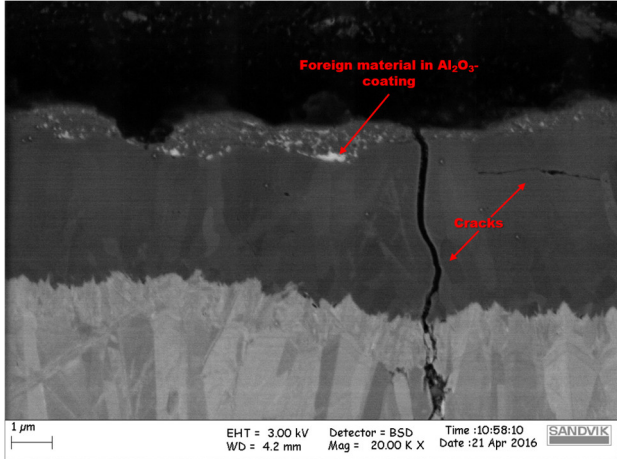


Figure 7.8. Close-up cross-sectional imaging (parallel to the cutting edge) of a CNMA type of tool from DP2 using channeling contrast in order to elaborate the internal structure of the alumina grains in the coating-layer. Bright spots and regions located in the topmost part (\leftrightarrow 1 μm) of the coating layer is clearly distinguishable from the image. The presence of cracks, which are elongated both laterally and vertically, is also visible in the image

7.6 Layer formation

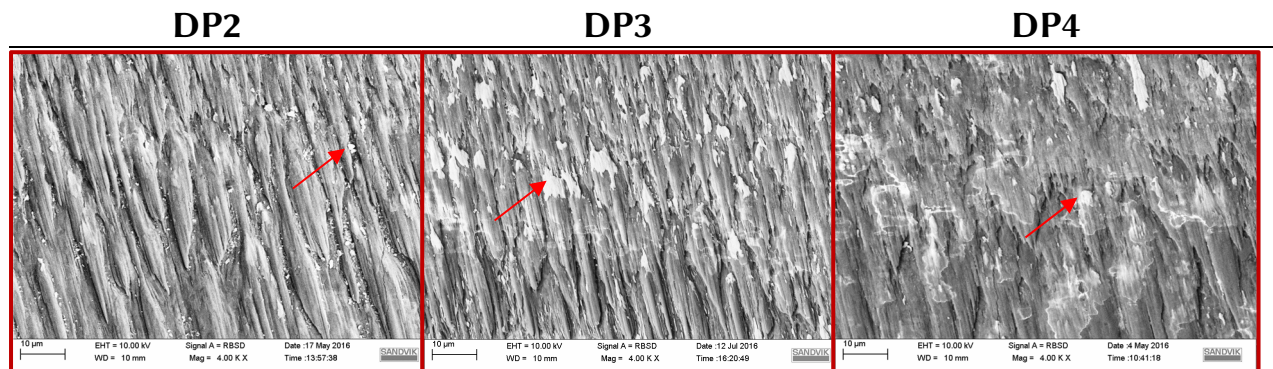
Table 7.2 demonstrates a comparison of the transitional 2nd-3rd wear band zone for non-etched CNMG tools originating from all three performed initial turning tests. As noted earlier, this zone corresponded to the area of the tools wear most of the wear had seemed to appear.

From these images, it may be deduced that foreign material, seen as white particles and smeared regions, did form on all the tools used in the three different initial turning tests. However, the amount of adhered material, along with the appearance of this material, did differ between the performed tests. This is most evident when comparing the surfaces from the tools belonging to DP2 (Ca-treated) with the tools from DP4 (not Ca-treated).

The transitional zone of DP2 seemed to demonstrate a slightly lower tendency for adhesion of workpiece material. This material had appeared as small isolated particles that was preferably located in the formed ridges of the tool. This was a deviation from the other two performed turning tests. This was particularly the case when comparing DP2 with DP4, where larger, smeared regions of workpiece material covered a larger part of the transitional region.

It is interesting to note that a large amount of workpiece material had appeared on the tools belonging to DP3, where no liquid coolant had been used. Therefore, these results indicate that the foreign material that were observed on the tools' surfaces may be derived directly to the machined workpiece material, and not from any possible contaminations found in the used coolant.

Table 7.2. Images comparing the relative amount of foreign material adhered on the transitional 2nd to 3rd wear band region on CNMG tools from all three performed initial turning tests. Foreign material is marked by a red arrow. A clear deviation between both the amount of adhered workpiece material and its appearance is evident from the images.



7.7 Surface analyses

7.7.1 Profilometry

Surface topographic images from unetched CNMA type of tools belonging to the turning tests DP2 and DP4, respectively, can be viewed in *Figure 7.9*. From these images, it can be seen that the topographical appearance of the transitional 2nd-3rd wear band region clearly deviated between the tool inserts from these performed turning test.

In essence, the tool surface from DP2 demonstrated a much more structured topographical appearance with evenly spaced ridges having a uniform depth. These ridges were also located below of the normalised reference plane. The maximum valley depth of these formed ridges, given as the S_v -value, was approx. 2.1 μm .

The topographical view of the DP4 demonstrated a slightly more non-structured appearance displaying a large part of material that had appeared above its normalised reference plane. This indicate that a larger amount of workpiece material had adhered on the tools from DP4, in comparison with the tools from DP2. Thus, these results are in accordance to the observations made from *Table 7.2*.

Nevertheless, some formed ridges can still be seen from the analysis of the DP4 tool, which had an S_v -value of 2.7 μm . This value was slightly larger than the one seen from the DP2 tools. This suggest that the formed ridges on the tools DP4 could be somewhat deeper.

Interestingly, even though the two surfaces clearly demonstrated different surface-topological appearances, their S_z value³ was shown to be nearly equal. This implies that the surface roughness between the tool samples were actually almost the same, in spite of their different visual appearances.

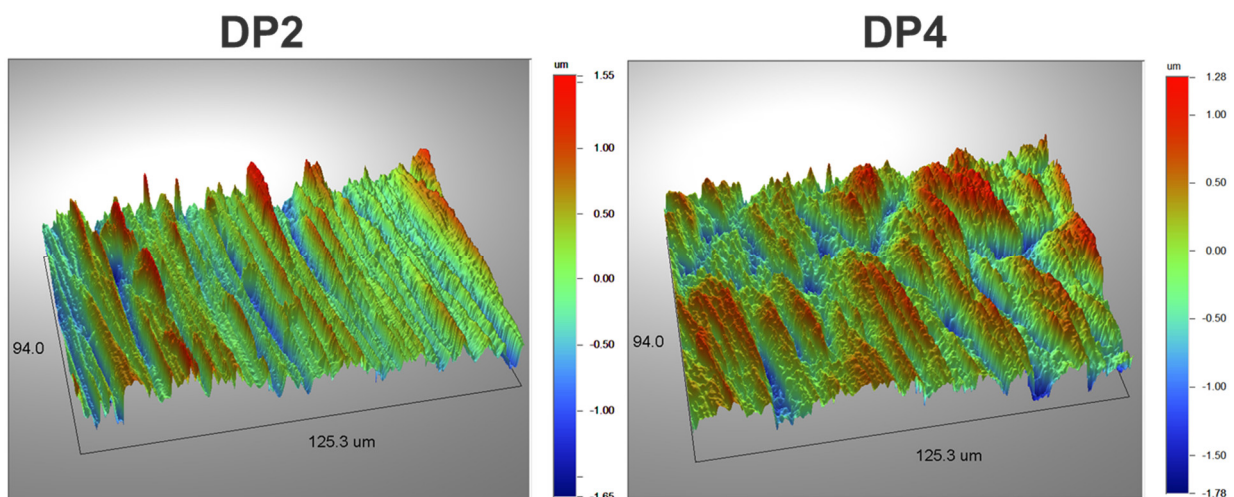


Figure 7.9. Surface topography images from Wyko taken on two separate CNMA tools from DP2 and DP4. Image taken at 50x magnification in the transitional 2nd-3rd wear band region.

³ The S_z value is defined as the difference between the maximum height value S_p and the maximum depth S_v .

7.7.2 Auger

Diagrams showing the relative atomic concentrations [At %] of different elements in the outer alumina coating in the examined tools are illustrated in *Figure 7.10*. Besides the obvious and expected signals from Al and O, the results showed that a significant amount of calcium was found in the topmost region of the alumina coating on the tools belonging to DP2 and DP3. No other elements were found to be present in the alumina layer whilst its thickness was successively reduced from the Ar-sputtering.

The calcium content was detected in the lower parts of the third wear band, that is, in the area 3 and 4 (see *Figure 6.3*). Interestingly, no calcium signal was detected in area 1 and 2 of these tools, which corresponded to the areas where the wear had seemed to be concentrating the most after 4 min of turning.

The tool from DP4 (non Ca-treated) distinguished itself for being the only tool sample where no calcium content could be detected. This was true for all of the evaluated areas on this tool.

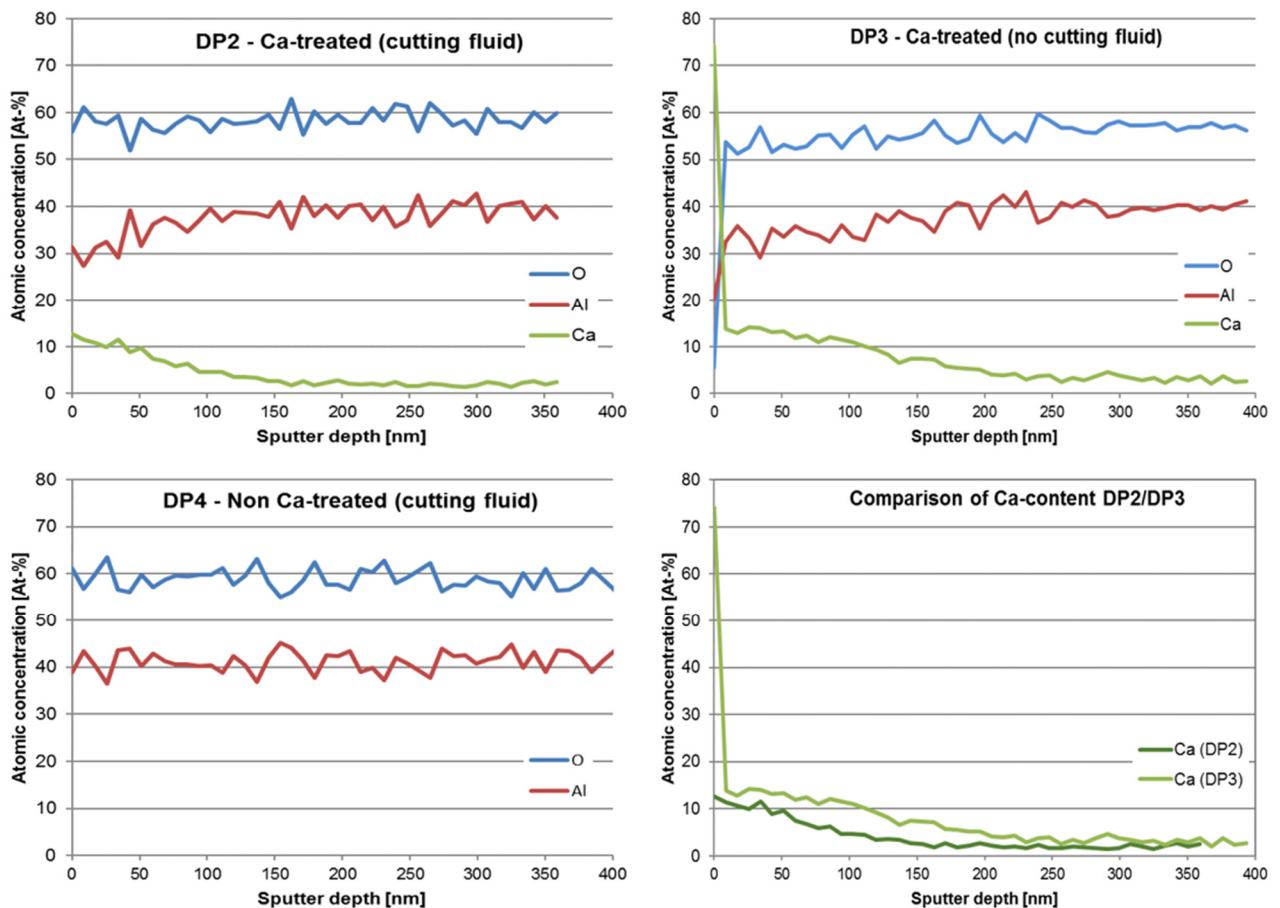


Figure 7.10. Diagrams displaying the relative atomic concentrations [At-%] of elements detected from Auger analysis in Area 4. A significant amount of calcium was found on the tools from DP2 and DP3. A comparison of Ca-content between these tool samples can be viewed from the figure. The tool from DP3 displayed a slightly higher overall Ca-content than the tool from DP2.

7.7.3 XRD

The two obtained x-ray diffractograms from DP2 and DP4 demonstrated a very similar appearance where reflections of tungsten carbide, alumina, and titanium-carbo-nitride were clearly visible. No other phases, such as calcium-containing ones, were visible from the XRD.

However, two unidentified peaks, located at 45° and 76° , were distinguishable from both sub-tests. These peaks showed a close resemblance to signals obtained by the presence of steel, although these particular peaks found from this evaluation were slightly shifted in their 2θ -positions compared with published data.

Even if the peaks obtained from the diffractogram were clearly visible, a modest overall increase of background noise were also evident from the diffractograms. This was most conspicuous around 30° angle, where a diffuse peak-signal was obtained from both evaluated tool samples. Given the relative amount of noise in the diffractogram, it is possible that this signal may represent an unidentified, semi-amorphous (e.g. nano-crystalline) and/or amorphous phase, that is present in both evaluated tool samples.

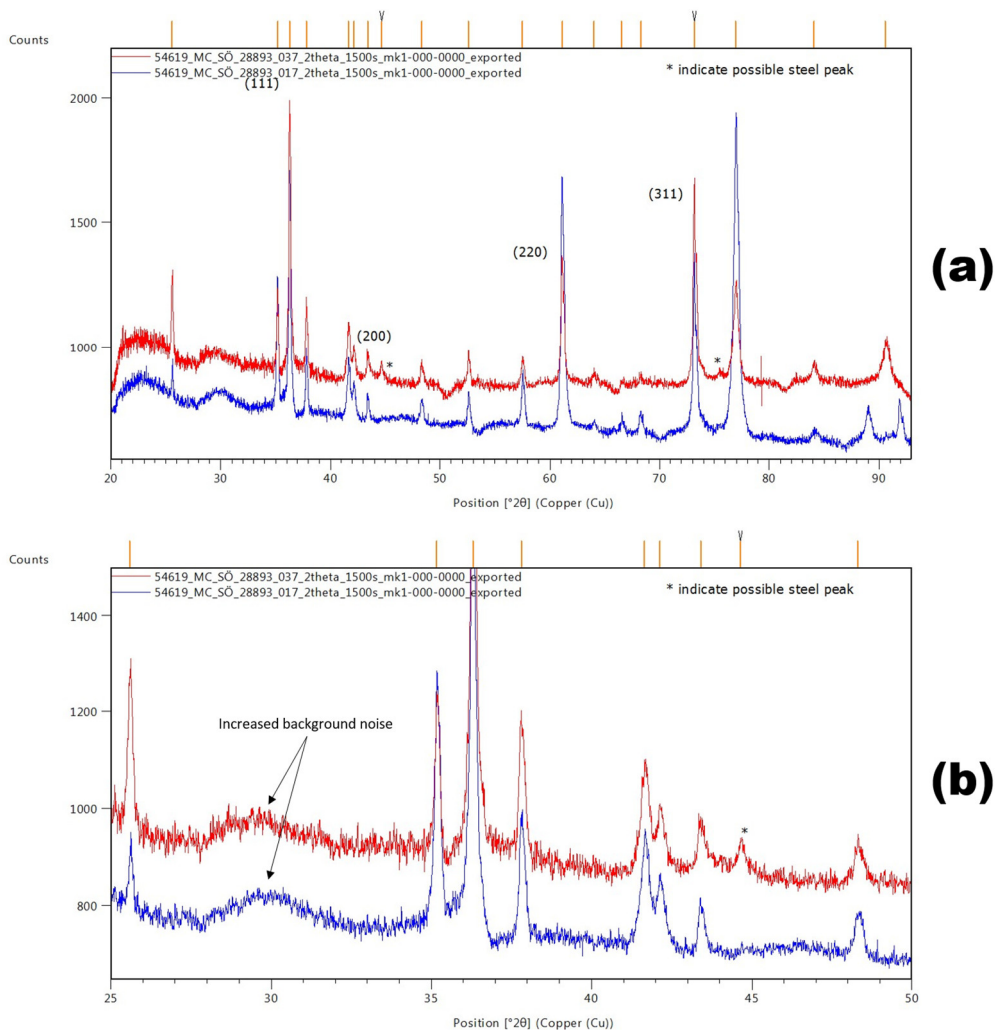


Figure 7.11. X-ray diffractograms of tool samples belonging to DP2 (red) and DP4 (blue). Note that the signal from DP2 have been slightly shifted upwards in order to easier distinguish coinciding peak signals. In (b) a closer magnification of the diffractogram in the interval $0-50^\circ$ can be seen. An increased background noise level at around 30° angle may here be distinguished for both evaluated tool inserts.

7.7.4 EPMA

Figure 7.13 and *Figure 7.15* displays the relative presence of each evaluated element in the smeared layers that were found on top of the alumina coating. Images of the analysed areas can be viewed from *Figure 7.12* and *Figure 7.14*, which also gives information of the relative location for each detected element in the two performed mapping sessions. It is recalled that the analysis was carried out on a cross-sectional tool sample from a single CNMA tool belonging to DP2. The cross-section was made to run parallel with the main cutting edge (as have been described in section 6.4.1).

Both performed mapping sessions revealed that the bright particles and regions, which had been detected from the cross-sectional SEM-images (*Figure 7.7* and *Figure 7.8*), primarily contained Fe but also elements such as Ni, Cr, Ti, Mn and Mg. These various elements were present in different concentrations and appeared as distinguishable bright phases when viewing the evaluated cross-sectional tool in the BSE-detector.

In addition, it was found that these bright phases were surrounded by a much darker phase, which contained elevated concentrations of Ca, Mn, S, Al and O. Because many of these elements (except for Al and O) are foreign and not a natural part of the tool's chemical composition, it can be concluded that they originate from the machined steel workpiece material. Moreover, since many of these detected elements are mostly localised to the steel's inclusions, it may also be safely assumed that the formed layers on the rake face stems from these inclusions. Thus, these results are in accordance with the literature for the formation of these layers, as have been reviewed earlier in this thesis.

When it comes to the concentrations of each individual element, it was found that particularly high amounts of Ca and S were present in the formed adhered layers. A small layer of C also seemed to be formed between the alumina coating and this smeared layer. However, the large ring-shaped signals present in the mappings of C are not likely to be a part of the tool's overall composition. Rather, they are more likely deposited contaminations from the electron beam in the instrument.

The reader should carefully note that a quantitative comparison between the detected elements in the elemental mappings are not possible, due to the limitations of the used EPMA-equipment. The signal for each detected element may originate from different channels and/or WDS-crystals, meaning that each elemental signal may contain a different number of registered counts. In other words, the colour scheme between two different elemental maps are not equally scaled; the colours may represent very different number of counts and hereby dissimilar elemental concentrations.

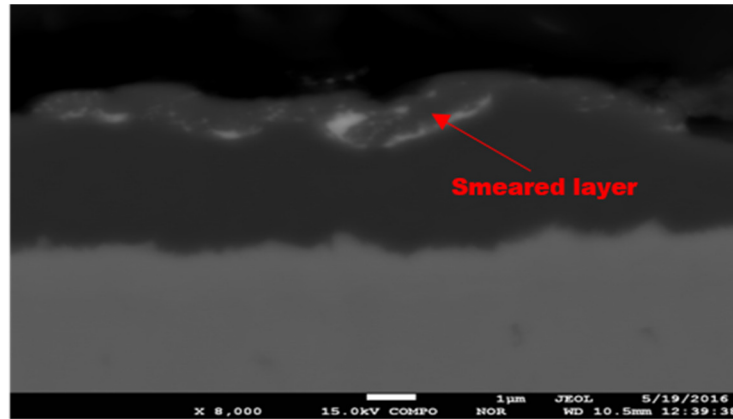


Figure 7.12. Image displaying the 1st map area analysed by the EPMA. A smeared transfer layer having different contrast to the underlying Al₂O₃ coating is clearly visible in the image.

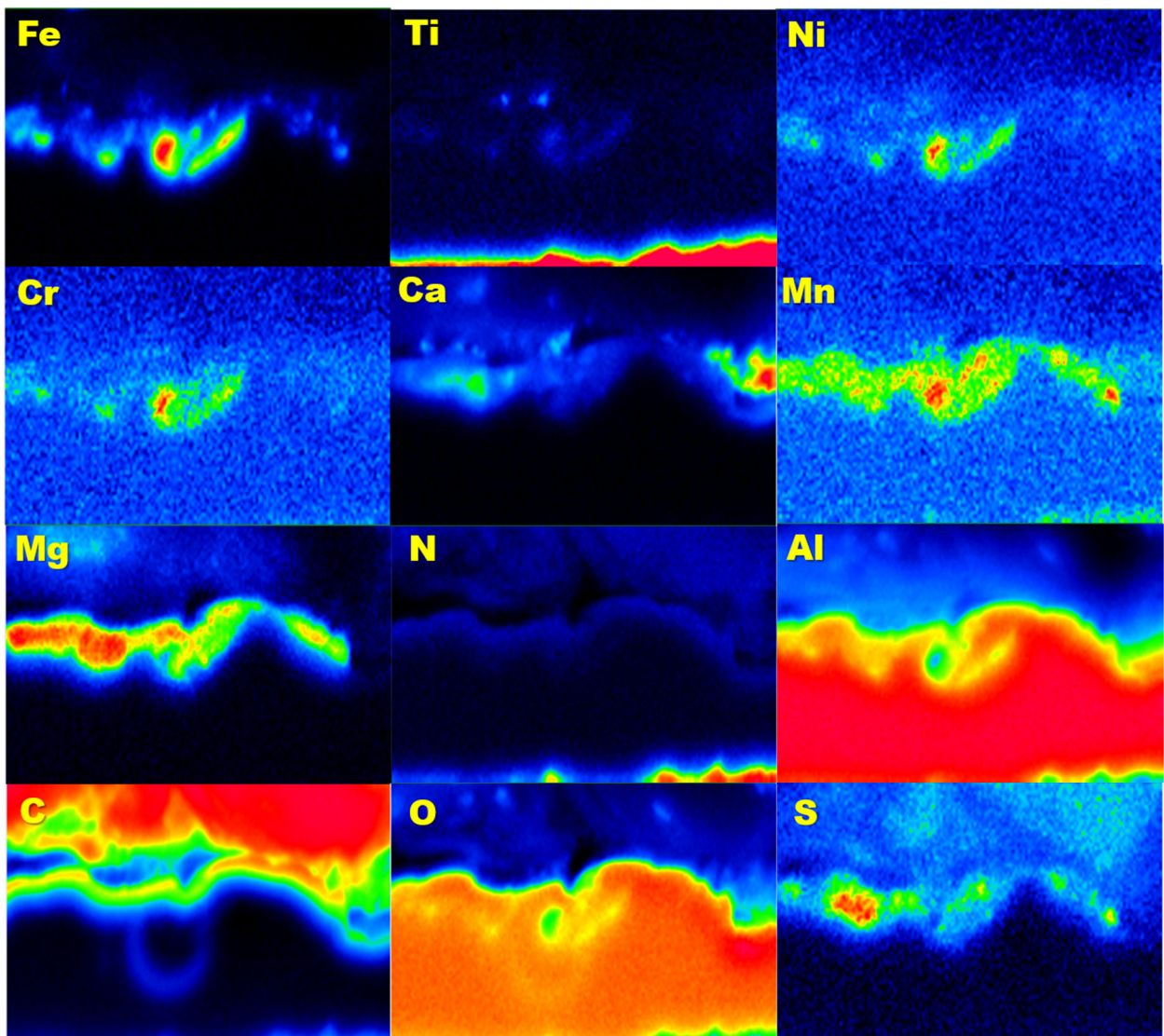


Figure 7.13. Elemental maps obtained from the analysed 1st area which displays the presence of the elements Fe, Ti, Ni, Cr, Ca, Mn, Mg, N, Al, C, O, S, respectively. Concentration follows a spectrum-scale in which red indicates for stronger elemental presence. Note that a quantitative, colour-based comparison of the detected elements between the maps are not possible. This is because the signal from each performed mapping session may represent a different number of registered counts and originate from different channels.

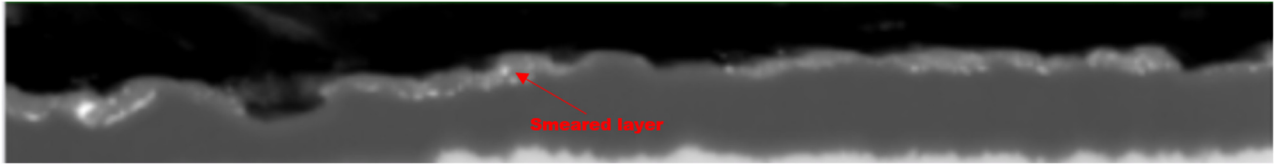


Figure 7.14. Image displaying the 2nd map area analysed by the EPMA.

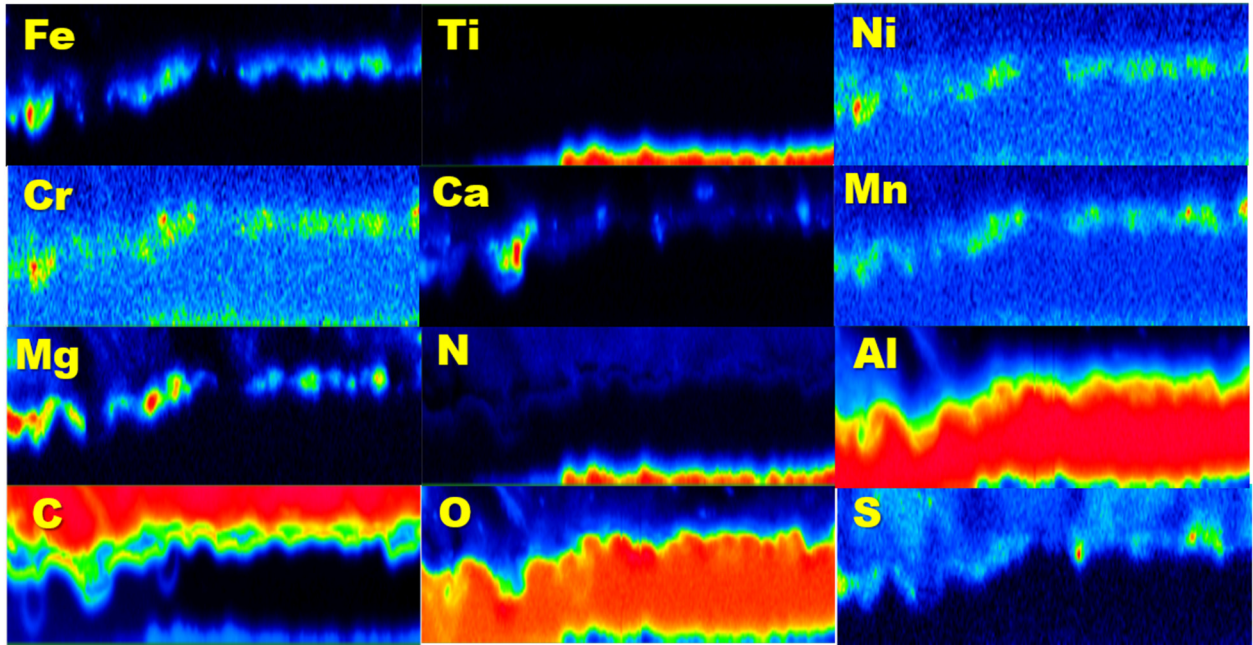


Figure 7.15. Elemental maps obtained from the analysed 2nd map displaying the presence of the elements Fe, Ti, Ni, Cr, Ca, Mn, Mg, N, Al, C, O, S, respectively. Concentration follows a spectrum-scale in which red indicates for stronger elemental presence. Note that a quantitative, colour-based comparison of the detected elements between the maps are not possible. This is because the signal from each performed mapping session may represent a different number of registered counts and originate from different channels.

8 Discussion

8.1 Summary of main results

➤ SEM and LOM investigations revealed that all tools used in the performed turning tests displayed a similar wear appearance on their rake faces. This was particularly true for the initial turning tests, where all tools demonstrated the development of three different and characteristic wear band regions. Each one of these had its unique appearance and wear pattern. Counting from the tools' cutting edges, these bands were listed as the 1st to the 3rd wear band. The 3rd wear band was distinguished by its highly ordered, alternating ridge-like pattern that ran mostly parallel with the chip-flow direction.

➤ Except for DP3 (Ca-treated, no coolant), wear seemed to be concentrating in the transitional region between the 2nd-3rd wear band. This was seen by the development of a bright region that progressed itself from an area close to the secondary cutting edge of the tools.

In addition, SEM-imaging of cross-sectional samples revealed that the outer alumina-coating in this region of the tools had been thinned. Thus, this region demonstrated the fastest wear rate on the tools. Based on these findings, it was considered that this bright region most likely represented the underlying Ti(C,N)-coating layer, which had been exposed to the detectors in SEM. However, it was not considered that the alumina-coating in this region had worn-through entirely to the underlying Ti(C,N)-coating layer. This was later confirmed from the SEM-imaging of the tools cross-sectional samples.

The tools belonging to DP3 (Ca-treated, no coolant) distinguished themselves for having their exposed Ti(C,N) region slightly shifted downwards, and was therefore entirely located in the 3rd wear band of these tools. This had left a small gap between the 2nd and 3rd wear band where no such white band could be seen on the tools from DP3.

➤ The performed longevity test (DP1) demonstrated, after LOM and SEM-investigations, that the width of this bright region increased at longer cutting times. This eventually resulted in the development of crater wear on the tools' rake faces. Ultimately, both types of tools (CNMG and CNMA) failed due to excessive plastic deformation. This was concluded based on the fulfilled tool-life ending criterion (i.e $V_B > 0.35$ mm) and from the overall appearance of the tools main flank side (*Table 7.1*). The fact that the tools had failed due to PD suggested that the tools used in the turning procedures had been exposed to very high and severe thermomechanical loads. In addition, since all tested tools demonstrated a similar appearance to their worn rake faces, it was deemed that they had undergone the same wear process when machining low-alloy SS2541 steel. The differences in machining usability time between CNMG and CNMA could therefore be explained from the equipped chip-breaking geometry on the CNMG-type of tools. This chip-breaker reduced the overall contact length between these tools' rake faces and the formed chips, thus reducing the progression of wear on these particular tools.

➤ All the tools used in the various performed turning test demonstrated the adhesion of foreign material on their surfaces. This could be viewed in the SEM as areas with lighter contrast and white-grey particles. These were distributed in all the different wear bands that had developed on the worn tools.

However, it was evident from the obtained results (*Table 7.2*) that the tools from the different turning tests demonstrated dissimilar tendencies for adhesion of material in their 2nd to 3rd transitional wear band regions. This was seen by the difference in amount and appearance of these adhered materials in this region, in particular when comparing the tools from DP2 (Ca-treated, coolant) with the tools from DP4 (Not Ca-treated, coolant).

The tools from DP2 also demonstrated less adhered material in their transitional region, whereas the tools from DP4 showed significantly more material in the same region of the tools. The foreign material adhered on the tools from DP4 had also appeared as being more smeared, and covered a larger part of the 3rd wear band.

Nevertheless, the cross-sectional tool samples (belonging to DP2) revealed that a thin layer of adhered material had indeed formed on these tools in the transitional region. These adhered material were preferably located in the formed ridges of the transitional region, i.e. the beginning of the 3rd wear band. Remarkably, it did also appear that some material, seen as small particles about in the nano-size, were located inside of the alumina matrix.

Because the tools from DP3 (where no liquid coolant had been used) demonstrated a similar tendency for the adhesion of foreign material on their rake faces, it was deemed that this material could not origin from the cutting fluid in the form of a possible contamination. Rather, the results strongly indicate that this material originated from to the workpiece material itself.

➤ When the adhered material on the tools were reviewed using EPMA, it was found out that its elemental composition consisted of various different elements, including Ni, Cr, Ti, Mn and Mg. These elements seemed to be surrounded by the elements Ca, Mn, S, Al and O.

All elements were mostly homogenously scattered across the tool surface; however, their respective concentrations at different locations seemed to differ. In addition, the relative amounts of each detected element also differed.

Because most of the detected elements may be directly localised to the steel's non-metallic inclusions, these findings suggest that the foreign material observed on the tools originates from these.

➤ When the tools were evaluated using Auger-spectroscopy, which is a highly surface-sensitive technique, some remarkable results were obtained. The results indicated that a significant amount of calcium were present inside the topmost part (~0.5 μm) of the alumina coating-layer on the tools from DP2 and DP3 but not from DP4. These results are interesting, since they are contradictory to the general belief that alumina are chemical inert during machining. Moreover, these results might indicate that a reaction occurs between the inclusion layer and the alumina coating (as discussed later).

➤ The XRD-analysis, which were used to support the characterisation of the adhered layers from AES and EPMA, did not reveal any presence of calcium-containing phases on its surfaces. Besides two unidentified peaks, which could resemble the possible presence of steel, the obtained diffractograms only gave responses to the presence of Al_2O_3 and $\text{Ti}(\text{C},\text{N})$, which are parts of the tools coating layers.

However, some interesting findings could still be made from the XRD-analysis. First, both obtained diffractograms demonstrated an increased level of background noise (and lower signal-to-noise ratio), which can be seen from the elevated base-line position. In addition, both obtained diffractograms also demonstrated the presence of a diffuse peak located at about 30° angle. Combined, these results indicate that a semi-amorphous (i.g. nano-crystalline) and/or amorphous phase may be present in the analysed tool samples.

8.2 Analyses of the results

The combined results from this thesis strongly suggest that a significant part of the wear that had appeared on the tools might be directly derived to the steel's inclusions. In addition, significant differences in the results were obtained when comparing the tools machined from DP2 (Ca-treated) with the similar tools from DP4 (not Ca-treated). Thus, the obtained results seem to depend on whether the machined workpiece material had been Ca-treated or not.

This suggest that calcium, as an element, may play an important part in how the wear develops on the tools used in the performed turning test. This conclusion, along with the observation that the steel's inclusions are important to the wear, are strengthened by the fact that:

- ✓ The adhered workpiece material, which had an elemental composition closely resembling to the ones found in the steel's inclusions, were present in the region of the tools where most wear had occurred initially. These adhered materials did also contain a large amount of calcium and sulphur, elements that from previous chemical analyses (Table 6.3) has been found to be abundant in the inclusions present in the machined SS2541 steel.
- ✓ Calcium was found to be present inside the alumina coating in the evaluated tool from DP2, but was not however found in the tools belonging to DP4. Additionally, the fact that calcium was also detected in the alumina layer in the tools from DP3, where no cutting fluid had been used, implicates that this calcium *did not* originate as a contamination from the used cutting fluid. Rather, the results indicate that the detected calcium indeed stems from the steel's inclusions.
- ✓ The 3rd wear band of the tools from DP2 and DP4 had a slightly different appearance. The tools machined in DP4 (not Ca-treated) demonstrated a larger tendency for layer formation than for DP2 (Ca-treated). Moreover, the tools from DP4 had a 3rd wear band that appeared to be more smooth and more broadened, which was evident from surface profilometry and SEM investigations. Since the cutting conditions for these two different machining test were exactly the same, the different appearances of the tool surfaces might therefore be related to whether the machined workpiece material had been Ca-treated or not.

- ✓ Calcium seems to accumulate on the tool surface although it exists in relative small amounts in the workpiece materials (*Table 6.1*). In addition, the amount of calcium in the machined steel materials differs depending on if the steel had been Ca-treated or not. The Ca-treated steel contained about 67 % more calcium than the non Ca-treated steel. Thus, a significant difference in the chemical properties for the Ca-containing inclusions in the Ca-treated steel should be expected compared with the non Ca-treated. This might explain why calcium was detected only in the tools from DP2 (Ca-treated) but not in the tools from DP4 (not Ca-treated).

Many of these observations are in accordance to the available literature concerning the wear of cutting tools when turning different steel grades, as have been described earlier in the sections 4.1.1 and 5.1 of this thesis.

Indeed, the nature of calcium, i.e. whether it acts detrimental or beneficial to the wear resistance from the tools, is an abstruse topic that has been discussed for more than 50 years in the literature. Since the opinions of this element is clearly divided among many authors in the field, it has been the ambition for the author of this thesis to try to disambiguate this topic to the furthest extent possible.

In this regard, it should be noted that the results from this thesis by itself cannot conclusively determine the exact nature that calcium has on the wear behaviour from the tools. Further investigations on this topic are still needed to be made. Some of these would likely require the use of highly sophisticated analytical techniques, such as transmission electron microscopy (TEM). This instrument could provide with much more detailed information about the worn rake faces of the tools. This instrument was not available during the course of this thesis.

Nevertheless, the combined results from this thesis do provide with many indications and clues on how calcium may influence the wear of the tools. Furthermore, the findings presented from this thesis might also contribute with the framework needed to give a comprehensive explanation on how the steel inclusions may participate in the wear of the tools.

In short, the results from this thesis indicate that calcium-containing inclusions, as found in the low-alloy SS2541 steel, might be detrimental for the overall wear resistance of the alumina coated tools. This might be explained from two possible ways, namely:

- I. By promoting a possible chemical wear mechanism in the 3rd wear band of the tools' rake faces.
- II. Act as a strong indication that a phase transformation of the alumina coating occurs, which further suggest that a superficial plastic deformation of the coating layer takes place.

8.2.1 I. – Possible chemical wear

The possibility for an occurring chemical wear mechanism of the tools' alumina coating has been commonly rejected in the literature on account for alumina's well-known and commonly accepted chemical inertness[34,38,92].

However, it is important to note that the term 'chemical inert' does not necessarily imply that the material in question is completely immune to undergo any form of chemical reaction. Rather, the term implicates that the material possesses a steep energetic barrier for a reaction to occur. In ordinary conditions, this means that the reaction rate for this material is very slow, though this might be greatly changed should the material be influenced by external conditions. Such conditions typically include applied mechanical stresses, high temperatures/pressures and large concentration differences between reacting elements. As remarked earlier in this thesis, many of these mentioned conditions are both present and severe during the machining of steel materials. For this reason, the aversion of alumina to undergo a chemical reaction during the machining of steel is a statement that may not stay completely true for metal cutting applications.

Nonetheless, there are remarkably little experimental evidence, if even any, present in the literature that may actually prove that a chemical reaction occurs in the alumina coating when machining of steel. In particular, few authors have been able to provide with reliable evidence suggesting that the calcium-rich inclusions may react with the alumina coating.

Frequently, many authors have ascribed the presence of the formed Ca-rich inclusion layers as a strong indication for a chemical wear mechanism to occur[43]. However, this does not actually verify that a chemical reaction is occurring, since it does not provide with any evidence for a 'chemical intermixing' to be present between this formed Ca-layer and the alumina coating. For machining applications, such chemical intermixing arises due to a solid-state reaction, i.e. a diffusion of solid species from the workpiece material that diffuse into the alumina coating, or vice-versa.

Accordingly, experimental results that may provide with evidence for this chemical intermixing to occur would act as one of the strongest indications that a chemical reaction of alumina is possible. Moreover, since the presence of a chemical reaction is deemed as a prerequisite for a chemical wear mechanism to occur, any such evidence would also support the theory that the diffused species are acting detrimental on the tools' wear resistance.

Therefore, the results from the performed AES investigations in this thesis (section 7.7.2) are particularly interesting, since they are able to show that a significant amount of calcium was present inside the topmost part of the alumina coating. These results have been verified on three different tools (both etched and unetched) belonging to DP2, which has been carried out on three separate and independent occasions. All these conducted measurements provided with the similar results, i.e. the significant presence of calcium inside the alumina coating layer of the examined tools.

These findings are interesting, as they do not only provide with strong evidence for a chemical reaction and hence possible chemical wear, but also because it has, to the authors best knowledge, not previously been published in the available literature. Assuming that these results are further repeatable and verified, they would challenge the common conception that alumina is chemical inert during the machining of Ca-treated steels.

Assuming that a chemical wear mechanism is present in the alumina coating, then a significant difference in the wear rate of the tools should be observed at varying cutting speeds. This is because this cutting parameter mainly governs the arisen temperatures at the tool-workpiece interfaces. Although no machining test were performed in this thesis using different cutting speeds, the results from DP3 may give a good answer on how the temperature influenced the wear of the tools. Since no coolant media was used in DP3, the temperatures reached in the tool-workpiece interfaces in this particular test are expected to be much higher than for the rest of the performed turning tests.

Accordingly, by comparing SEM images of the rake faces of the tools machined in DP2 and DP3 (*Figure 7.2* and *Figure 7.3*) it becomes evident that the tool belonging to DP3 had worn much quicker. This can be seen by the more progressed exposure to the underlying Ti(C,N) coating layer, i.e. the larger “white band” formation, on the DP3 tool. Since the temperature reached in the tool-workpiece is the only significant aspect differencing DP2 from DP3, it may be concluded that this increase in wear is mainly a temperature-governed process. This notion would then favour the presence of a chemical wear mechanism, which indeed is a highly temperature-dependent wear mechanism (as described in *Section 2.4*).

In addition, the influence of the temperature to the wear of the tools is also highlighted by the fact that the exposed Ti(C,N) layer had occurred slightly lower on the tool belonging to DP3 (*Figure 7.3*), and was thereby mainly located in its 3rd wear band. This was a clear deviation in comparison with the tools belonging to the other performed turning tests. The relocation of this exposed Ti(C,N) region did also seem to occur without any apparent alteration of the other wear features of the DP3 tool, such as the development of its three wear bands. It is noted that these bands did appear on all of the tested tools regardless of what cutting test they belonged to.

Therefore, the change in position for this exposed Ti(C,N) layer seemed to have occurred independently from the mechanisms governing the formation of the three wear bands. By knowing that the position for this exposed Ti(C,N) layer appears to be highly temperature-dependent, it further suggest that the a chemical wear mechanism may be one cause for this exposed Ti(C,N) layer.

Lastly, a notion should be made regarding the relative position for the detected calcium in the AES-investigation and how this may correlate to a suggested chemical wear mechanism. It is briefly recalled that calcium was only detected by AES in the lower regions of the 3rd wear band, and not in its topmost region where the most wear and exposed Ti(C,N) layer had mostly appeared on the tools.

The reason why no calcium was detected in this concentrated wear region may be explained by the fact that the Al₂O₃-layer was thinner in this region, suggesting that the calcium-contaminated surface had simply been worn away. This could potentially be due to a chemical-dissolution mechanism as proposed by some authors[43].

However, this might be very hard to prove experimentally. This is because (a): the very low detection limits and analytical thresholds needed to detect tool fragments in the formed chips and (b): accurately determine if these chemical phases actually originate from the cutting tool.

One suggested method, albeit perhaps being a rather complex one, to further prove the existence for a chemical wear mechanism would be to utilize energy filtered transmission electron

microscopy (EFTEM). With this technique, highly magnified elemental mappings of the concentrated worn area of the tools could be made. This might reveal any presence of a chemical wear of the tools. Such technique has previously been employed in the determination of a chemical wear mechanisms on cubic boron-based tool inserts when machining steels. [93].

8.2.2 II. – Indication for a phase transformation of alumina

In the previous section, it was shown that a chemical wear mechanism of the alumina coating might be a plausible wear feature of the tools when machining Ca-treated steels. Nevertheless, the continuously reported chemical inertness of alumina, made by many authors in the field, still contradicts this proposition.

This inconsistency should not be neglected. In fact, the reason to why alumina has been deemed as the “material-of-choice” in wear-resistant coatings for steel machining has mainly been based on its well-known chemical resistance. Since experimental evidence from this thesis suggest that calcium is able to diffuse into the alumina coating, which hence acts as strong evidence that a chemical solid-state reaction actually occurs, a credible explanation on how this reaction might occur must be given.

From an interdisciplinary point of view, it appears that the observed reactivity of alumina towards calcium might be explained due to structural phase transformation of the alumina, which is likely caused from a plastic deformation of this coating layer. Such phase transformations of alumina has, to the authors knowledge, not been thoroughly investigated in the literature concerning metal cutting applications. However, it has been demonstrated from other scientific fields that alumina’s reactivity increases for its nano-crystalline[94] and possibly also amorphous state. Besides alumina’s crystalline α -phase, it has been reported that alumina may be stabilised in an amorphous phase[45].

For example, alumina is commonly used as a biomaterial in living systems, in which a good bio-compatibility between this material and the living tissue is essential. In this field, it has been reported that conventional polycrystalline alumina is bio-inert, i.e. unable to interact with living tissue, whereas its nanocrystalline structures, on the other hand, are bio-compatible and able to react with other elements. In particular, an increased reactivity of nano-crystalline alumina has been reported towards hydroxyapatite, which is a highly calcium-rich mineral commonly found in bone tissue.[94] Thus, these findings might be adopted to explain the presence of calcium inside the alumina coating of the machined tools, as demonstrated from this thesis.

In other words, this suggests that the reaction between the alumina coating on the tools and the calcium-containing inclusions in the Ca-treated steels are enabled due to a structural phase transformation of the crystals in the alumina coating.

Although no unequivocal conclusion for the presence of such phase transformation can be made from the results in this thesis, there are indications from the performed XRD-analyses that may suggest that such transformation may exist. This is seen from the obtained diffractograms, which revealed not only a clear increase of the background noise (and thus a decrease in the signal/noise-ratio) but also both contained a diffuse, unidentified peak-signal at 30° angle. These observations support the presence of a semi-amorphous and/or nano-crystalline phase in the examined tool specimens.

However, one should note that the causes for an increased background noise in XRD may have several possible causes, and that these results by themselves are not enough to support the theory that such phase transformation exist in the machined tool samples. Since these phase transformations are quite subtle and surface-localised, and because they occur on a small atomic scale, it seems that high magnification TEM-investigations are the primary choice for further investigations of this matter.

Interestingly, recent reports concerning the tool wear on textured alumina coatings have demonstrated from TEM-evaluations that these layers may undergo a structural nano-crystalline phase transformation. In one article, presented by Roland Bejjani and Marianne Collin from Sandvik Coromant, a nano-crystalline alumina layer was found in the topmost part of this coating, after machining low-alloy SS2541 steel[27]. These recent findings support the belief that the textured alumina-coating may have undergone this type of structural phase transformation in the performed turning tests from this thesis as well.

In addition, it may be demonstrated theoretically that such phase transformation of textured alumina is not only possible but also highly likely to occur during a machining process. This insight has for this thesis led to the development of an entirely new, detailed and comprehensive wear model that may describe how these tools wears on an atomic scale. Furthermore, this model puts an extra emphasis on the role of the inclusions found in the steel, and how these may influence the wear. This model is presented in the following *Section 8.3* of this thesis.

It should be emphasised that this model does not necessitate the presence of calcium in the alumina coating layer in order to be valid. Rather, the model can provide with a detailed explanation to why calcium may diffuse into the damaged and nano-crystalline alumina layer.

8.3 Amorphous transitional breakdown model

In the literature, there have been several different models and theories proposed to describe how alumina-coated tools wear when turning different steel grades. These different models may be grouped as:

- The superficial plastic deformation model
- The abrasive model
- The chemical-dissolution model

From a tribological point of view, these models are all related by their attempts to comprehensively explain the characteristic ‘scorns’ and ‘ridge-like’ wear patterns that tend to appear when steel workpiece materials are being machined. On the rake face, these wear patterns arise exclusively in the 3rd wear band of the tools. As have been demonstrated in the results of this thesis, this area corresponds to the region where the wear seems to be the most pronounced on the machined tools, both initially and at the end of their lifetime. Thus, it may be concluded that the expansion of the 3rd wear band, along with the tribological mechanism(s) that occurs in the beginning of this band, are the most important factors that determines the continuous wear of alumina-coated cutting tools when machining steels.



Figure 8.1. Illustration of the three main models acknowledged for describing the wear behavior of alumina-coated tools during metal cutting applications. Each model is here regarded as stand-alone models with little dependency of one another.

Even though all of these presented models aim to give a plausible explanation for the arisen wear patterns discussed above, they still lack many details to give a full, comprehensive description of the link between these arisen wear patterns to the macroscopic wear behaviour of the alumina coated tool. All of these models contain their individual limitation(s) that needs to be addressed. For example, the superficial plastic model, originally introduced by Dearnley[79], cannot thoroughly explain why deformation is only localised to the topmost parts of the alumina coating.

Similarly, the chemical dissolution model, acknowledged by authors such as Barry and Byrne[43], has shown to have very limited experimental evidence. This idea is also commonly rejected due to the general opinion that alumina is chemical inert in metal cutting applications.

Lastly, the abrasive model[13,27,77], which present a reasonable experimentally-based model that the river-like patterns are caused by the sliding of hard inclusions, also have its limitations. In essence, this model cannot entirely explain the ordered, alternating lamellar structure having a high aspect ratio that indeed characterise this wear region. First, if it were true that these wear patterns had arisen solely due to the sliding of inclusions, then a more chaotic and less ordered scratch pattern had been more likely to appear. This is due to the effect from free-rolling particles ('third-body wear'). In fact, even an impingement of these inclusions, which would cause so called 'two-body abrasive wear', would not seem to be likely to produce this microscopically well-arranged pattern. It is recalled that this worn area in the 3rd wear band of the tools (DP2) demonstrated a nearly identical depth from its ridges and also a similar spacing between them (see *Figure 7.3*).

Furthermore, all of these varying models have so far appeared to presented as a "stand-alone" explanation for the arisen wear patterns of the machined tools. Few attempts, if even any, have yet been made by scientists to link these models with each other, and even fewer have opted for discussing the possibility that they may coexist during the machining process. Rather, scientists have chosen to argue that these independent models occur solely as 'either-one'. This has likely contributed to the many divided opinions for the models that exist to describe the wear behaviour of these types of alumina-coated tools.

However, the deformational behaviour of alumina has actually been thoroughly investigated in many other scientific areas. These include, for example, its possible usages as a protection from ballistic projectiles. In these fields, a different approach has been adopted to explain the behaviour of alumina.

This approach mainly focuses on the properties of alumina as a ceramic material, linking its behaviour to its crystal structure and the atomic mechanisms that occurs in its lattice during the influence of large stresses, temperatures and/or pressures. To the author's knowledge, such a profound explanation has not yet been invoked to explain the wear of alumina in metal cutting applications.

Therefore, the reader will here find one of the first models presented that links the arisen wear patterns and corresponding wear behaviour of alumina to its atomic arrangement and crystal structure. The model is based on the mechanisms that occurs in alumina's lattice during deformation, and also constitutes to one of the first attempts made to link the previous presented models to this underlying one. It is emphasised that many of the erratic behaviours of alumina, along with the limitations from the previous presented models, may be explained from this new model approach.

The model presented in this thesis is based on an interdisciplinary literature review, and is therefore not entirely based from the experimental results obtained in this thesis. This would have required investigations using highly detailed TEM-equipment. However, many of the references presented to support this new model have used TEM-investigation to support their respective findings.

The model has been named as “Amorphous transitional breakdown model” (abbreviated as ATBM) and may be summarized by the following five individual steps:

- I. Plastically-induced shear deformation from the activation of predominantly basal slip systems, which causes basal twinning and stacking faults on α -Al₂O₃'s (0001) plane.
- II. Activation of pyramidal slip systems due to shock-induced strain rates, caused by the sliding of abrasive particles (inclusions) across the top-surfaces of the alumina crystals.
- III. Nano-crystallisation and/or amorphisation, due to a shuffling of the cationic arrangement in the alumina crystals' interior.
- IV. Formation of micro-cracks due to dislocation pile-ups, decreased plastic resistance for the alumina crystals in the coating and possible chemical wear.
- V. Coupling of microcracks, resulting in accelerated tool wear and subsequent failure due to excessive wear.

8.3.1 General description of slip and dislocation movement

In order to fully understand the model describing the wear of alumina, one has to consider the deformation of the material on an atomic scale. This inevitably requires the introduction of concepts such as dislocation movements, slip systems and critical resolved shear stresses, which will be briefly introduced to the reader in this section.

The deformation of materials on an atomic scale is generally governed by the coordinated movement of various types of defects that are present in the material's lattice structure. These defects are known as *dislocations*, and the movement from these dislocations are ascribed to the permanent plastic deformation of solid materials.[95]

In materials, the movement from these dislocations (known as '*slip*' or '*glide*') tend to occur in different predefined *slip systems*, which are composed of a *slip direction* and a *plane* where the dislocation is moving in.[95] For polycrystalline materials, it is usually considered that a total number of 5 independent slip systems must be simultaneously activated in order for uniform plastic deformation to occur. This criterion is known as the *Von Mises criterion*[43].

However, in the case of textured materials, the number of available slip systems for an applied load direction are greatly limited, which alters the possibilities for these materials to undergo uniform plastic deformation. These materials may therefore deform in quite complex and unexpected ways. For example, such materials may display unusual plastic behaviours that are not ordinary attributed to the material's polycrystalline phases. In addition, many materials having a h.c.p structure, which includes most ceramic compounds, already have a limited number of available slip systems to begin with[96].

Alumina have been identified to possess three different kinds of slip systems, which are denoted as *basal*, *prismatic* and *pyramidal*, depending on what geometrical plane the dislocation moves in into the crystal.[52]

During the influence from an applied load, these different slip systems will be more or less easily activated, depending on how effortlessly it is for the dislocations to move in this particular slip system[97]. This may depend on aspects such as interplanar distances between atoms, sterical hindrances, electrostatic repulsions etc. These factors induce forces that opposes the movement from dislocations in the crystal. Therefore, the combined forces that impede the movement of dislocations in the crystal, and are thus needed to move the dislocation in the plane, are known as *Pierls-Nabarro forces*. [97]

Slip is initiated when these Pierls-Nabarro forces are overcome in the crystal, which occurs at a critical stress level known as the '*Critical Resolved Shear Stress*' (CRSS)[97]. The value of the resolved shear stress, in turn, is determined from *Schmid's law*, given as

$$m = \sigma \times \cos(\phi) \times \cos(\lambda) \quad (\text{eq 8.2.1})$$

Where σ is the stress applied, ϕ is the angle of the slip direction and the slip plane's normal, and λ represent the angle between the applied stress and the slip direction.[97] The slip system first reaching its CRSS-value is the one who is first activated[97].

For alumina, the slip system having the lowest CRSS is the basal slip[48], occurring at the plane perpendicular to the [0001] direction (i.e. the basal plane), followed by prismatic slip and lastly pyramidal slip. The pyramidal slip system is generally considered to be the hardest slip system to activate in the alumina crystal. An approximate description of the direction of this different slips are given in *Figure 8.2*.

External factors, such as temperature and induced pressures, are known to influence the CRSS needed to activate any of the mentioned slip systems found in alumina. Moreover, these external factors may also alters the order in which they occur in the crystal.[52].

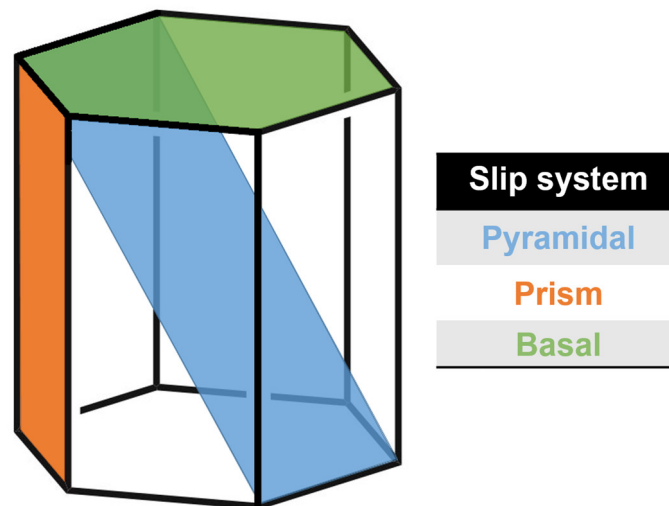


Figure 8.2. Schematic illustration depicting the three different available slip systems (pyramidal, prismatic and basal) present in the α -alumina crystal. Their geometrical expansion and direction is viewed in the figure. At elevated temperatures, such as the ones reached in a metal cutting procedure, the pyramidal slip system is the hardest one to activate, followed by prismatic and then basal.

8.3.2 I – Shear deformation and basal twinning formation

The compressive strength of an alumina single-crystal is approximately ~3 GPa, depending on its orientation[54,98]. This value is, however, greatly reduced if the material is influenced by high temperatures and pressures. As earlier described in this thesis, such conditions may be induced on the tool's alumina-coated rake face during the turning of different steel materials.

During these conditions, the CRSS for the available slip systems in alumina are greatly reduced and slip is thus more easily activated. Accordingly, the induced compressional stresses acting on the tool's rake face during a machining process will be enough to surpass the alumina-coatings compressive strength. This will initiate a shearing of the alumina crystals topmost (0001) planes. This shearing is caused by an activation of alumina's most energetically favoured slip systems. At elevated temperatures, these systems predominantly corresponds to the basal ones[52,99].

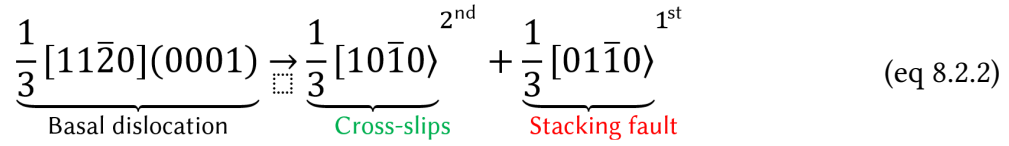
Once these slip systems are activated, the basal dislocations will start to migrate across the alumina crystal's topmost parts. These dislocations will move at directions perpendicular to the crystals growth direction, i.e. the [0001]-direction, which is also known as crystal's c-axis (see *Figure 3.2*).

On an atomic scale, the migration of these basal dislocations have been thoroughly investigated by many authors, both experimentally and theoretically, by employing highly sophisticated TEM-investigations[100]. Now, in accordance to the model originally presented by the authors Bilde-Sørensen, Pirouz and Lawlor and Geipel *et al.*[52,99,100], the movement from these basal dislocations may be regarded as a displacement of Al^{3+} cations in a single dimensional direction, i.e. the basal slip direction. This is because the basal slip plane lies right between two puckled Al^{3+} cation layers in the crystal's stacking sequence[48,51,52]. Since these cations are, in turn, surrounded by three oxygen anions, the displacement of the Al^{3+} cation will be accompanied by a stretching of the Al-O bond distances in the alumina crystals found in the alumina coating[52].

However, the extension of the atomic positions caused by the movement from these basal dislocations are actually quite confined, due to the electrostatic interactions[46] that exists in the alumina crystal. The Al^{3+} cations can only be displaced a certain length in the crystal, but no longer, since this will put two Al^{3+} in too close proximities to one another. Such configuration induces excessively large Pierls-Nabarro forces in the lattice that acts as an effective energy-barrier. This barrier impedes the further movements from basal dislocations that are moving in the same crystallographic direction.[99,100]

Therefore, once these Pierls-barriers are formed in the slightly sheared alumina crystal lattice, it becomes more energetically favourable for the basal dislocations to change their slip direction, and move to other available slip planes. This is achieved from a process known as cross-slip, in which the basal dislocations may move to a prismatic slip plane to further continue the shearing of the crystal. This process is favoured by the fact that not all octahedral holes of the alumina crystal are filled. The empty octahedral interstices act as vacancies which facilitates this cross-slip process for an 'stationed' basal dislocation.[99]

Hence, shearing from activated basal dislocations is described as a two-step process in the deformed Al₂O₃-crystal, in which the original basal dislocation is dissociated into two acting partials[48]. To exemplify, this may in crystallographic notions be described as



Where the 1st partial shears the alumina lattice and causes a stacking fault[48,51], and the other partial may *cross-slip* to a prismatic slip plane and continue the shearing of the crystal.

The stacking fault means that the stacking sequence of the alumina crystal changes, due to the coordinated movement of cations caused by the movement from the 1st partial dislocation[52]. It is emphasized that the 2nd formed partial cannot move in the same slip direction as this first partial. This is due to the large energy barrier that is induced from this arisen stacking fault.[51,99]

As a result of the cross-slip, a pinned L-shaped screw dislocation is formed lying both in the basal plane and the prismatic one[48]. This screw dislocation may act as a so called Frank-Read source that, under an applied stress, may induce the repeated formation of new dislocations lying in the same crystallographic plane.[51] Metaphorically, this occurs in a similar manner as how ripples are formed on water, i.e. by the formation of continuously expanding loops.[48,99]

The generated dislocations from this pinned screw dislocation cannot, however, converge in the same crystallographic plane. This is once again due to energetic reasons[99]. Instead, they may undergo a special type of cross-slip[101], referred to in literature as a *Friedel-Escaig mechanism*[102,103], where two dislocations undergo a synchronous double cross-slip to form a new, pinned dislocation segment. These may then again act as a new “Frank-read source” to repeat the dislocation process as previously described.[99]

As a result, a stair-like and alternating appearance of the alumina topmost surface takes form, which are composed of nano-thin, lamellar-like bands that are (i) equally spaced[51] and (ii) extended in a similar crystallographic orientation[104]. These bands are referred to in literature as *twin bands*[105], and the formation process to create these bands, as described earlier, is known as *basal twinning*[51,52,56].

The repeated cross-slip and Frank-Read formation in the alumina crystals causes a thickening[105] of these formed lamellas[48,51], which hereby eventually makes them macroscopically visible[99]. Thus, this might explain the appeared ridge-like morphology from the 3rd wear band of the tools.

Furthermore, because the bands are formed in pairs[51] (due to the double cross-slip) and provides an energetically necessitated pathway[51,101] for the basal dislocations to move into, they may extend themselves a significant distance in the topmost part of the alumina coating[106]. This is a presumed explanation for the surprisingly high aspect ratio of the lamellas seen in this third wear band of the worn tools.[104]

In addition, an explanation to why deformation is localized to the topmost part of the alumina coating may be based on the fact that the basal twinning formation mechanism forms many surface-localised and crystallographically constrained dislocations[106]. In other words, the basal twinning formation produces dislocations that lies mainly in the same crystal plane. The activity from these formed dislocations are much higher close to the alumina coatings top surface than to its bulk, due to the decreased coordination number of the atoms in this part of the coating.

8.3.3 II: Activation of pyramidal slip systems due to the sliding of hard inclusions

Among the three different kind of slip systems that exist in the alumina crystal, it is generally found that the pyramidal slip systems are the ones being the most difficult to initiate[54]. These type of slip systems are rarely seen to be activated from a compressional load only. From molecular dynamic simulations[51,101], it has been shown that extremely high temperatures and large stresses are simultaneously required to initiate these systems from a compressional load. The temperatures needed are typically close to alumina's melting point, and the stresses needed are in the magnitude of more than 10 times the value for the maximum compressive strength of alumina. Although it is true that the conditions at the tool-workpiece interface are severe, it is unlikely that such extreme conditions are induced on the tools from an ordinary steel machining process.

However, the pyramidal slip systems can actually be activated from other type of induced stresses in the alumina crystal. For example, it has been continuously reported in literature that these slip systems are activated if the alumina crystal(s) are subjected to the rubbing of hard, sliding, abrasive particles. In fact, the activation of these slip systems may occur even in spite that no compressional stresses are being applied to the alumina crystals. Hence, some authors that has discussed the activation of these pyramidal slip systems have even refereed this mechanism as "the *mild* wear of alumina".[54,106]

There are two principal reasons that can explain why these pyramidal slip systems are difficult to initiate from a compressional load only, and why they may instead be activated from the sliding of hard particles. First, as viewed in the *Figure 8.2*, the pyramidal slip plane intersects the intrinsic parts of the alumina crystal lattice in a diagonal direction. This means that the dislocations that moves in this plane are greatly affected by the electrostatic and sterical hindrances that are found in the interior of the alumina crystal[46]. As a result, the dislocations moving in these pyramidal planes must surmount very steep Piers-Nabarro barriers. This is highly unlikely, unless the temperatures and stresses induced in the crystals are extreme (as previously mentioned).[51]

Secondly, the movement from the dislocations on these pyramidal planes occurs in a very narrow angle that is close to the same direction as for the applied load. In accordance with Schmid's law (formulated in eq 8.2.1) this results in a very low λ -value that are close to or nearly equal to zero. Consequently, this results in a very low value for the RSS, i.e the resolved shear stress, which means that there is a large unlikelihood that these slip systems will be activated in the crystal.

Considering both these factors, it may appear surprising that these pyramidal slip systems actually can be activated in alumina from a machining application. To understand why these still may be activated, one must look into the atomic structure of alumina.

Most ceramic materials, including alumina, are highly sensitive against thermal and mechanically induced shocks. That is, large rapid pulses of energy that originates from a mechanical and/or thermally applied peak load.[41,98,104] This is particularly true for textured alumina, which transmits energetic disturbances unevenly across its atoms in its crystal lattice. This is due to alumina's crystal structure and to its anisotropic material behavior[51].

Accordingly, when a hard particle (such as an oxide-based inclusion) slides across the top surface of the alumina crystal, it may induce a sharp, large and instantaneous peak load to the crystal's interior.

Because this load only acts for an extremely short time interval, supposedly less than a fraction of a second, the detrimental forces developed within the crystal may be enormous. This is illustrated by an extremely high *strain rate*, which mathematically is expressed as

$$\dot{\epsilon} = \frac{v}{r_a} \quad (\text{eq 8.2.3})$$

Where v is the velocity of the sliding particle and r_a the width of the formed groove caused by this particle, i.e the relative radius of the inclusion[54]. Even though the sliding velocity for the abrasive particle may be relatively moderate from a macroscopic point of view, the small size of the inclusion (typically in the size of a few μm) will cause the development of strain rates reaching a magnitude of 10^6 s^{-1} . Such extremely high strain rates develop forces within the crystal that are significantly larger than those commonly reached from a continuous applied compressional load only. Hence, these developed strain rates are efficiently able to shock the comprising atoms inside the alumina crystals. This will hereby activate the pyramidal slip systems.[54]

The pyramidal slip systems, which acts as the last remaining slip systems for the alumina crystal, are essentially needed for the crystal in order to handle these developed peak strains. The large and rapid energetic disturbances caused by the sliding from hard particles cannot be efficiently transmitted nor removed from the already activated slip systems. This energetically necessitates the activation from these pyramidal slip systems in order to relief the crystal from these experienced peak loads[51].

Moreover, it should be mentioned that the critical resolved shear stress for the available slip systems in most crystal structures are greatly affected when experiencing high strain rates. Therefore, a significantly large strain rate will be able to drastically lower the CRSS for the available pyramidal slip systems in the alumina crystals which makes them easier to activate.[54]

In summary, the sliding of hard particles on the top surface of textured alumina causes sharp, intense and instantaneous increases to the strains experienced within its crystals. These strains develop forces in the crystal lattice that cannot be resolved by the already activated slip systems. Hence, this necessitates the activation from the pyramidal slip systems in order to resolve these developed forces to the alumina crystals.

8.3.4 III: Nano-crystallisation and/or amorphisation

The activation of the pyramidal slip systems, which are normally inoperative in the alumina crystal even at large compressional stresses, are known to cause a dramatic disturbance to the crystals interior parts[51,101]. Specifically, the movement of dislocations in these pyramidal planes have in literature been demonstrated to induce some severe phase transformations of alumina[51,104,107]. In these phase transformations, alumina loses most of its ordered appearance and adapt a nano-crystalline and/or amorphous appearance. Also, these phase transformations are accompanied by a drastically change of alumina's chemical and mechanical properties. As have been previously described in section 3.3 in this work, these material properties are highly related to the appearance of alumina's crystal structure.

The full details on how this amorphous transition occurs are still not entirely understood[49]. However, since it is known that the cationic arrangement inside alumina is vital for its geometrical structure of its crystals [44], it is likely that a migration from the cations inside these crystals may enable for this transition to occur. Based on this notion, a hypothetical explanation for the amorphous transition of alumina may be given. A schematic description of this procedure can be viewed in *Figure 8.3* on the following page.

When dislocations move along a pyramidal plane, they are able to cause a “synchro-shear[52]” to the alumina crystals' cationic interior, meaning that a synchronous movement between cations and linked anions will occur in the crystal. Since aluminium ions are located close to the pyramidal slip systems[44], the movement from any dislocation in this plane will cause some large electrostatic disturbances to these cations[52]. These disturbances force the cations to migrate in the lattice at random directions, which are done by either switching their octahedral positions to vacant ones or, alternatively, taking positions into some of the tetragonal vacancies that are available in the crystal.[44]

The effect from the migration of the cations are twofold. First, the displacement of these cations causes a subsequent rearrangement of the oxygen anions surrounding these migrated Al^{3+} -cations[44,105]. Since the cations move at different directions due to short-range diffusion[44], the displacement of the oxygens will occur randomly, resulting in a large variation of bond angle distribution in deformed alumina[49]. This means that parts of the alumina crystals will lose their long-range periodicity and ordered appearance. Thus, this contributes into an overall amorphisation of the material.

In addition, some of these cationic migrations will cause a far too great strain on the Al-O and Al-O-Al bonds present in the material. Consequently, these bonds will dissociate[44,51], which favours the fracturing of some alumina crystals into smaller nano-crystallites[107].

In other words, the movement of dislocations on the pyramidal slip planes will cause a ‘cationic shuffling[52]’ of the interior parts of the deformed alumina crystals. This may induce an overall amorphisation of the material along with a nano-crystallisation[107] due to the rupturing of highly strained Al-O bonds.

As a consequence of this “cationic shuffling”, the bond length of the atoms in alumina, as well as its interatomic spacing between neighbouring atomic planes[57], will start to vary in the crystal[49,108]. In particular, the nano-crystallisation will leave a large part of the ruptured Al-O bonds with undercoordinated atoms in the alumina lattice[51,101]. Due to the missing atoms adjacent to these undercoordinated atoms, an increased number of voids will fill the

deformed alumina crystal's structure[49,51]. This will lower the materials density and hence also its mechanical properties[49], making the alumina crystals more susceptible for further plastic deformation.

Last of all, these undercoordinated atoms have an increased number of unpaired valence electrons which creates “dangling bonds” in the crystal structure[109]. These dangling bonds enhances the overall chemical reactivity of alumina, making what once was a chemical inert material into a more reactive one. For this reason, this might explain the possibility for calcium to react with the alumina coating that were found from the employed AES-investigations in this thesis.

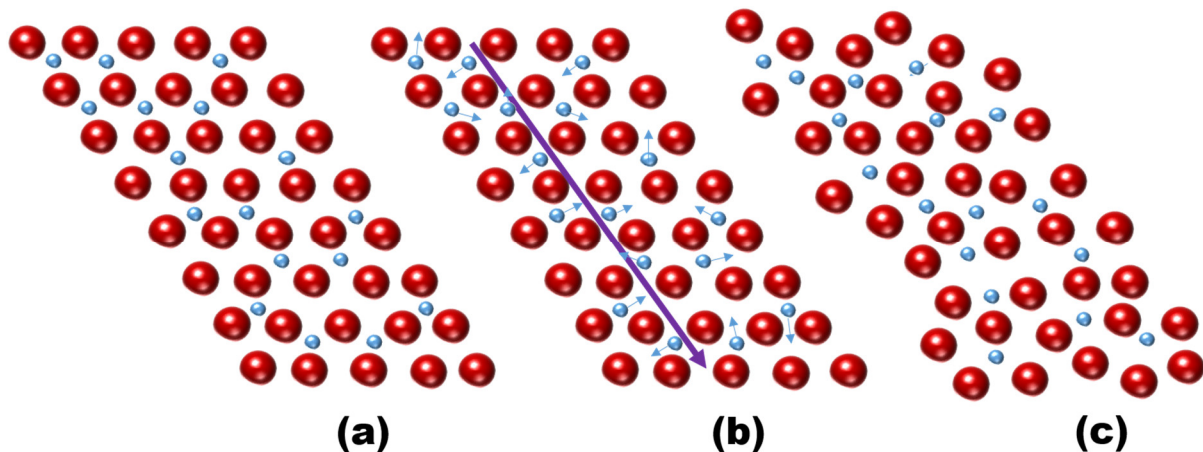


Figure 8.3. Schematic description of an induced amorphisation/nano-crystallisation in a shocked α - Al_2O_3 crystal due to the activation of pyramidal slip systems. In the figure, O^{2-} anions are shown in red and Al^{3+} cations are shown in blue. In (a) an undamaged crystal lattice is shown having an irregular stacking of Al^{3+} anions in the interior of the crystal. When a pyramidal slip is induced in (b) it causes a short-range diffusion of the crystal's intrinsic cations (i.e a “cationic shuffling”) that alters the cationic arrangement in the crystal. This leads to (c) a loss of the long-range periodicity and the short-range stacking sequences of the crystal, thus causing an nano-crystallisation and/or amorphisation of the crystal.

8.3.5 IV: Microcrack formation

As the turning process proceeds, the formed dislocations will start to gather in the grain boundaries that are found in between the alumina crystals in the coating. This causes an increased dislocation density[106] in these areas known as “pile-ups”[54]. The interaction between dislocations in these areas may act as nucleation sites for the further growth of microcracks in the coating layer[101]. These microcracks are preferably extended in the grain boundaries and will eventually cause cracking between neighbouring grains in the alumina coating[106]. It is also possible that these formed cracks may interact with the twinned surface structure of the deformed alumina crystals, which might favour their expansion and growth.[51,54,104,106]

8.3.6 V: Coupling of micro cracks and end of tool-life

At intermediate stages of the turning process, the growth of these micro cracks may extend down through the entire alumina coating layer and into the underlying Ti(C,N)-layer. At these stages of the turning process, an increased wear rate is likely to be observed due to a contribution of a chemical dissolution wear of the substrate[110]. This wear is facilitated by

the growth of these formed micro cracks, which acts as effective diffusion channels for the migration of tool elements. Hence, this contribution results in an overall increase of the observed crater wear on the tools.

Ultimately, at the final stages of the tool's lifetime, the extensive number of formed cracks will start to interact and grow together into a puzzle-like pattern. Eventually, this results in a loss of large tool fragments from the rake face and excessive crater wear.

9 Suggestions for further work

The results from this thesis, along with the model presented describing the wear process of the alumina coated tools, may present many new opportunities for the possible further research on the topic of tool wear and the machining of steels. Some of these may be summarized as follows:

- *Experimental verification of suggested wear model by employing TEM-investigations*

In order to validate the authenticity of the presented model from experimental findings, it is strongly suggested that further TEM-investigations are needed to be made. Moreover, this technique could also provide the necessary resolution to clarify many of the assertions made in the discussion part of this thesis. For instance, TEM observations may prove if a nano-crystalline/amorphous transition has occurred in the tools' coatings, if any pyramidal slip systems have been activated, if any chemical wear mechanisms is present and so on. This instrument has not been available for use during the course of this thesis.

- *Evaluation of tool wear when machining newly developed steel grades*

Newly developed, high-performance steel grades may contain very low levels of impurities and practically no inclusions in their matrix. Since it is suggested in this work that these inclusions are important for the continuous wear of the tools, it would be interesting to evaluate the tools' performance when machining these type of new steel grades. If the theory behind the presented model holds, then the abrasive wear of the tools would be suppressed when machining these materials, since there are few sliding particles that may activate the pyramidal slip systems.

10 Summary and conclusions

In this work, a detailed and comprehensive study have been made to evaluate how wear develops on the textured alumina coatings for two different cutting tool types, CNMA and CNMG, when turning low-alloy steel. Two different kind of steel materials (SS2541) have been used, one Ca-treated and the other not Ca-treated.

The work has been specifically aimed to elucidate what role the inclusions have for the wear of the tools and, in this respect, evaluate the presence of adhered layers and their possible influence for the wear. A literature review has suggested that these type of layers may both act as beneficial (by retarding the wear on the tools) and detrimental (by promoting the wear).

Four different types of turning tests have been conducted to evaluate the wear performance of the tools. In this evaluation, several different types of analytical techniques have been employed.

The results from this thesis showed that all the machined tools demonstrated a similar wear pattern after 4 min of turning. It was possible to separate the wear features on the tools into three separate, highly distinctive wear bands, numbered in order from the cutting edge and down on the tools. Among these bands it was clear that most wear had appeared in the top-most part of the 3rd wear band close to the end of the 2nd wear band. This was shown from cross-sectional SEM-imaging.

It was therefore concluded that this area played the most significant role for the continued development of wear on the tools. This was further experimentally validated by the performed longevity test (DP1). The result from this test indicated that the developed crater wear propagated from the 3rd wear band on both tool types, ultimately resulting in crater wear and failure from plastic deformation as a consequence.

All the tools machined demonstrated the smearing of workpiece materials on their rake faces. Most adhered material was found on the tools from DP3 (Ca-treated steel no coolant) and DP4 (not Ca-treated steel coolant). This was particularly evident when reviewing the tools surface topography, where it was shown that DP4 demonstrated a significantly larger amount of adhered materials on their surfaces in comparison with the similar tools from DP2 (Ca-treated coolant).

The adhered material on the tools were analysed using an electron-probe micro analyser (EPMA). This revealed that adhered materials had formed on the machined tools, in particular in the concentrated wear area, i.e. 2nd-3rd wear band. It was found that the adhered material that had appeared close to the formed ridges in the 3rd wear band contained elevated levels of various elements. This were deemed to originate from the machined steel. These elements included relatively high levels of iron, calcium and sulphur. Because calcium and sulphur are two elements that are principally found in the steel's inclusions, it was concluded that these layers originated from these.

It was difficult to deduce if these adhered layers were acting protecting or not for the tools overall wear resistance. Nonetheless, it was clear that the calcium treatment of the workpiece material played an important part on how the wear developed on the machined tools. This suggests that calcium, in particular calcium-rich inclusions, may have an important role for the wear behaviour of these alumina-coated tools.

From the Auger-investigations, it was shown that a significant amount of calcium was present in the topmost part (i.e. $\leftrightarrow 0,5 \mu\text{m}$) of the alumina coating. This result indicates that the presence of calcium in the alumina layer may be attributed to a diffusion mechanism, i.e. a reaction between the alumina coating and the calcium-containing inclusions. To the authors' knowledge, such results have not yet been presented in the available literature.

The nature of calcium, and whether this element may act as beneficial or detrimental to the wear resistance of the alumina-coating, has been thoroughly discussed. Based on the results from this thesis, it was decided that calcium was most likely detrimental to the tools' overall wear resistance. This could be due to two suggested reasons: (a) promoting a possible chemical wear of the alumina coating and/or (b) acting as an indication that a structural phase transformation of the alumina coating into a nano-crystalline/amorphous state has occurred. Such a transformation would be able to drastically increase the chemical reactivity of alumina towards other elements.

Although there are some small indications that such a transformation may have occurred from the XRD results in this thesis, it is difficult to draw any certain conclusions. Nonetheless, recent articles concerning the machining of low-alloy steel have shown that such a transformation, namely a nano-crystallisation, is indeed possible to occur in the tool's alumina coating. This supports the belief that such a transformation may have occurred in the worn tools used in this thesis as well.

Furthermore, it has been shown that such a phase transformation of alumina is possible theoretically. Based on the results from this thesis, along with a breakdown of available literature about the behaviour of single-crystalline alumina during deformation, a new wear model has been developed and presented. This model may describe how wear develops on textured alumina coatings throughout the entire machining process and is based on alumina's crystalline structure and atomic arrangement.

From this model, it is strongly emphasized that an amorphisation and nano-crystallisation of the alumina crystals may occur due to the activation of so-called pyramidal slip systems. These may be activated due to the sliding of hard, abrasive particles. When machining low-alloy steel, these mainly correspond to the steel's inherent inclusions.

To conclude, the following remarks on the following page could be made from this master thesis:

- Wear on the tools tends to concentrate in the top part of the 3rd wear band (i.e. transitional 2nd-3rd wear band region). This region was characterised by the appearance of small, alternating scorns and grooves, which formed into an ordered, ridge-like wear pattern.
- All tool samples demonstrated the presence of adhered workpiece material that formed into smeared layers on the tools. These layers were found to contain a large mixture of different elements. EPMA revealed that they mostly contained iron, sulphur and calcium.
- Auger-measurements demonstrated that a significant amount of calcium was found inside the alumina coating of some of the tested tools. This indicates that calcium may react with the alumina coating through a solid-state reaction (i.e. diffusion). It further suggests that crystalline alumina may be transformed into a nano-crystalline state and/or become amorphous. It is also possible that calcium may participate in a chemical wear of the tools.
- Based on these results and a literature breakdown, a new model describing the wear of textured alumina have been developed.

11 Acknowledgements

The author of this thesis would like to pay his sincere thanks to all the kind co-workers at Sandvik Coromant Västberga whom, during my time here as a master thesis student, has greatly supported me in all my work. Among these persons there are some that I especially would like to thank.

First and foremost, I would like to thank my mentor *Marianne Collin* for all the kind help, support and trust during my entire stay here in Västberga.

In no particular order, I would also like to thank:

Kalle Erixon, for all the help with the performed turning tests.

Christer Fahlgren and *Svend Fjordvald*, for all the help with the SEM-equipment and image-taking.

Magnus K Berglund, for the help with the imaging from the Wyko-instrument.

Elias Nyrot, for the help with the EPMA-results.

Mikael Kritikos, for the help with the performed XRD.

And *Mikael Olsson*, Professor Högskolan Dalarna, who provided me with the results from the AES-measurements.

Last but not least, I would like to thank all the colleagues in CDTF who have made my stay here at Sandvik Coromant Västberga into a very joyful period.

Thank you all!

Sebastian Öhman
14/06/2016,

1st revision 19/08/2016
2nd revision 02/09/2016

12 References

1. Industrial Revolution - Facts & Summary [Internet]. HISTORY.com. [citerad 12 juni 2016]. Hämtad från: <http://www.history.com/topics/industrial-revolution>
2. Heinrichs J, Olsson M, Jacobson S. Surface degradation of cemented carbides in scratching contact with granite and diamond—The roles of microstructure and composition. *Wear*. 2015;342–343:210–21.
3. Cemented carbide -- Britannica Online Encyclopedia [Internet]. [citerad 12 juni 2016]. Hämtad från: <http://academic.eb.com.ezproxy.its.uu.se/EB-checked/topic/101853/cemented-carbide>
4. metallurgy: Powder metallurgy -- Britannica Online Encyclopedia [Internet]. [citerad 12 juni 2016]. Hämtad från: <http://academic.eb.com.ezproxy.its.uu.se/EB-checked/topic/377665/metallurgy/81903/Powder-metallurgy>
5. Sawka A, Kwatera A, Woźnicki A, Zasadziński J. Cemented carbide cutting tools life with nanocrystalline Al₂O₃ layer deposited by MOCVD. *Arch. Civ. Mech. Eng.* 2016;16:351–64.
6. Ånmark N, Lövquist S, Vosough M, Björk T. The Effect of Cleanliness and Micro Hardness on the Machinability of Carburizing Steel Grades Suitable for Automotive Applications. *Steel Res. Int.* 2016;87:403–12.
7. Motorcu AR. Tool life performances, wear mechanisms and surface roughness characteristics when turning austenised and quenched AISI 52100 bearing steel with ceramics and CBN/TiC cutting tools. *Indian J. Eng. Mater. Sci.* 2011;18:137–46.
8. Ånmark N, Karasev A, Jönsson PG. The Effect of Different Non-Metallic Inclusions on the Machinability of Steels. *Materials*. 2015;8:751–83.
9. machine tool -- Britannica Online Encyclopedia [Internet]. [citerad 07 maj 2016]. Hämtad från: <http://academic.eb.com.ezproxy.its.uu.se/EB-checked/topic/354662/machine-tool>
10. Gurbuz H, Kurt A, Ciftci I, Seker U. The Influence of Chip Breaker Geometry on Tool Stresses in Turning. *Stroj. Vestn. – J. Mech. Eng.* 2011;57:91–9.
11. Collin M, inter alios. *Wear Guide - Education material from Performance testing in Västberga* August 2013. 1:a uppl.
12. Pu CL, Zhu G, Yang SB, Yue EB, Subramanian SV. Effect of dynamic recrystallization at tool-chip interface on accelerating tool wear during high-speed cutting of AISI1045 steel. *Int. J. Mach. Tools Manuf.* 2016;100:72–80.
13. Fallqvist M, Olsson M, Ruppel S. Abrasive wear of texture-controlled CVD α -Al₂O₃ coatings. *Surf. Coat. Technol.* 2007;202:837–43.
14. Astakhov VP. The assessment of cutting tool wear. *Int. J. Mach. Tools Manuf.* 2004;44:637–47.
15. Jacobsson S, Hogmark S. *Tribologi - Friktion, Smörjning, Nötning*. 2:a uppl.
16. Ko TJ, Kim HS. Surface Integrity and Machineability in Intermittent Hard Turning. *Int. J. Adv. Manuf. Technol.* 2001;18:168–75.
17. Zemzemi F, Rech J, Ben Salem W, Dogui A, Kapsa P. Identification of a friction model at tool/chip/workpiece interfaces in dry machining of AISI4142 treated steels. *J. Mater. Process. Technol.* 2009;209:3978–90.
18. Abukhshim NA, Mativenga PT, Sheikh MA. Heat generation and temperature prediction in metal cutting: A review and implications for high speed machining. *Int. J. Mach. Tools Manuf.* 2006;46:782–800.
19. Yuan J, Boyd JM, Covelli D, Arif T, Fox-Rabinovich GS, Veldhuis SC. Influence of Workpiece Material on Tool Wear Performance and Tribofilm Formation in Machining Hardened Steel. *Lubricants*. 2016;4:10.
20. Qi HS, Mills B. Formation of a transfer layer at the tool-chip interface during machining. *Wear*. 2000;245:136–47.

21. Kulkarni AP, Joshi GG, Sargade VG. Dry Turning of AISI 304 Austenitic Stainless Steel Using Al-TiCrN Coated Insert Produced by HPPMS Technique. *Procedia Eng.* 2013;64:737–46.
22. Chandrasekaran H, Granfors M, M'Saoubi R. Tribological aspects of tool–chip and tool–work contact in machining and the application of laser spectrometry. *Wear.* 2006;260:319–25.
23. Gekonde HO, Subramanian SV. Tribology of tool–chip interface and tool wear mechanisms. *Surf. Coat. Technol.* 2002;149:151–60.
24. Rogström L, Johansson-Jöesaar MP, Landälv L, Ahlgren M, Odén M. Wear behavior of ZrAlN coated cutting tools during turning. *Surf. Coat. Technol.* 2015;282:180–7.
25. Zhou F. A new analytical tool-chip friction model in dry cutting. *Int. J. Adv. Manuf. Technol.* 2013;70:309–19.
26. wear | physics [Internet]. *Encycl. Br.* [citerad 07 maj 2016]. Hämtad från: <http://global.britanica.com/science/wear>
27. Bejjani R, Collin M, Thersleff T, Odelros S. Multi-scale study of initial tool wear on textured alumina coating, and the effect of inclusions in low-alloyed steel. *Tribol. Int.* [Internet]. [citerad 07 maj 2016]; Hämtad från: <http://www.science-direct.com/science/article/pii/S0301679X16000335>
28. Yin Z, Huang C, Yuan J, Zou B, Liu H, Zhu H. Cutting performance and life prediction of an Al₂O₃/TiC micro–nano-composite ceramic tool when machining austenitic stainless steel. *Ceram. Int.* 2015;41:7059–65.
29. Senthil Kumar A, Raja Durai A, Sornakumar T. Wear behaviour of alumina based ceramic cutting tools on machining steels. *Tribol. Int.* 2006;39:191–7.
30. Markov D, Kelly D. Mechanisms of adhesion-initiated catastrophic wear: pure sliding. *Wear.* 2000;239:189–210.
31. Jr WDC, Rethwisch DG. *Materials Science and Engineering: An Introduction 8th Edition Binder Ready Version with Binder Ready Survey Flyer Set.* John Wiley & Sons, Incorporated; 2010.
32. Šimůnek A, Vackář J. Hardness of Covalent and Ionic Crystals: First-Principle Calculations. *Phys. Rev. Lett.* 2006;96:85501.
33. Haddag B, Makich H, Nouari M, Dhers J. Characterization and Modelling of the Rough Turning Process of Large-scale Parts: Tribological Behaviour and Tool Wear Analyses. *Procedia CIRP.* 2015;31:293–8.
34. Rупpi S. Enhanced performance of α -Al₂O₃ coatings by control of crystal orientation. *Surf. Coat. Technol.* 2008;202:4257–4269.
35. Jianxin D, Jiantou Z, Hui Z, Pei Y. Wear mechanisms of cemented carbide tools in dry cutting of precipitation hardening semi-austenitic stainless steels. *Wear.* 2011;270:520–7.
36. Fang XD, Zhang D. An investigation of adhering layer formation during tool wear progression in turning of free-cutting stainless steel. *Wear.* 1996;197:169–78.
37. Ciftci I. Machining of austenitic stainless steels using CVD multi-layer coated cemented carbide tools. *Tribol. Int.* 2006;39:565–9.
38. Gerth J, Gustavsson F, Collin M, Andersson G, Nordh L-G, Heinrichs J, m.fl. Adhesion phenomena in the secondary shear zone in turning of austenitic stainless steel and carbon steel. *J. Mater. Process. Technol.* 2014;214:1467–81.
39. Rупpi S. Deposition, microstructure and properties of texture-controlled CVD α -Al₂O₃ coatings. *Int. J. Refract. Met. Hard Mater.* 2005;23:306–16.
40. Rупpi S, Larsson A, Flink A. Nanoindentation hardness, texture and microstructure of α -Al₂O₃ and κ -Al₂O₃ coatings. *Thin Solid Films.* 2008;516:5959–66.
41. Mao WG, Shen YG, Lu C. Deformation behavior and mechanical properties of polycrystalline and single crystal alumina during nanoindentation. *Scr. Mater.* 2011;65:127–30.
42. Krell A, Bakun OV. High-temperature hardness of Al₂O₃-base ceramics. *Acta Metall.* 1986;34:1315–9.
43. Barry J, Byrne G. Cutting tool wear in the machining of hardened steels: Part I: alumina/TiC cutting tool wear. *Wear.* 2001;247:139–51.
44. Levin I, Brandon D. Metastable Alumina Polymorphs: Crystal Structures and Transition Sequences. *J. Am. Ceram. Soc.* 1998;81:1995–2012.
45. Lizárraga R, Holmström E, Parker SC, Arrouvel C. Structural characterization of amorphous alumina and its polymorphs from first-principles XPS and NMR calculations. *Phys. Rev. B.* 2011;83:94201.

46. Marinopoulos AG, Elsässer C. Microscopic structure and bonding at the rhombohedral twin interface in α -Al₂O₃. *Acta Mater.* 2000;48:4375–86.
47. Atkins P, Paula J de. *Atkins' Physical Chemistry*. OUP Oxford; 2010.
48. Heuer AH, Lagerlöf KPD, Castaing J. Slip and twinning dislocations in sapphire (α -Al₂O₃). *Philos. Mag. A.* 1998;78:747–763.
49. Le V-V, Nguyen V-H, Nguyen V-H, Pham K-H. The structure and mechanical properties in amorphous alumina under pressure. *Comput. Mater. Sci.* 2013;79:110–7.
50. Chiang Y-M, Birnie DP, Kingery WD. *Physical Ceramics: Principles for Ceramic Science and Engineering*. Wiley; 1996.
51. Zhang C, Kalia RK, Nakano A, Vashishta P, Branicio PS. Deformation mechanisms and damage in α -alumina under hypervelocity impact loading. *J. Appl. Phys.* 2008;103:83508.
52. Bilde-Sørensen JB, Lawlor BF, Geipel T, Pirouz P, Heuer AH, Lagerlöf KPD. On basal slip and basal twinning in sapphire (α -Al₂O₃)—I. Basal slip revisited. *Acta Mater.* 1996;44:2145–52.
53. Kottada RS, Chokshi AH. The high temperature tensile and compressive deformation characteristics of magnesia doped alumina. *Acta Mater.* 2000;48:3905–15.
54. Barceinas-Sánchez JDO, Rainforth WM. On the role of plastic deformation during the mild wear of alumina. *Acta Mater.* 1998;46:6475–83.
55. Haney EJ, Subhash G. Static and dynamic indentation response of basal and prism plane sapphire. *J. Eur. Ceram. Soc.* 2011;31:1713–21.
56. Kollenberg W. Plastic deformation of Al₂O₃ single crystals by indentation at temperatures up to 750° C. *J. Mater. Sci.* 1988;23:3321–5.
57. Mao WG, Shen YG, Lu C. Nanoscale elastic-plastic deformation and stress distributions of the C plane of sapphire single crystal during nanoindentation. *J. Eur. Ceram. Soc.* 2011;31:1865–71.
58. Nordgren A, Melander A. Deformation behaviour of different types of inclusion during chip formation in turning of quenched and tempered steels. *Mater. Sci. Technol.* 1989;5:940–51.
59. Helistö P, Helle AS, Pietikäinen J. Interface phenomena between oxide layers and cemented carbide tools. *Wear.* 1990;139:225–34.
60. Joo Hyun Park HT. Control of MgO·Al₂O₃ Spinell Inclusions in Stainless Steels. *ISIJ Int.* 2010;50:1333–46.
61. Ånmark N, Björk T, Ganea A, Ölund P, Hogmark S, Karasev A, m.fl. The effect of inclusion composition on tool wear in hard part turning using PCBN cutting tools. *Wear.* 2015;334–335:13–22.
62. Krauss G. *Steels: Processing, Structure, and Performance, Second Edition*. ASM International; 2015.
63. Barry J, Byrne G. Cutting tool wear in the machining of hardened steels: Part II: cubic boron nitride cutting tool wear. *Wear.* 2001;247:152–60.
64. Nordgren A, Melander A. Tool wear and inclusion behaviour during turning of a calcium-treated quenched and tempered steel using coated cemented carbide tools. *Wear.* 1990;139:209–23.
65. Matsui N, Watari K. Wear Reduction of Carbide Tools Observed in Cutting Ca-added Steels for Machine Structural Use. *ISIJ Int.* 2006;46:1720–7.
66. Qi HS, Mills B. On the formation mechanism of adherent layers on a cutting tool. *Wear.* 1996;198:192–6.
67. M. Stanford, P.M. Lister, K.A. Kibble, C. Morgan, T. Sihra. Tool wear investigation whilst turning BS970-080A15 carbon steel using TiCN-Al₂O₃ CVD coated carbide tooling in gaseous and liquid nitrogen environments. *Ind. Lubr. Tribol.* 2013;65:236–44.
68. Tieu AK, Fang XD, Zhang D. FE analysis of cutting tool temperature field with adhering layer formation. *Wear.* 1998;214:252–8.
69. Mills B, Hao CS, Qi HS. Formation of an adherent layer on a cutting tool studied by micro-machining and finite element analysis. *Wear.* 1997;208:61–6.
70. Akasawa T, Sakurai H, Nakamura M, Tanaka T, Takano K. Effects of free-cutting additives on the machinability of austenitic stainless steels. *J. Mater. Process. Technol.* 2003;143–144:66–71.
71. Experimental study of Built-Up Layer formation during machining of high strength free-cutting steel [Internet]. [citerad 05 juli 2016].

Hämtad från: <http://www.science-direct.com.ezproxy.its.uu.se/science/article/pii/S0924013616301480>

72. Larsson A, Rupp S. Structure and composition of built-up layers on coated tools during turning of Ca-treated steel. *Mater. Sci. Eng. A*. 2001;313:160–9.

73. Atlati S, Haddag B, Nouari M, Moufki A. Effect of the local friction and contact nature on the Built-Up Edge formation process in machining ductile metals. *Tribol. Int.* 2015;90:217–27.

74. von Herwart O, Gappisch M, König W, Pape R, Adalbert W. Einfluß oxydischer Einschlüsse auf die Bearbeitbarkeit von Stahl Ck 45 mit Hartmetall-Drehwerkzeugen. *Arch. Für Eisenhüttenwesen Vom Ver. Dtsch. Eisenhüttenleute Max-Planck-Inst. Für Eisenforschung*. 1962;Jahrgang Heft 12:841–51.

75. Ohgo K. The adhesion mechanism of the built-up edge and the layer on the rake face of a cutting tool. *Wear*. 1978;51:117–26.

76. Lo Casto S, Lo Valvo E, Lucchini E, Maschio S, Ruisi VF. Wear rates and wear mechanisms of alumina-based tools cutting steel at a low cutting speed. *Wear*. 1997;208:67–72.

77. Rupp S, Högrelius B, Huhtiranta M. Wear characteristics of TiC, Ti(C,N), TiN and Al₂O₃ coatings in the turning of conventional and Ca-treated steels. *Int. J. Refract. Met. Hard Mater.* 1998;16:353–68.

78. Brandt G, Mikus M. An electron microprobe and cathodoluminescence study of chemical reactions between tool and workpiece when turning steel with alumina-based ceramics. *Wear*. 1987;115:243–263.

79. Dearnley PA. Rake and Flank Wear Mechanisms of Coated Cemented Carbides. *Surf. Eng.* 1985;1:43–58.

80. Senthil Kumar A, Raja Durai A, Sornakumar T. The effect of tool wear on tool life of alumina-based ceramic cutting tools while machining hardened martensitic stainless steel. *J. Mater. Process. Technol.* 2006;173:151–6.

81. Sun F, Li Z, Jiang D, Chen B. Adhering wear mechanism of cemented carbide cutter in the intervallic cutting of stainless steel. *Wear*. 1998;214:79–82.

82. Collin M. Wear Point CVD. A Study of Flank Wear on CVD Coatings. Västberga; Report No.: TM CDTF85936.

83. Sandvik Coromant. Material Evaluation of ISO P Workpiece Materials. Report No.: TM CTEV69193.

84. 4340 High tensile steel datasheet [Internet]. Australia: Bohler Uddeholm; Hämtad från: <http://www.ssm.co.nz/sitefiles/4340.pdf>

85. Exova. Test report SS2541. Report No.: K401732.

86. Lövquist S. Evaluation of workpiece material 34CrNiMo6+QT for Västberga - Technical Memo. Sandviken: Sandvik Materials Technology (SMT); 2016 maj s. 5. Report No.: 22.

87. Raveendra S, Raghuvveer G. Inclusions Assessment of SS2541 Steel Grade. Tech. Rep. - Res. Dev. AB Sandvik Coromant. 2014;2014.

88. Sandvik Coromant. Product information: CNMA 12 04 08-KR [Internet]. [citerad 09 maj 2016]. Hämtad från: <http://www.sandvik.coromant.com/en-gb/products/Pages/productdetails.aspx?c=cnma%2012%2004%2008-kr%203025&m=5725025>

89. Sandvik Coromant. Product information: CNMG 12 04 08 - PM [Internet]. [citerad 09 maj 2016]. Hämtad från: <http://www.sandvik.coromant.com/en-gb/products/pages/productdetails.aspx?c=CNMG%2012%2004%2008-PM%204325&m=6265883>

90. Säkerhetsdatablad Blasocut BC 935 SW [Internet]. , CH - 3415 Hasle - Rüegsau (Schweiz); Hämtad från: <http://www.duroc.com/media/1062009/01935-65-blasocut-bc-935-sw-1312.pdf>

91. Product Data Sheet - Blasocut BC 935 [Internet]. BLASER Swissslube Ltd., CH - 3415 Hasle - Rüegsau (Schweiz); Hämtad från: http://www.cuttingfluids.com.mx/es/wp-content/uploads/2014/09/Blasocut_BC935.pdf

92. Azhar AZA, Choong LC, Mohamed H, Ratnam MM, Ahmad ZA. Effects of Cr₂O₃ addition on the mechanical properties, microstructure and wear performance of zirconia-toughened-alumina (ZTA) cutting inserts. *J. Alloys Compd.* 2012;513:91–6.

93. Angseryd J. Microstructure of a cubic boron nitride tool material and its degradation during hard turning operations. Göteborg: Department of Applied Physics - CHALMERS UNIVERSITY; 2011 Sweden. Report No.: Ny serie 3169.

94. Ahn ES, Gleason NJ, Nakahira A, Ying JY. Nanostructure Processing of Hydroxyapatite-based Bioceramics. *Nano Lett.* 2001;1:149–53.
95. Aifantis EC. The physics of plastic deformation. *Int. J. Plast.* 1987;3:211–47.
96. University of Cambridge. Slip in HCP metals 1: slip systems [Internet]. DoITPoMS. Hämtad från: http://www.doit-poms.ac.uk/tlplib/slip/slip_in_hcp1.php
97. University of Cambridge. Slip geometry: the critical resolved shear stress [Internet]. Hämtad från: http://www.doit-poms.ac.uk/tlplib/slip/slip_geometry.php
98. Acharya S, Bysakh S, Parameswaran V, Kumar Mukhopadhyay A. Deformation and failure of alumina under high strain rate compressive loading. *Ceram. Int.* 2015;41:6793–801.
99. Pirouz P, Lawlor BF, Geipel T, Bilde-Sørensen JB, Heuer AH, Lagerlöf KPD. On Basal slip and basal twinning in sapphire (α -Al₂O₃)—II. A new model of basal twinning. *Acta Mater.* 1996;44:2153–64.
100. Geipel T, Bilde-Sørensen JB, Lawlor BF, Pirouz P, Lagerlöf KPD, Heuer AH. On basal slip and basal twinning in sapphire (α -Al₂O₃)—III. HRTEM of the twin/matrix interface. *Acta Mater.* 1996;44:2165–74.
101. Zhang C, Kalia RK, Nakano A, Vashishta P. Hypervelocity impact induced deformation modes in α -alumina. *Appl. Phys. Lett.* 2007;91:71906–71906.
102. Caillard D, Martin JL. Thermally Activated Mechanisms in Crystal Plasticity. Elsevier; 2003.
103. Friedel J. Dislocations and Mechanical Properties of Crystals. John Wiley Sons Inc. 1957:330–2.
104. Chen MW, McCauley JW, Dandekar DP, Bourne NK. Dynamic plasticity and failure of high-purity alumina under shock loading. *Nat. Mater.* 2006;5:614–8.
105. Wang YG, Bronsveld PM, De Hosson JTM, Djuričić B, McGarry D, Pickering S. Twinning in θ Alumina Investigated with High Resolution Transmission Electron Microscopy. *J. Eur. Ceram. Soc.* 1998;18:299–304.
106. Inkson BJ. Dislocations and twinning activated by the abrasion of Al₂O₃. *Acta Mater.* 2000;48:1883–95.
107. Sarobol P, Chandross M, Carroll JD, Mook WM, Bufford DC, Boyce BL, m.fl. Room Temperature Deformation Mechanisms of Alumina Particles Observed from In Situ Micro-compression and Atomistic Simulations. *J. Therm. Spray Technol.* 2015;25:82–93.
108. Furuichi H, Matsuura K, Yamazaki K, Watanabe S. Amorphous state formation and structural changes in a alumina by repeated rubbing. *Wear.* 1995;189:86–90.
109. Nakamura A, Lagerlöf KPD, Matsunaga K, Tohma J, Yamamoto T, Ikuhara Y. Control of dislocation configuration in sapphire. *Acta Mater.* 2005;53:455–62.
110. Dearnley P, Thompson V. Evaluation of failure mechanisms of ceramics and coated carbides used for machining stainless steels. *Surf. Eng.* 2013;